รายงานวิจัยฉบับสมบูรณ์

โครงการ การออกแบบและพัฒนาตัวเร่งปฏิกิริยาโลหะออกไซด์ผสม สำหรับการเปลี่ยนสารอนุพันธ์จากชีวมวลให้เป็นผลิตภัณฑ์แกมมาวาเลโรแลคโตน

โดย นายสัญชัย คูบูรณ์

เดือน ปี ที่เสร็จโครงการ

มีนาคม 2562

สัญญาเลขที่ TRG6080004

รายงานวิจัยฉบับสมบูรณ์

โครงการ การออกแบบและพัฒนาตัวเร่งปฏิกิริยาโลหะออกไซด์ผสม สำหรับการเปลี่ยนสารอนุพันธ์จากชีวมวลให้เป็นผลิตภัณฑ์แกมมาวาเลโรแลคโตน

นายสัญชัย คูบูรณ์
ศูนย์นาโนเทคโนโลยีแห่งชาติ สำนักงานพัฒนาวิทยาศาสตร์และเทคโนโลยีแห่งชาติ

สนับสนุนโดยสำนักงานกองทุนสนับสนุนการวิจัยและต้นสังกัด
(ความเห็นในรายงานนี้เป็นของผู้วิจัย สกว.และต้นสังกัดไม่จำเป็นต้องเห็นด้วยเสมอไป)

บทคัดย่อ

กระบวนการไฮโดรจีเนชันแบบส่งผ่านโดยใช้ตัวเร่งปฏิกิริยาโลหะเพื่อเปลี่ยนอนุพันธ์ของชีวมวลให้เป็นสารมูลค่าเพิ่มถือเป็นกระบวนการที่สามารถนำมาใช้ประโยชน์ในอุตสาหกรรมพลังงานและเคมีชีวภาพได้ ซึ่งกระบวนการนี้ไม่ต้องใช้แก๊สไฮโดรเจนซึ่งมีราคาแพงและสามาถลุกติดไฟ แต่ในปัจจุบัน ขั้นตอนของการกระตุ้นตัวเร่งปฏิกิริยาให้สามารถใช้งานได้นั้นยังมีความจำเป็นต้องใช้แก๊สไฮโดรเจนอยู่ งานวิจัยชิ้นนี้จึงมุ่งเน้นการพัฒนาตัวเร่งปฏิกิริยาโลหะออกไซด์ผสมของคอปเปอร์ที่สามารถถูกกระตุ้นได้ในตัวทำละลายแอลกอฮอล์ และสามารถเร่งปฏิกิริยาเพื่อผลิตสารแกมมาวาเลโรแลคโตนจากสารเมธิลลิวูลิเนตได้โดยไม่ต้องเติมแก๊สไฮโดรเจนเข้าไปในระบบ แอลกอฮอล์หลายชนิดได้ถูกนำมาใช้ศึกษาเพื่อเป็นแหล่งผลิตไฮโดรเจนสำหรับการกระตุ้นตัวเร่งปฏิกิริยา และใช้สำหรับกระบวนการไฮโดรจีเนชัน ผลการศึกษาชี้ให้เห็นว่า ตัวเร่งปฏิกิริยาทั้งสี่ชนิด ได้แก่ CuNiO, CuCoO, CuCrO, และ CuFeO มีความสามารถในการเร่งปฏิกิริยาเพื่อผลติสารแกมมาวาเลโรแลคโตนได้ที่อุณหภูมิ 200 องศาเซลเซียสภาในเวลา 3 ชั่วโมง และ 2-โพรพานอล และ 2-บิวทานิล เป็นแอลกอฮอล์ที่สามารถผลิตไฮโดรเจนสำหรับกระบวนการเร่งปฏิกิริยาได้ดีที่สุด งานชิ้นนี้แสดงให้เห็นว่าการทำงานร่วมกันระหว่างตัวเร่งปฏิกิริยาโลหะผสมและแอลกอฮอล์เป็นปัจจัยสำคัญที่ทำให้สามารถผลิตสารแกมมาวาเลโรแลคโตนได้สำเร็จ.

Abstract

Catalytic transfer hydrogenation (CTH) of biomass-derivatives to value-added chemicals over metal-based catalysts is a promising process in biorefinery. This reaction does not require high pressure of expensive and flammable hydrogen gas (H_2). However, an activation of metal-based catalysts using H_2 pretreatment prior to the CTH process limits this advantage. Here, Cu-based mixed metal oxides are introduced as simultaneously activated catalysts (SACs) in the presence of alcohol for a production of gamma-valerolactone (GVL) from methyl levulinate (ML) without requirement of additional H_2 gas during both catalyst pretreatment and hydrogenation steps. Different alcohols including ethanol (EtOH), 1-propanol (1-PrOH), 2-propanol (2-PrOH), 2-butanol (2-BuOH), and cyclohexanol (CyOH) are selected to function as hydrogen sources for both catalyst activation and ML hydrogenation. All four Cu-based mixed metal oxides including CuNiO, CuCoO, CuCrO, and CuFeO show high potential as catalysts for ML conversion to GVL at 200 ^{o}C for 3 h. Among various alcohols investigated in this work, 2-PrOH and 2-BuOH exhibit effective roles as hydrogen sources for simultaneous reduction of the catalysts to generate metal active sites and provide hydrogen species

for hydrogenation of ML to GVL. The complementary cooperation between secondary alcohols and Cu-based mixed-metal oxides is the important key for the high GVL production yield over the novel simultaneously activated catalysts (SACs) in this work.

Project Code (รหัสโครงการ) : TRG6080004

Project Title (ชื่อโครงการ) : Design and development of mixed metal oxides catalysts for production of gamma valerolactone from biomass derivatives

Investigator (ชื่อนักวิจัย) : Mr. Sanchai Kuboon, National Nanotechnology Center, National Science and Technology Development Agency

E-mail Address : sanchai@nanotec.or.th

Project Period (ระยะเวลาโครงการ) : 2 Years

Objective(s) (วัตถุประสงค์)

1. To design, synthesize, and characterize mixed metal oxides catalyst for conversion of glucose to levulinic acid or its derivatives to GVL
2. To study reaction mechanism of levulinic acid or its derivatives conversion to GVL on bimetal oxide catalysts
3. To optimize reaction conditions for maximizing GVL productivity

1. Introduction (บทนำ)

The consumption of fossil fuel keeps increasing with some concern of how long it would last as well as its impact on global warming.[1-5] Various renewable resources including agricultural lignocellulosic biomass becomes increasingly recognized as a valuable feedstock for biofuel and biochemical production due to its abundance and renewability.[6-10] Gamma-valerolactone (GVL), a biomass-derived chemical is a non-toxic and versatile organic compound which could be employed as a starting material or a

solvent in energy and polymer industries.[11-17] Generally, GVL is produced via hydrogenation of levulinic acid (LA) or its esters.[18-33] Good number of reports have demonstrated great potential of LA as a starting material for GVL production. For examples, Cervantes and García showed that GVL could be produced from LA successfully after 24 h using Ru nanoparticle catalyst at 130 ^{o}C[19]. Yan and Chen found that Cu-Fe showed good activity on GVL production from LA at 200 ^{o}C for 10 h.[20] Moreover, a high GVL yield obtained from LA conversion over Ni–Cu/Al_2O_3 catalyst at 250 ^{o}C after 6 h was also reported by Obregón et al.[21] However, due to the fact that levulinic acid could not be separated easily from its acid matrix that used in an extraction process from biomass feedstock, its esters were then becoming more suitable choices for GVL production.[9,27] In addition, methyl levulinate has been suggested as one of the most suitable esters for GVL production over metal catalysts.[34-36] Conventionally, H_2 gas is used directly as a hydrogen source for hydrogenation of LA or its esters which is not favorable considering its risk of explosion from exothermic heat under high reaction pressures.[18,20,21] Catalytic transfer hydrogenation (CTH), on the other hand, is more preferable because of its endothermic nature and its low reaction pressure caused by a replacement of hydrogen gas with organic compounds which could promote superior product selectivity.[28,29,31-33,35-37] Particularly, effective catalysts play the most important role in CTH for accelerating conversion of feedstock and controlling high product yield. In general, Ru-based materials were reported as efficient noble metal catalysts for conversion of LA or its esters to GVL.[19,26] Non-noble metal-based catalysts including nickel, cobalt, copper, chromium, iron or their alloys have also been reported as alternative catalysts for hydrogenation of LA or its esters to GVL as well as other related reactions.[18,20-25,27-29,31,32,50] Among many works reported recently, Song et al. demonstrated an effective Ni/NiO composite catalyst for GVL production from LA. They found that the metal/oxide active sites is the key for its high activity.[50] Another work by Ashok et al. suggested that a suitable loading of CuO promoted a hydrogen spillover effect which could decrease NiO reduction temperature to metallic nickel.[38] Furthermore, our previous report on methyl levulinate (ML) conversion over Ni-Cu-O catalyst indicated that the nickel and copper mixed metal oxides could be employed as catalysts for GVL production.[51] Additionally, Said et al. had reported that CuO–NiO nanocomposites were effective catalysts for 2-propanol dehydrogenation due to enhancement of electrical conductivity and basicity.[49] This good agreement from the previous reports of copper mixed oxides or composites on their promising catalytic

performance in both hydrogenation and dehydrogenation reactions is advantageous for the catalyst design in CTH.

The purpose of this work is; therefore, to integrate the hydrogen spillover effect of CuO with various alcohols as reducing agents for activation of copper mixed metal oxide catalysts and to propose their reaction mechanism for GVL production. A systematic study of catalyst reduction behaviors using Hydrogen temperature programmed reduction (H_2-TPR), alcohol-assisted simultaneous reaction (ASR), *in situ* X-ray diffraction (*in situ* XRD) reduction, and X-ray photoelectron spectroscopy (XPS) were combined with the catalytic performance of GVL production. The obtained knowledge from this work could lead us to a new catalysis concept of simultaneously activated catalysts (SACs) for advanced catalytic transfer hydrogenation (CTH).

2. Experimental

2.1 Catalyst preparation. All metal nitrate salts were purchased from Ajax Finchem Pty Ltd. with minimum purity of 98%. Metal oxide and their Cu–based mixed metal oxides were simply prepared by thermal decomposition of metal nitrate salts. For metal oxide preparation, a chosen nitrate salt of 0.042 mole of each metal was dissolved in 10 ml of DI water. While a mixture of 0.021:0.021 mole ratio of $Cu(NO_3)_2{\cdot}3H_2O$ and one of the other metal (Ni, Co, Cr, or Fe) nitrate was selected for Cu–base mixed metal oxide preparation. After dissolution of metal salts in DI water, the sample was dried and calcined at 800 ^{o}C for 5 h in air and collected after cooling down at room temperature.

2.2 Catalysts Characterization. Powder X–ray diffraction (XRD) patterns of samples from both conventional and *in situ* experiments were analyzed by an X–ray diffractometer (D8 ADVANCE, Bruker, Ltd., Germany) using Cu K_α radiation at 40 kV and 40 mA over the 2θ range of $10 < 2\theta < 80$ degree. For the *in situ* experiment, the sample was heated with a heating rate of 12 ^{o}C /min under hydrogen atmosphere (99.99%) at the flow rate of 20 ml/min from room temperature to 600 ^{o}C on a Rh–Pt alloy substrate. Hydrogen temperature programmed reduction (H_2-TPR) was carried out using CHEMBET–Pulsar Quantachrome Instruments (Germany) equipped with a thermal conductivity detector (TCD). The catalyst (20 mg) was reduced in 5 vol% H_2 in argon at a flow rate of 30 ml/min with a heating rate of 10 ^{o}C /min from room temperature to 800 ^{o}C. X-ray photoelectron spectroscopy (XPS) was conducted using PHI 5000 Versaprobe II (ULVAC-PHI, Inc., Japan). The obtained data was fitted and interpreted using XPSPEAK4.1 program.

2.3 Evaluation of catalytic properties. All catalytic transfer hydrogenation reactions were carried out in a 130 ml stainless steel autoclave with a magnetic stirrer (500 rpm). 0.58 ml of methyl levulinate (ML), 24 ml of alcohol, and 1 g of a metal oxide or mixed metal oxide catalyst were loaded in an autoclave and heated up to 200 ^{o}C with heating rate of 5 ^{o}C /min. A liquid sample analyzed by gas chromatograph using a flame ionization detector or GC-FID (GC–2010, Shimadzu, Japan) and a mass spectrometry detector or GC-MS (GCMS–QP2020, Shimadzu, Japan), and a capillary column (DB–WAX, Agilent technologies, USA) with 30 m in length, 0.25 mm inner diameter, and 0.25 µm film thickness). The methyl levulinate conversion and the GVL product yield were calculated using the following equations:

$$Conversion\ (\%) = \left(\frac{mole\ of\ consumed\ ML}{mole\ of\ ininitial\ ML}\right) \times 100 \qquad (1)$$

$$Yield\ (\%) = \left(\frac{mole\ of\ produced\ GVL}{theoretical\ mole\ of\ GVL}\right) \times 100 \qquad (2)$$

The numbers of mole of ML and GVL were obtained from the peak area analysis using GC–FID while other by–products were detected by GC–MS. Hydrogen content remaining in the reaction was calculated according to the ideal gas law. In brief, the final pressure was recorded after the reactor was cooled down to room temperature. The value of remaining pressure in atm was then subjected to equation (3).

$$n = \frac{PV}{RT} \qquad (3)$$

where V = 0.1 L (actual volume of the reactor), R = 0.08206 L.atm/(mol.K) and T = 298.15 K.

The gas was later analyzed using micro-GC for acquiring purity of hydrogen (CP 4900, Agilent Technologies, USA) and multiplied with the calculated total mole number of remaining gas.

3. Results and discussion

3.1 Catalytic performance. Single phase metal oxides and mixed metal oxides catalysts were compared for GVL production from ML. Initially, five single phase metal oxides including CuO, NiO, Co_3O_4, Cr_2O_3, and Fe_2O_3 were tested as catalysts for production of gamma–valerolactone (GVL) from methyl levulinate (ML) by catalytic transfer hydrogenation (CTH) in a 2–propanol (2-PrOH) system. Their crystal structure information can be found in Fig. S2 and their surface area was shown in Table S1. Catalytic evaluation results of these metal oxides showed neither catalytic behavior toward 2-propanol dehydrogenation nor GVL production at 200 ^{o}C during the reaction

period of 3 h. These results were supported by unchanged reaction pressures caused by 2-propanol evaporation and undetectable or negligible hydrogen gas, acetone, methanol, or GVL throughout the course of the reactions. Consecutively, the four Cu–based mixed oxides were employed as catalysts giving catalytic results provided in Fig. 1a. CuNiO showed high catalytic property which was in good agreement with our previous report[51]. The order of catalytic performance in terms of ML conversion and GVL yield is as follows; CuNiO > CuCoO > CuCrO > CuFeO. The superior catalytic properties of CuNiO and CuCoO catalysts are in accordance with those nickel and cobalt catalysts reported in other studies, namely Raney-nickel[28,29], Ni/Al_2O_3[23,25], and Co-based catalysts.[24,27] The formation of H_2 was labelled as amount of remaining hydrogen in Fig. 1a. For the CuNiO catalyst, it was quite obvious that both 2-PrOH dehydrogenation and ML hydrogenation could take place effectively. CuCoO and CuCrO also showed similar behavior to CuNiO but with less catalytic activity. On the other hand, CuFeO did not show high ML conversion but gave almost the same amount of remaining H_2 as that of CuNiO. This indicated that CuFeO catalyst tended to be an active catalyst for 2-PrOH dehydrogenation but was not effective for ML hydrogenation. XRD patterns of the catalysts before and after the reaction were also shown in Fig. 1. It could be seen that CuO was completely reduced to Cu metal while NiO was partially reduced to Ni metal after the reaction. As it was reported by Song et al. on their study in GVL production from LA using Ni/NiO composite catalyst. They found that the reactant was more likely to adsorb on the NiO sites while the H_2 molecules preferred to stay on the Ni metallic sites. Therefore, the presence of Ni/NiO structure could enhance the catalytic perfamance.[50] In this work, although ML was used as a reactant instead of LA, the Ni/NiO phase with the presence of Cu metal could provide efficient GVL production. The XRD pattern of CuCoO showed complete reduction of both CuO to metallic Cu and Co_3O_4 to metallic Co, respectively. The conversion of ML over this catalyst was around 80%. Zhou et al. had used metallic Co, Ni, and Fe for conversion of ethyl levulinate (EL) to GVL. They found that metallic cobalt was the most active catalyst for GVL production.[27] The CuCrO catalyst showed moderate catalytic activity for both 2-PrOH dehydrogenation and ML conversion. According to the study of Yan and Chen, they found that Cu-Cr catalyst with the 1:2 ratio of Cu^{2+}/Cr^{3+} was an active catalyst for the conventional hydrogenation of LA to GVL using H_2 gas of 70 bar at 200 ^oC for 10 h.[18] They suggested that Cu^{2+} had an important role for H_2 dissociation where the Cu^{2+}/Cr^{3+} ratio significantly influenced the effectiveness of hydrogenation. In this work only 1:1 ratio of Cu^{2+}/Cr^{3+} was employed under the reaction pressure below 40 bar

(generated from the 2-PrOH and its produced H_2) only for 3 h. It might be the unsuitable Cu^{2+}/Cr^{3+} ratio, lower reaction pressure and shorter reaction time that was responsible for its lower activity. The XRD pattern after reaction of CuCrO catalyst represented in Fig. 1c showed 2 phases of Cu metal and $CuCr_2O_4$ which was different from the spent Cu-Cr catalyst reported by Yan and Chen. The higher catalyst reduction temperature used in their work and the low reduction temperature in this work could lead to the phase difference. CuFeO catalyst did not show high activity towards GVL production but provided large amount of hydrogen gas. Yan and Chen also studied the Cu-Fe catalyst for GVL production from LA which indicated that the optimum Cu^{2+}/Fe^{3+} ratio was 1:1 under H_2 pressure of 70 bar at 200 ^{o}C for 10 h. Although the Cu^{2+}/Fe^{3+} ratio from this work and their work were similar but the lower reaction pressure and shorter reaction time in this work could result in its lower catalytic activity. In addition, the Cu-Fe and CuFeO catalysts after reaction showed different phases. The spent Cu-Fe had two phases of $CuFe_2O_4$ and $CuFeO_2$ while the spent CuFeO contained Cu metal and Fe_3O_4 phases. Hence, the synergy of various oxidation states (Cu^0, Fe^{2+}, Fe^{3+} and O^{2-}) in Cu and F_3O_4 system during the dehydrogenation process should be responsible for its good H_2 production. Additionally, substrates for GVL production, besides methyl levulinate were expanded to levulinic acid, ethyl levulinate, and butyl levulinate over the NiCuO catalyst. The results shown in Table S7 suggested that conversion of other feedstocks or GVL product could barely be detected after 3 h of the reaction at 200 ^{o}C. This indicated that the NiCuO catalyst is highly selective toward methyl levulinate substrate.

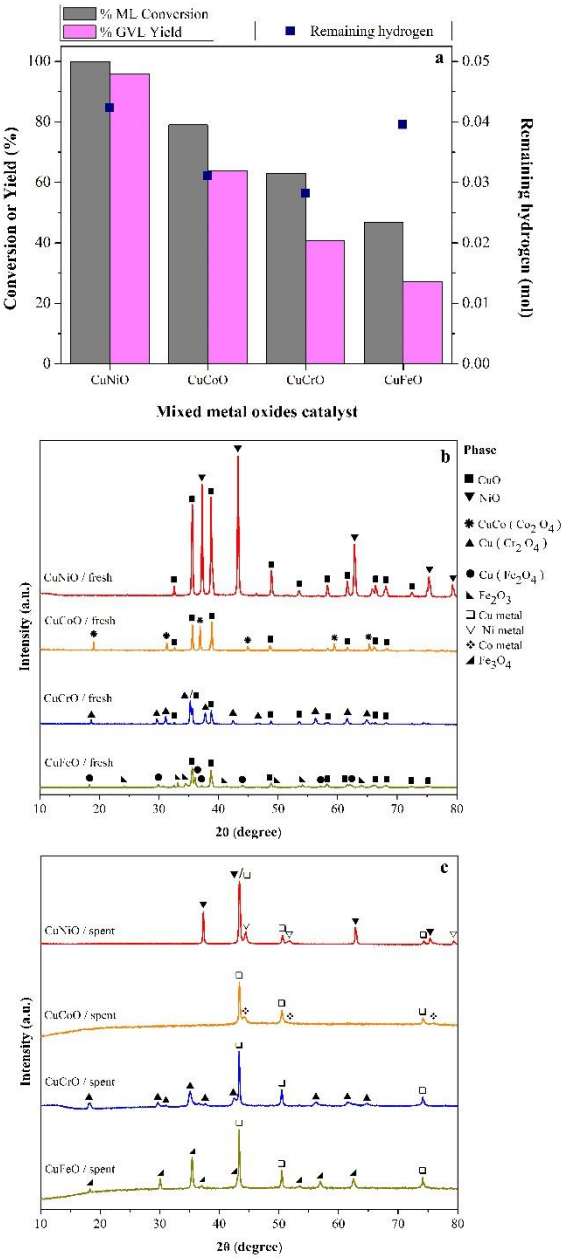

Fig. 1 (a) Catalytic performance in terms of ML conversion, GVL yield, and hydrogen production of copper mixed oxide catalysts at 200 ^{o}C for 3 h using 0.2 M ML in 24 ml of 2-PrOH, (b) XRD patterns of (a) fresh catalysts and (c) spent catalysts.

3.2 Hydrogen temperature programmed reduction (H_2-TPR). To further elucidate the reduction behaviors associated with the catalytic performance of the Cu–based mixed oxide catalysts and their host metal oxides, the hydrogen temperature programmed reduction (H_2–TPR) was conducted and the results were shown in Fig. 2., where their peak areas were displayed in Table S2.CuO catalyst showed a large bell peak at 439 ^{o}C representing a complete reduction from Cu^{2+} to Cu^{0} showing a good agreement with that reported by Tang et al.[39] NiO catalyst showed a major reduction peak at 500 ^{o}C

suggesting a reduction of Ni^{2+} to Ni^{0} as reported by Sá et al.[40] and Zhu et al.[41] In addition, an appearance of a low intensity flat curve at around 620 ^{o}C could be related to a difficultly reduced species of high crystalline NiO (Fig. S2). Co_3O_4 catalyst showed only one broadly asymmetric reduction peak at 514 ^{o}C which was similar to that reported by James and Maity.[42] Fe_2O_3 catalyst was reduced at two different temperatures of 506 and 665 ^{o}C, in accordance with studies by Valenzuela et al.[43] and Liang et al.[44] In contrast, there was a small peak observed at around 380 ^{o}C in Cr_2O_3 catalyst. This result was different from Cr_2O_3 reduction behavior reported by Amrute et al.[45] and Bai et al.[46] They mentioned that the reduction process of Cr_2O_3 underwent two steps including Cr^{6+} to Cr^{3+} at lower temperature and Cr^{3+} to Cr^{2+} at higher temperature. Hence, a very small reduction peak found in this work of the Cr_2O_3 catalyst could be attributed to the reduction of small portion of Cr^{6+} presented in Cr_2O_3 to Cr^{3+}. Moreover, it was clear that all five single phase metal oxides catalysts prepared in this work showed smaller degree of reduction or appeared at higher reduction temperature compared to the similar metal oxides synthesized at lower calcination temperatures in other reports. The inferior reduction behavior of all metal oxides which resulted in a lack of their active metallic sites lead to their poor catalytic performance towards GVL production. Further investigation in the H_2-TPR study of the copper mixed oxide catalysts indicated that each catalyst had at least two reduction peaks as shown in Fig. 2b. The CuNiO catalyst showed two main reduction peaks at 408 and 440 ^{o}C with a very broadly flat curve at around 700 ^{o}C. As it could be observed in the corresponding XRD pattern (Fig. 1b), two phases of CuO and NiO were presented in the CuNiO catalyst.

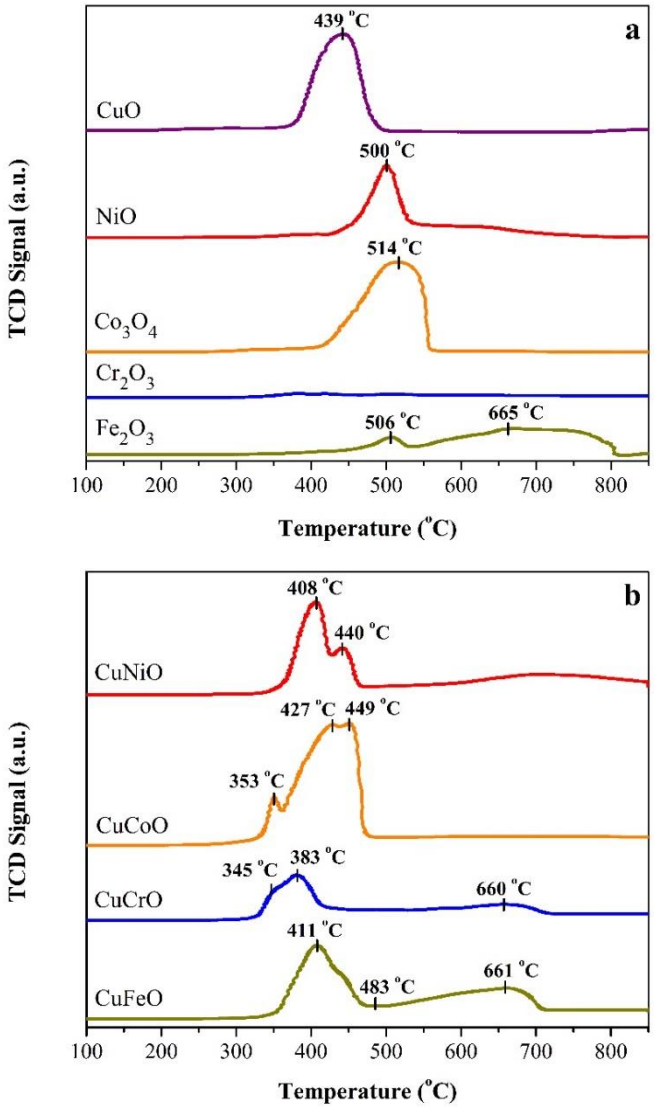

Fig. 2 H_2-TPR profiles of (a) single phase metal oxide (b) mixed metal oxides catalysts.

The first reduction peak belonged to the reduction of CuO to metallic copper (Cu^0) while the second peak was assigned to the reduction of NiO to metallic nickel (Ni^0). CuCoO showed three reduction peaks at 353, 427, and 449 °C. Based on the XRD pattern of CuCoO catalyst shown in Fig. 1b, this catalyst had two major phases of CuO and $CuCo(Co_2O_4)$ spinel. Therefore, the first small peak at the lowest temperature should be assigned to the easily reduced CuO phase while the peak at 427 °C should correspond to the reduction of Cu^{2+} to Cu^0 and Co^{3+} to Co^{2+} in the spinel structure. The highest reduction peak at 449 °C belonged to the reduction of Co^{2+} to metallic Co.[47] Interestingly, XRD pattern of CuCrO showed two different phases of CuO and $Cu(Cr_2O_4)$ spinel without the presence of Cr_2O_3 phase. This meant that the formation of copper oxide and chromium oxide could alter the oxidation states of chromium. In

addition, TPR profile of CuCrO displayed two overlapped peaks at 345 and 383 ^{o}C as well as another broad peak at 660 ^{o}C. The first peak at 345 ^{o}C was attributed to the reduction of Cu^{2+} in CuO to Cu^{0}. The second peak at 383 ^{o}C was a reduction of Cu^{2+} in the $Cu(Cr_2O_4)$ spinel to Cu^{0} and the last peak at 660 ^{o}C was attributed to the reduction of Cr^{3+} in $Cu(Cr_2O_4)$ spinel to Cr^{2+}. Lastly, CuFeO also showed three reduction peaks at 411, 483, and 661 ^{o}C while its XRD pattern in Fig. 1b showed three phases of CuO, $Cu(Fe_2O_4)$ and Fe_2O_3. The first peak at 411 ^{o}C indicated the reduction of Cu^{2+} in CuO to Cu^{0}. A shoulder appeared at around 450 ^{o}C could be assigned to the reduction of Fe^{3+} in Fe_2O_3 to Fe^{2+} in a spinel Fe_3O_4. A very small peak shown at 483 ^{o}C could represent the reduction of Cu^{2+} in $Cu(Fe_2O_4)$. Finally, the broad asymmetric peak at 661 ^{o}C could both be attributed to the partial reduction of Fe^{3+} in $Cu(Fe_2O_4)$ to Fe^{2+} in $(CuFe)(Fe_2O_4)$ spinel and the complete reduction from Fe^{3+} in both rhombohedral and spinel structures to FeO and/or Fe^{0}. In brief, the CuNiO was composed of two separated phases of CuO and NiO; however, the reduction temperature of both CuO and NiO were lower than their host metal oxides. On the other hand, the addition of copper oxide to the cobalt oxide (CuCoO) created the new phase of $CuCo(Co_2O_4)$ spinel structure while maintaining the CuO phase but without the presence of pure the Co_3O_4 phase. The reduction profile of CuCoO indicated that CuO could be reduced at low temperature. The formation of copper oxide and chromium oxide created the more reducible phase of $Cu(Cr_2O_4)$. Finally, the formation of copper and iron mixed metal oxides (CuFeO) could create the new $CuFe_2O_4$ phase but still maintained their host metal oxides of CuO and Fe_2O_3. All reductions of Cu^{2+} and Fe^{3+} were shifted to lower temperatures. In all cases, the reducibility of metal ions were improved after the mixed oxide formation with copper oxide. The alteration of catalyst redox behaviors was strongly related to the enhanced catalytic performance.

3.3 Alcohols-assisted simultaneous reaction evaluation (ASR). With the consistent results among XRD, H_2-TPR, and catalytic performance evaluation, it could be confirmed that the CuNiO was the most effective catalyst for GVL production from ML. Subsequently, various alcohols including aliphatic primary alcohols (ethanol, EtOH and 1-propanol, 1-PrOH), aliphatic secondary alcohols (2-propanol, 2-PrOH and 2-butanol, 2-BuOH), and a cyclic secondary alcohol (cyclohexanol, CyOH) were selected for catalytic testing to verify effect of alcohol types on GVL production over the CuNiO catalyst. Catalytic results presented in Fig. 3a showed that the secondary alcohols were more suitable than primary alcohols in this reaction. EtOH and 1–PrOH gave about 30%

of ML conversion and less than 10% of GVL yield. Formation of a stronger bond between the catalyst active sites and alkoxide species generated from the primary alcohol compared to that of the secondary alcohol could support the ineffectiveness of the primary alcohols.[30] On the other hand, the aliphatic secondary alcohols (2-PrOH and 2-BuOH) showed drastically better catalytic activity than the cyclic secondary alcohol (CyOH). This was due to a high adsorption tendency of CyOH over the catalyst surface.[30] In addition, its high viscosity (Table S4) could also affect ML dispersion in the solution which lowered ML conversion. In addition, the efficiency of CyOH in GVL production from ML reported here was different from the GVL production from EL reported by Cai et al.[32] Although similar CuNi-based catalysts were employed in both studies, alcohol had additional role in facilitating metal oxide reduction in our investigation.

A very low amount of H_2 generated after reaction as shown in Fig. 3a indicated that CyOH has low tendency for hydrogen production. Both 2–PrOH and 2–BuOH provided high ML conversion and more than 95% of GVL yield which is in good agreement with the previous reports.[28-32] In addition, the highest remaining hydrogen amount was obtained in the 2–PrOH system. As mentioned above, generated hydrogen species from alcohol could perform as a reducing agent for the activation of metal oxide catalyst to generate metal active sites. Phase alteration of CuNiO catalyst after reactions in various alcohols was determined by XRD technique as shown in Fig. 3b. In the primary alcohol system, Cu metal phase was formed with the presence of CuO and NiO. Aliphatic secondary alcohols; on the other hand, showed higher degree of catalyst reduction where metallic nickel was also observed. Surprisingly, although low ML conversion, low GVL yield, and low H_2 production were observed in CyOH system (Fig. 3a) both metallic Cu and Ni were generated after the reaction. This means that the CyOH could reduce CuNiO catalyst. However, its strong adsorption on the catalyst as well as its high viscosity could be the reasons for its ineffective role in GVL production.

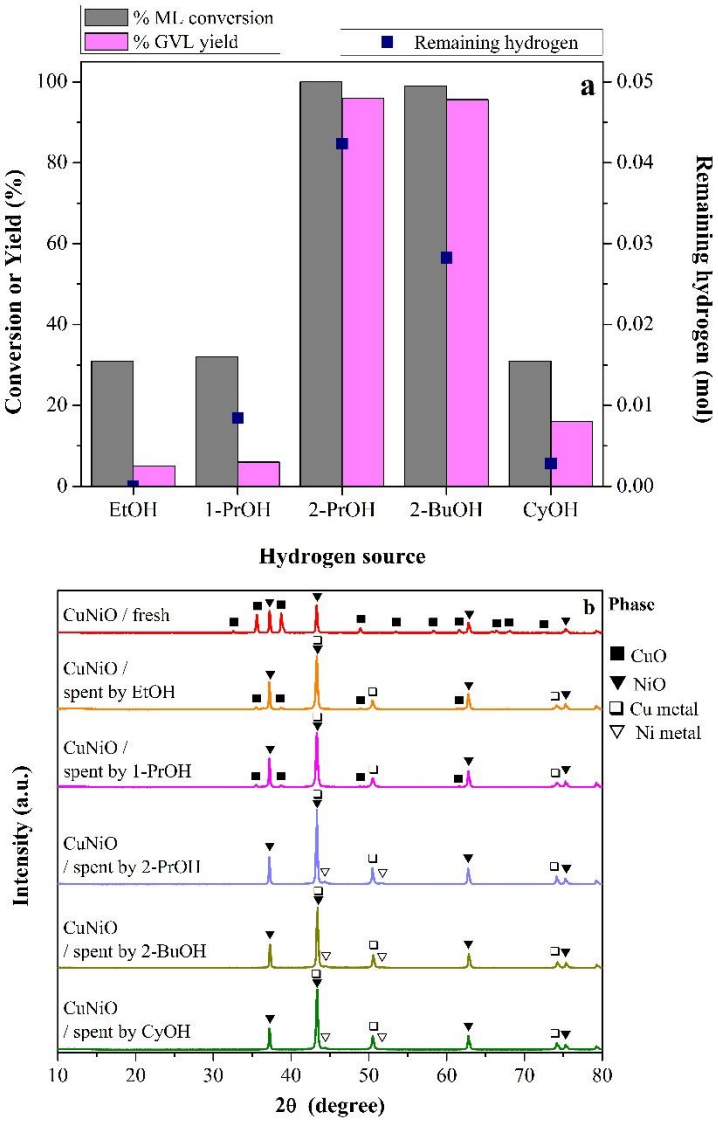

Fig. 3 (a) Catalytic performance in terms of ML conversion, GVL yield, and hydrogen production of CuNiO catalyst at 200 °C for 3 h using 0.2 M ML in 24 ml of various alcohols and (b) XRD patterns of fresh and spent CuNiO catalyst after the reaction.

3.4 *In situ* XRD reduction: Role of CuO in copper mixed metal oxide catalysts. To confirm and gain more insight information on the reducibility enhancement of CuO addition in the copper mixed oxide catalysts, the CuNiO was further selected for an *in situ* XRD reduction experiment in comparison with the CuO and NiO catalysts.[53] Phase transformation of each catalyst was recorded while the catalyst was reduced under pure hydrogen atmosphere at elevated temperature. The *in situ* reduction of CuNiO result shown in Fig. 4a indicated that CuO was reduced to form metallic copper at around 150 °C, following by NiO reduction to form metallic nickel at around 155 °C. While the reduction profile of CuO shown in Fig. 4b indicated that Cu metal was created when the temperature reached 130 °C. The reduction behavior of NiO was displayed in Fig. 4c

where Ni metal was generated at 200 ^{o}C. It can be seen that CuO phase in the CuO catalyst was reduced to Cu metal at lower temperature than CuO in CuNiO while NiO phase in the NiO catalyst was reduced at higher temperature than that of the CuNiO catalyst. The shift of CuO reduction temperature to higher temperature (from 130 to 150 ^{o}C) and the shift of NiO reduction temperature to lower temperature (from 200 to 155 ^{o}C) was an important evidence of the complementary reduction between CuO and NiO in this catalyst. In addition, the occurrence of CuO and NiO reduction temperatures in the CuNiO catalyst at a very close values (150 and 155 ^{o}C, respectively) could support that there was a good interaction between these two oxides in the structure. In brief, the *in situ* XRD results obtained here could confirm the spillover effect of hydrogen species from the created Cu metal to its neighboring NiO for generating nickel metal active sites at lower temperature.

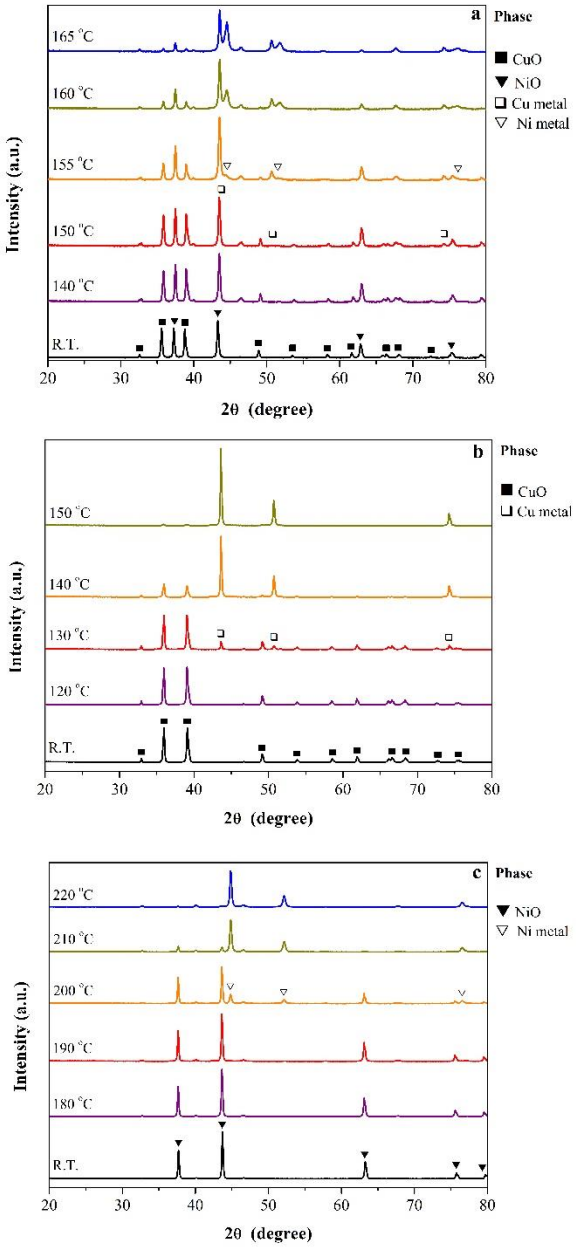

Fig. 4 *In situ* XRD patterns during reduction of (a) CuNiO, (b) CuO, and (c) NiO catalysts under pure H_2 gas flow of 20 ml/min.

3.5 Reusability and versatility of the catalyst. The spent CuNiO catalyst was employed for four more times for the GVL production. The results depicted in Fig. 5a revealed that this catalyst showed only a small decrease in terms of ML conversion and GVL yield after the fourth time. The XRD patterns of the fresh and the 4^{th} reuse of the catalyst were shown in Fig. 5b. It indicated that the spent catalyst still had the same three phases including Cu metal, Ni metal, and NiO as it was reported earlier in Fig. 2b. The small decrease of the catalytic activity might be resulted from the fact that some metallic sites became agglomerated (Fig. S5). The number of phases existed in the CuNiO catalyst before and after the reaction led to a further challenge to find out whether the catalytic performance of the mechanically mixed CuO and NiO would be similar or different from that of the CuNiO catalyst as well as its completely reduced form (alloy). The comparative results of the three scenarios were shown in Fig. 5c. The mechanically mixed CuO+NiO catalyst gave 17% of ML conversion with negligible GVL yield and H_2 production. The improvement in terms of ML conversion compared with the inactive CuO and NiO suggested that the presence of both CuO and NiO in the same system promoted the catalytic activity. The similar XRD patterns of the catalyst before and after reaction without the presence of reduced species (Cu or Ni metal) indicated that the oxide phases in the mechanically mixed metal oxide catalyst might have some capability to accelerate ML conversion; however, metallic sites were required for producing GVL (Fig. 5d). On the other hand, a completely reduced CuNiO labelled as CuNi_alloy showed only one single phase of CuNi alloy. Surprisingly, this alloy catalyst showed comparable ML conversion and GVL yield to those of the pristine CuNiO catalyst. These results suggested that the ML could be converted either on mixed metal oxides or metal/alloy active sites, however, the high selectivity of GVL product preferred the suitable ratio of metal oxides/metallic active sites. In addition, in terms of H_2 production, the alloy catalyst was not comparable to the CuNiO catalyst suggesting that the 2-PrOH dehydrogenation preferably took place over the mixed metal oxide catalysts. Comparative H_2-TPR results of the mechanically mixed CuO + NiO, CuNiO, CuO, and NiO catalysts were shown in Fig. S3. Higher reduction peaks of the mechanically mixed catalyst than that of the CuNiO could explain why there was no metal phase generated after the catalyst utilization. As it was described above, CuNiO showed its impressive catalytic activity in all forms namely, pristine mixed metal oxides (CuNiO), partially

reduced composite (Cu + Ni/NiO), and completely reduced solid solution (CuNi alloy). This is the important proof to confirm that CuNiO was a versatile catalyst for GVL production.

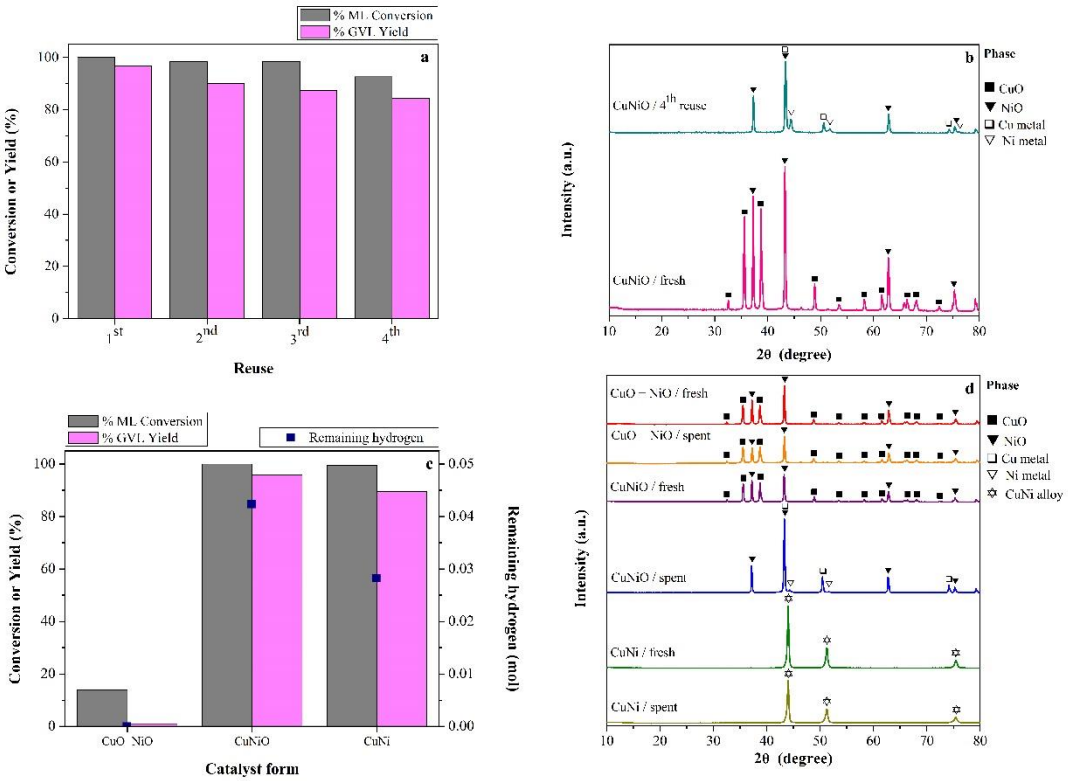

Fig. 5 (a) Catalytic performance of reused CuNiO catalyst up to 4 times at 200 ^{o}C for 3 h using 0.2 M ML in 24 ml of 2-PrOH, (b) XRD patterns of fresh CuNiO and after its 4th reuse, (c) catalytic performance of mechanically mixed CuO+NiO, CuNiO, and CuNi at 200 ^{o}C after 3 h using 0.2 M ML in 24 ml of 2-PrOH, and (d) XRD patterns of mechanically mixed CuO+NiO, CuNiO, and CuNi after reaction at 200 ^{o}C for 3 h in 2-PrOH.

3.6 Metal valences and surface species. To gain more understanding about good performance of the mixed metal oxide catalyst, the Cu/Ni molar ratio of 1.00 and 1.03 were observed in the pristine CuNiO and CuNi_alloy catalysts by using XRF method, respectively (Table S6). Surface analysis results using XPS technique of the pristine CuNiO, spent CuNiO, and CuNiO after 4th reuse were compared in Fig. 6. According to the Cu2p spectra (Fig. 6a, b, c), the pristine CuNiO was originally composed of CuO and $Cu(OH)_2$. After its first use, CuO was completely transformed to Cu metal, while the $Cu(OH)_2$ was still existed. The 4th reuse catalyst also showed these two species but with higher Cu metal/$Cu(OH)_2$ peak ratio. Ni2p spectra (Fig. 6d, e, f) also showed two species of NiO and $Ni(OH)_2$ in the pristine catalyst while the Ni metal was observed along with these two species both in the spent and 4th reuse catalysts. The O1s spectra

(Fig. 6 g, h, i) showed good agreement with the Cu2p and Ni2p results on their surface metal oxides and metal hydroxides formation. Additionally the high binding energy at around 532.6 – 532.7 eV in the spent catalyst and the 4th reuse samples indicated the physically adsorbed water and/or organic compounds (i.e. ML, GVL, 2-PrOH) over NiO species. This could be implied that the NiO was an important site for ML or 2-PrOH adsorption during the ML conversion to GVL. The XPS results revealed various types of surface species including Cu, Ni, CuO, NiO, $Cu(OH)_2$, and $Ni(OH)_2$. While the CuO was found in the pristine catalyst but disappeared after its first use in the reaction. The role of CuO was consistent with the *in situ* XRD results stated above for facilitating NiO reduction at low temperature. The mutual presence of Cu, Ni, NiO, $Cu(OH)_2$, and $Ni(OH)_2$ on the surface were responsible for high catalytic performance of CuNiO catalyst. There was a report by Tang et al. that CuO in form of nanostructure could be also employed as catalysts for GVL production from ML in the presence of methanol directly without catalyst pretreatment[54]. An investigation by combining the findings of their work and the current study to prepare nanostructured mixed metal oxides catalysts for more effective GVL production could be an interesting aspect to conduct in the future.

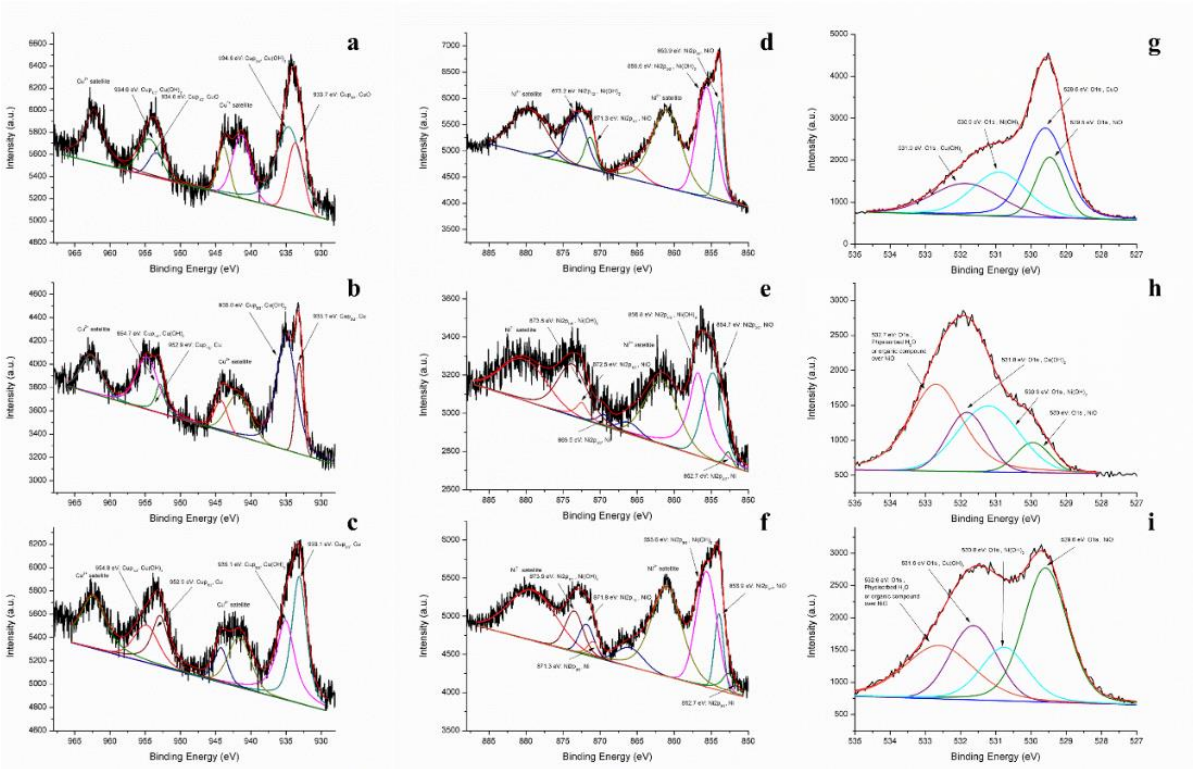

Fig. 6 XPS spectra of CuNiO (a, d, and g); spent CuNiO (b, e, and h); and CuNiO after 4th reuse (c, f, and i) in terms of Cu2p, Ni2p, and O1s, respectively

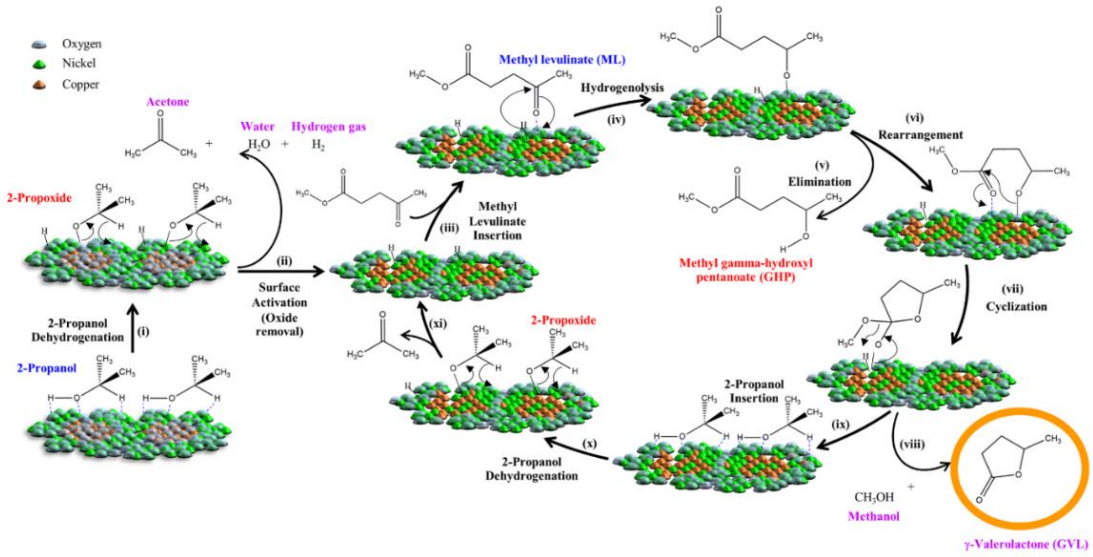

Scheme 1 Proposed reaction mechanism

3.6 Proposed mechanism of alcohol-assisted simultaneous activated copper mixed oxide catalysts for GVL production. Generally, catalytic transfer hydrogenation mechanism over heterogeneous catalysts can take place either through direct catalytic transfer (MPV) or metal hydride mechanism depending on catalyst active sites.[29-31,37] If both Lewis acid and Brønsted basic sites are presented next to each other on the catalyst, the reaction would undergo via MPV mechanism. On the other hand, the reaction would proceed through the metal hydride mechanism if only a Lewis acid or the metal active site is presented. Therefore, in this work, it is worth proposing a reaction mechanism of ML to GVL conversion over the CuNiO catalyst to clarify its simultaneous reduction behavior and promising catalytic performance under 2-PrOH system (Scheme 1). As it was shown in Fig. S4, CuNiO showed the highest acidity compared with other mixed metal oxide catalysts while the acidity could be doubled after the reduction of CuNiO to form CuNi alloy. Moreover, the CO_2-TPD results (Fig. S6c and d) also confirmed that the CuNi alloy has the highest basicity (Table S3). This data could strongly support that the catalytic performance of ML conversion to GVL is not only dependent on catalysts' reducibility but also their acid and base properties. Typically, two major steps including (1) alcohol dehydrogenation to activate surface of the catalyst and (2) hydrogenation of ML followed by simultaneous cyclization to produce GVL. In the first major step, 2-propanol was oxidized over a mixed metal oxide catalyst (containing both Lewis acid and Brønsted base sites) to form 2-propoxide on the catalyst surface[52] (step i). This dehydrogenated intermediate generated hydrogen species and acetone via direct catalytic transfer or MPV mechanism (step ii). Then, the hydrogen species reduced metal oxides surface simultaneously to form metal active sites (Lewis acid) and this process generated water (Table S5) which could partially

reoxidize the metals to metal hydroxides. After ML was inserted to the active metal sites (step iii) under adequate reaction pressure resulted from generated hydrogen gas and alcohol vapor at 200 ^{o}C, ML could then spontaneously react with adsorbed hydrogen species on the catalyst surface to form methyl gamma-hydroxypentanoate (GHP) adsorbed on the surface (step iv).[29-31,37] Some of this intermediate could be eliminated from the surface (step v) while the others underwent cyclization (step vii) leading to GVL production as well as methanol (MeOH) formation (step viii). The vacant active sites were then filled with 2-propanol (step ix) to generate active hydrogen species after 2-propanol dehydrogenation (step x) and acetone elimination (step xi). This led to an active site ready for the next cycle of GVL production. Due to the fact that there were less number of Lewis acid (metal or alloy) than Brønsted base (species on the catalyst active sites at the beginning of the reaction, both alcohol dehydrogenation and GVL production preferably underwent trough MPV mechanism.[37] However, after the first cycle of reaction both MPV and metal hydride are crucial pathways for 2-PrOH dehydrogenation and ML hydrogenation

Conclusions (สรุปผลการวิจัย)

The catalytic transfer hydrogenation was successfully employed in both activation of copper mixed oxide catalysts and production of GVL consecutively. By using H_2-TPR technique, alcohol-assisted reduction evaluation (ASR), *in-situ* XRD reduction, and XPS analysis, it was evident that the good synergistic behaviour between the secondary alcohols and the H_2 spillover effect in copper mixed oxide catalysts is the key for the superior catalytic performance. All catalysts showed potential performance for GVL production from ML in the 2-PrOH system at 200 ^{o}C within 3 h. The most efficient catalyst, CuNiO could be recycled up to four times with only slight decrease of GVL yield. The reaction mechanism in alcohol dehydrogenation and ML hydrogenation underwent through both MPV and metal hydride routes. The discovery in this work could pave the way for a new sustainable concept in catalysis over simultaneously activated mixed metal oxide catalysts.

Suggestions (ข้อเสนอแนะสำหรับงานวิจัยในอนาคต)

1. The amount of catalyst used for catalytic process should be minimized by preparing catalyst over supported materials for controlling the active sites' shape and size.

2. The kinetics study of this materials should be investigated under different reaction temperatures and times.
3. The catalysts prepared in this work should be extended to other hydrogenation processes.

Supporting Information (ข้อมูลสนับสนุนผลการวิจัยเพิ่มเติม)

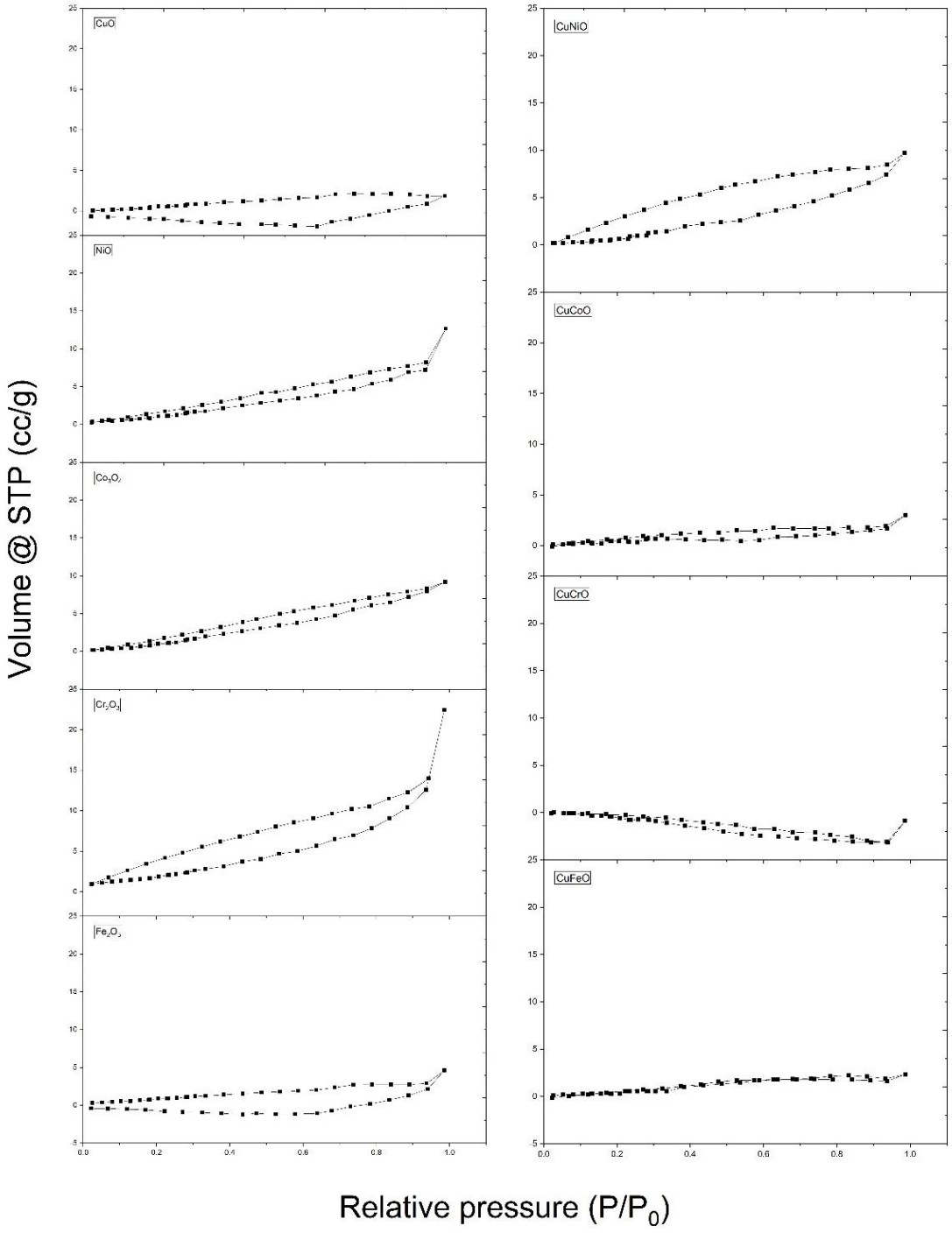

Figure S1. Adsorption-desorption isotherms of catalysts were analyzed at -196 ^{o}C with nitrogen adsorption-desorption technique (Nova 2000e, Quantachrome, Germany).

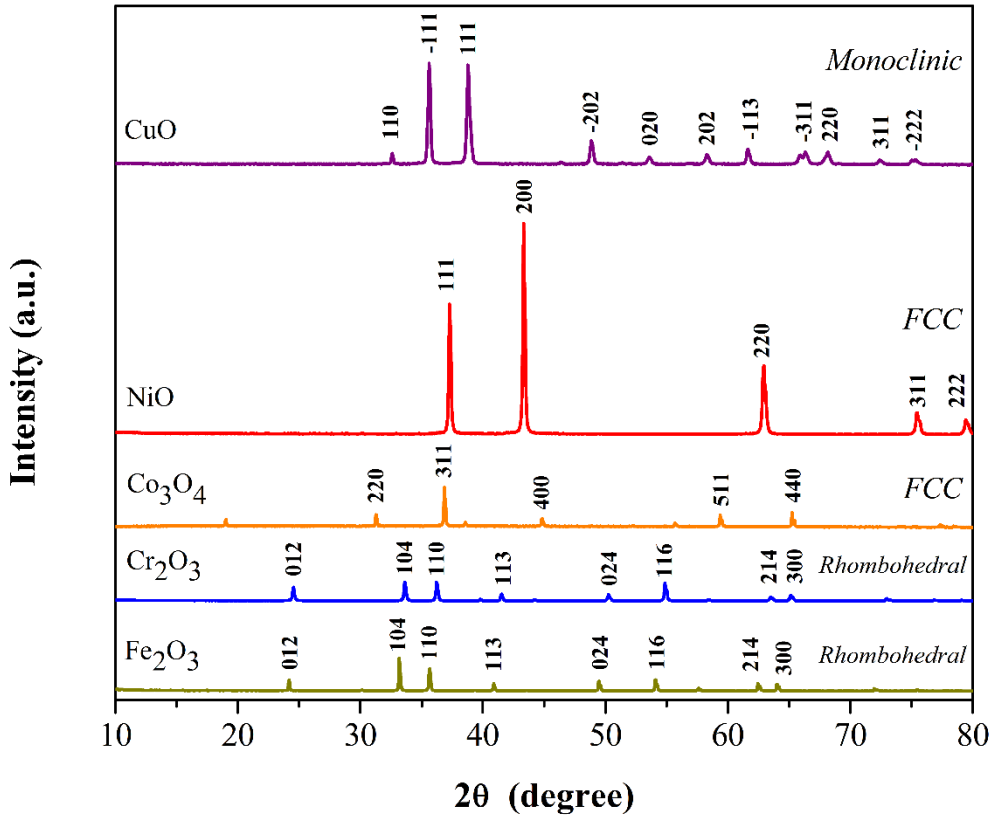

Figure S2. XRD patterns of single phase metal catalysts

Bruker (D8 ADVANCE) X–ray diffractometer was used for determining catalyst crystal structure at room temperature.

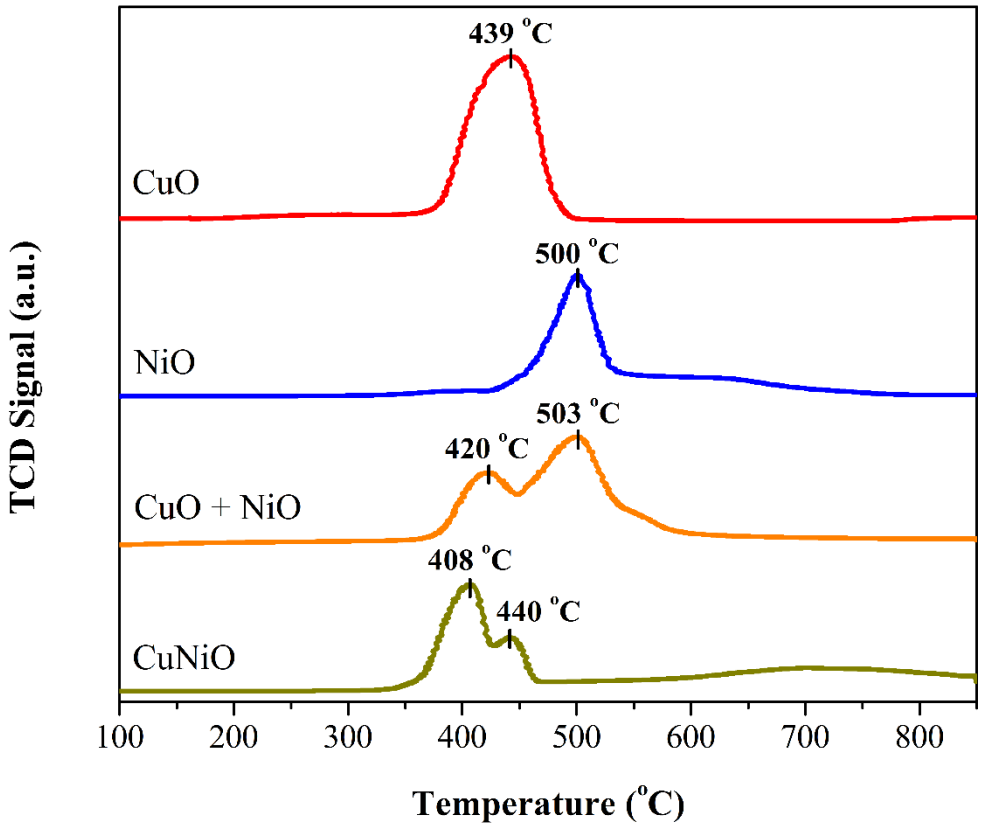

Figure S3. H_2-TPR profile of the mechanically mixed CuO + NiO catalyst compared with CuNiO catalysts and their host metal oxides.

Hydrogen temperature programmed reduction (H_2–TPR) was carried out to determine reduction behavior of the catalyst (CHEMBET–Pulsar Quantachrome, Germany).

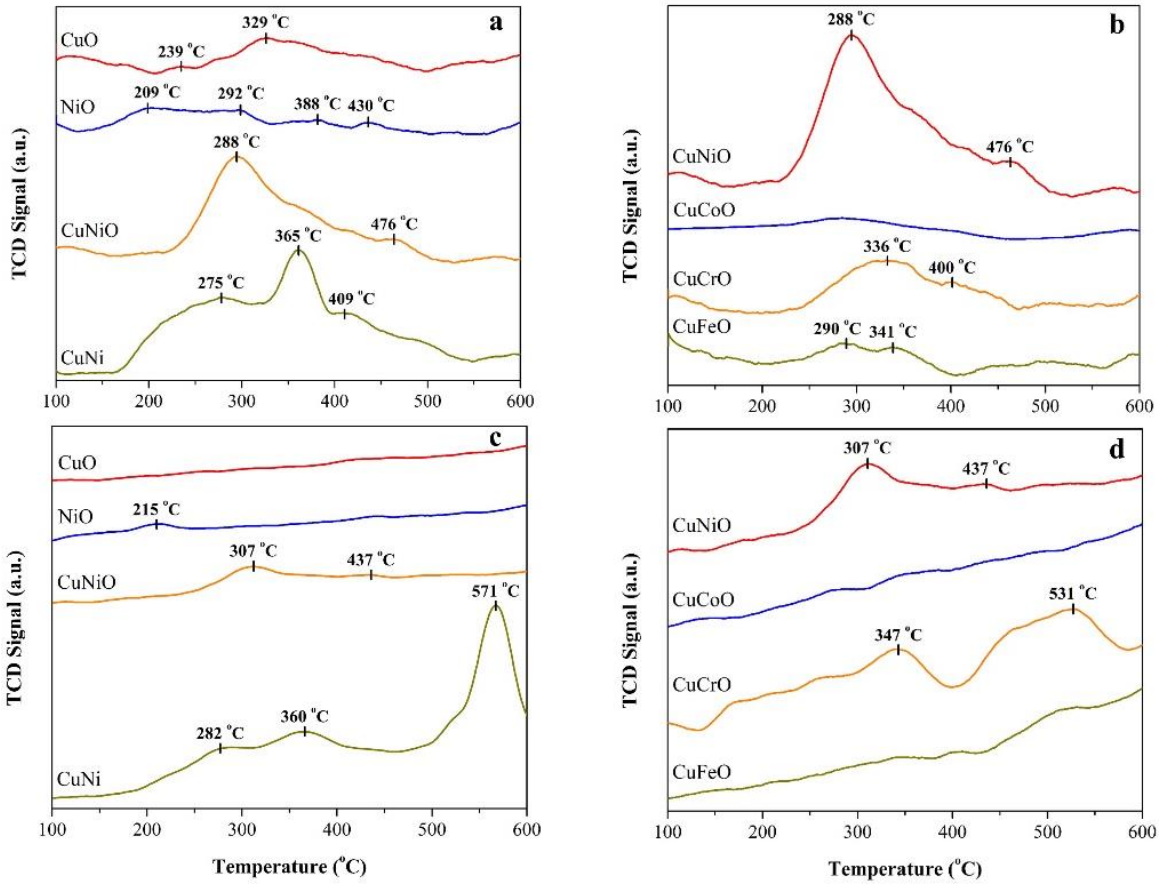

Figure S4. NH_3-TPD profiles of CuNiO catalyst (a) with their host metal oxides and alloy (b) with other Cu-based mixed metal oxides and CO_2-TPD profiles of CuNiO catalyst with (c) with their host metal oxides and alloy (d) with other Cu-based mixed metal oxides.

Acid-based properties of catalysts were evaluated using temperature programmed desorption techniques, NH_3-TPD and CO_2-TPD, respectively (ChemStar, Quantachrome, Germany). Briefly, each sample was adsorbed with 10% NH_3/He or CO_2 at constant temperature, then it was heated up to 800 ^oC with heating rate of 5 ^oC/min under He atmosphere while the signal from TCD detector was recorded.

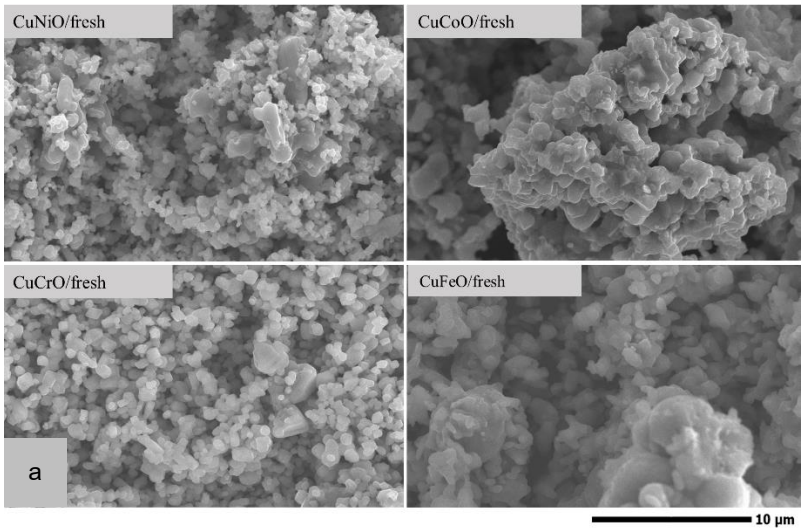

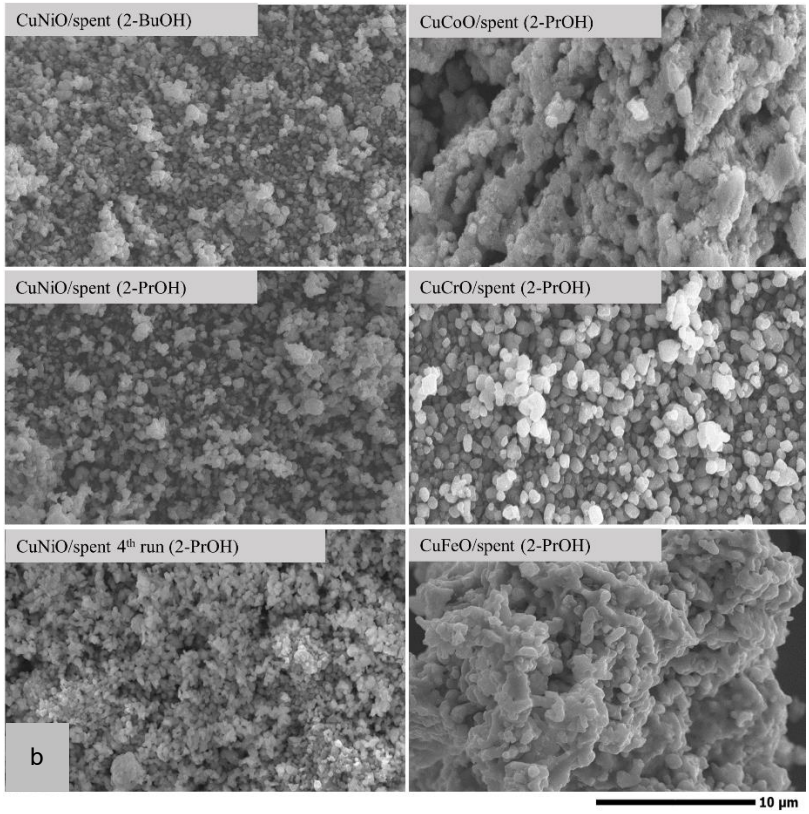

Figure S5. SEM images of (a) fresh catalysts and (b) spent catalysts.

Catalyst morphology was observed by a scanning electron microscope at the magnification of 5,000X (SEM; Hitachi–S3400N, Japan).

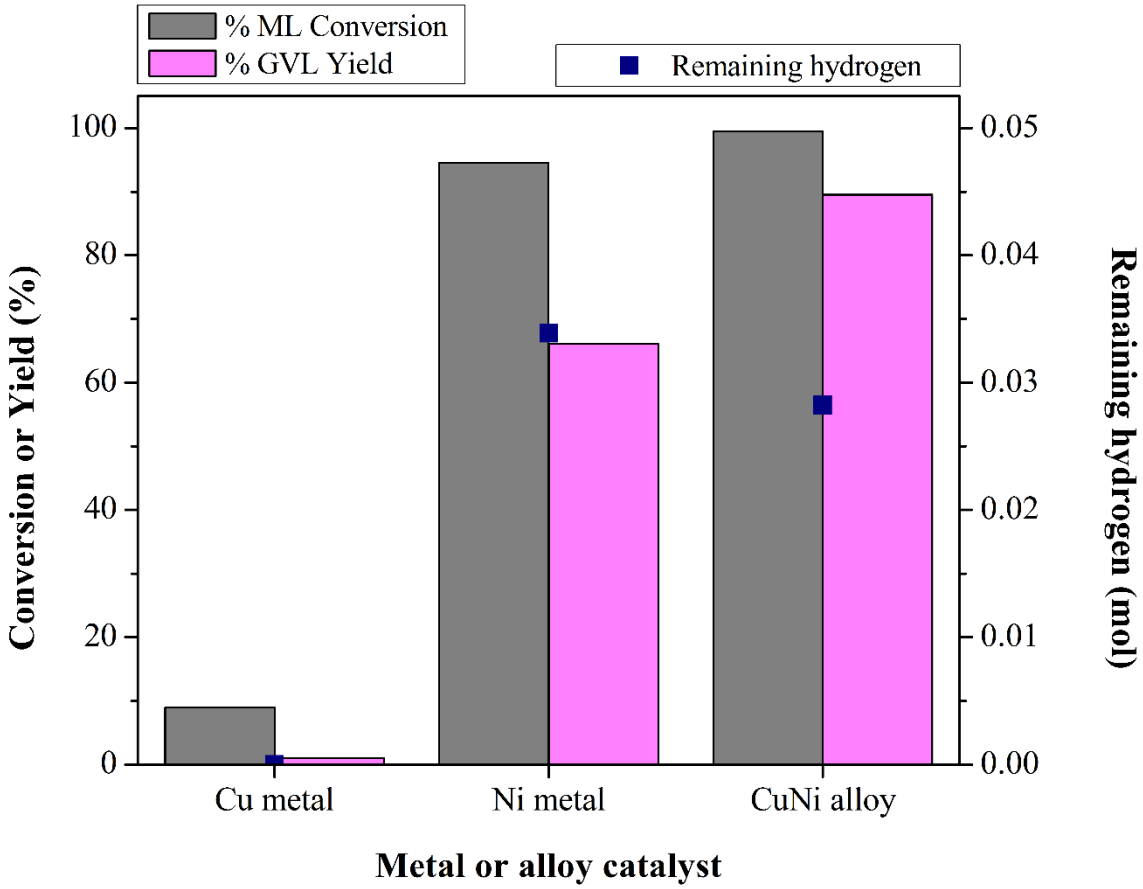

Figure S6. Catalytic performance of Cu metal, Ni metal, and CuNi alloy catalysts

Cu metal, Ni metal, and CuNi alloy, were evaluated at 200 °C for 3 h using 0.2 M ML in 24 ml of 2-PrOH.

Table S1. Surface areas of different catalysts.

Single phase metal oxide	**Surface area (m^2/g)**	**Mixed metal oxides or alloy**	**Surface area (m^2/g)**
CuO	45	CuNiO	9
NiO	7	CuCoO	5
Co_3O_4	13	CuCrO	9
Cr_2O_3	9	CuFeO	6
Fe_2O_3	4	CuNi	undetectable

Table S2. Peak area from H_2-TPR technique

Single phase metal oxide	**Total peak area (a.u.)**	**Mixed metal oxides or alloy**	**Total peak area (a.u.)**

CuO	15,677	CuNiO	11,097
NiO	13,144	CuCoO	17,512
Co_3O_4	20,190	CuCrO	8,008
Cr_2O_3	2,038	CuFeO	14,408
Fe_2O_3	15,684	CuNi	N/A

Hydrogen temperature programmed reduction (H_2–TPR) was carried out to determine reduction behavior of the catalyst (CHEMBET–Pulsar Quantachrome, Germany).

Table S3. Acidity and basicity of catalysts.

Catalysts	**Acidity (μmol/g)**	**Basicity (μmol/g)**	**Acidity/basicity ratio**
CuO	19.2	2.1	9.1
NiO	5.5	3.1	1.8
CuNiO	19.9	11.9	1.7
CuCoO	Undetectable	Undetectable	N/A
CuCrO	1.5	9.1	0.2
CuFeO	6.9	Undetectable	N/A
CuNi	38.5	63.5	0.6

Table S4. Properties of alcohols.

Alcohol	**Purity (%)**	**Boiling point (°C)**	**Density (g/cm^3, at 25 °C)**	**Viscosity Dynamic (cP)**	**Kinematic (cSt)**
EtOH	99.90	78.4	0.79	1.6	2.0
1-PrOH	99.50	97.0	0.80	2.0	2.5
2-PrOH	99.50	82.6	0.79	2.2	2.8
2-BuOH	99.50	99.5	0.81	3.0	3.7
CyOH	99.00	162.0	0.96	57.2	59.6

Brookfield (DV–III Ultra, USA) programmable rheometer was used for analyzing viscosity of solvent at room temperature.

Table S5. Generated water content in 2-PrOH after the reaction at 200 ^{o}C for 3 h of various catalysts.

Sample	Water content (wt. %)
2-PrOH	undetectable
CuNiO	1.1
CuCoO	2.7
CuCrO	3.6
CuFeO	1.6
CuNi	undetectable

A volumetric water by-product content in 2-PrOH was determined using a Karl Fisher titrator (Metrohm 870 KF Titrino plus, Switzerland) at room temperature.

Table S6. Compositions of metals in mixed metal oxide and alloy catalysts.

Catalyst	Element	K_a Intensity (a.u.)	Weight %	Atomic %	Cu/M* molar ratio
CuNiO	Cu	16597.02	52.06	50.09	1.00 ± 0.10
	Ni	15442.70	47.94	49.91	
CuCoO	Cu	13273.22	56.78	55.31	1.24 ± 0.12
	Co	21540.96	43.22	44.69	
CuCrO	Cu	15534.24	56.43	51.45	1.06 ± 0.12
	Cr	15221.31	43.22	48.55	
CuFeO	Cu	12577.12	58.18	55.01	1.22 ± 0.12
	Fe	17955.25	41.82	44.99	
CuNi	Cu	17411.08	52.71	50.74	1.03 ± 0.10
	Ni	15809.33	47.29	49.26	

*M = Ni, Co, Cr, or Fe

Metal compositions of the catalysts were determined using Orbis Micro X-ray Fluorescence (Micro-XRF, USA) Analyzer.

Table S7. Catalytic performance of CuNiO over various feedstocks.

Feedstock	ML conversion (%)	GVL yield (%)
Methyl Levulinate (ML)	98.6	95.8
Ethyl Levulinate (EL)	Negligible	Negligible
Butyl Levulinate (BL)	Negligible	Negligible
Levulinic Acid (LA)	Negligible	Undetectable

Each experiment was conducted at 200 ^{o}C for 3 h using 0.2 M of each feedstock in 24 ml of 2-PrOH.

References (อ้างอิง)

1. M. Hoel and S. Kverndokk, Depletion of fossil fuels and the impacts of global warming, Resour. Energy Econ., 18 (1996) 115-136.

2. J. Hansen, M. Sato, R. Ruedy, A. Lacis and V. Oinas, Global warming in the twenty-first century: An alternative scenario, Proc Natl Acad Sci., 97 (2000) 9875-9880.

3. A. Midilli and I. Dincer, Hydrogen as a renewable and sustainable solution in reducing global fossil fuel consumption, Int. J. Hydrog. Energy, 33 (2008), 4209-4222.

4. A. Zecca and L. Chiari, Fossil-fuel constraints on global warming, Energy Policy, 38 (2010) 1-3.

5. C. McGlade and P. Ekins, The geographical distribution of fossil fuels unused when limiting global warming to 2 °C, Nature, 517 (2015), 187-190.

6. D. M. Alonso, J. Q. Bond and J. A. Dumesic, Catalytic conversion of biomass to biofuels, Green Chem., 12 (2010) 1493-1513.

7. D. M. Alonso, S. G. Wettstein and J. A. Dumesic, Bimetallic catalysts for upgrading of biomass to fuels and chemicals, Chem. Soc. Rev., 41 (2012) 8075-8098.

8. Y. Liu, L. Chen, T. Wang, Q. Zhang, C. Wang, J. Yan and L. Ma, One-Pot Catalytic conversion of raw lignocellulosic biomass into gasoline alkanes and chemicals over $LiTaMoO_6$ and Ru/C in aqueous phosphoric acid, ACS SUSTAIN CHEM ENG, 3 (2015) 1745-1755.

9. D. Ding, J. Xi, J. Wang, X. Liu, G. Lu and Y. Wang, Production of methyl levulinate from cellulose: selectivity and mechanism study, Green Chem., 17 (2015) 4037-4044.

10. M. J. Biddy, R. Davis, D. Humbird, L. Tao, N. Dowe, M. T. Guarnieri, J. G. Linger, E. M. Karp, D. Salvachúa, D. R. Vardon and G. T. Beckham, The techno-economic

basis for coproduct manufacturing To enable hydrocarbon fuel production from lignocellulosic biomass, ACS SUSTAIN CHEM ENG, 4 (2016) 3196-3211.

11. I. T. Horváth, H. Mehdi, V. Fábos, L. Boda and L. T. Mika, γ-Valerolactone—a sustainable liquid for energy and carbon-based chemicals, Green Chem., 10 (2008) 238-242.

12. D. Fegyverneki, L. Orha, G. Láng and I. T. Horváth, Gamma-valerolactone-based solvents, Tetrahedron, 66 (2010) 1078-1081.

13. J. Q. Bond, D. M. Alonso, D. Wang, R. M. West and J. A. Dumesic, Integrated catalytic conversion of γ-valerolactone to liquid alkenes for transportation fuels, Science, 327 (2010) 1110-1114.

14. Y. Zhao, Y. Fu and Q.-X. Guo, Production of aromatic hydrocarbons through catalytic pyrolysis of γ-valerolactone from biomass, Bioresource Technology, 114 (2012) 740-744.

15. J. C. Serrano-Ruiz, D. J. Braden, R. M. West and J. A. Dumesic, Conversion of cellulose to hydrocarbon fuels by progressive removal of oxygen, Appl Catal B., 100 (2010) 184-189.

16. D. M. Alonso, S. G. Wettstein and J. A. Dumesic, Gamma-valerolactone, a sustainable platform molecule derived from lignocellulosic biomass, Green Chem., 15 (2013) 584-595.

17. A. Kumar, Y. E. Jad, J. M. Collins, F. Albericio and B. G. de la Torre, Microwave-assisted green solid-hhase peptide synthesis using γ-valerolactone (GVL) as solvent, ACS SUSTAIN CHEM ENG, 6 (2018) 8034-8039.

18. K. Yan and A. Chen, Efficient hydrogenation of biomass-derived furfural and levulinic acid on the facilely synthesized noble-metal-free Cu–Cr catalyst, Energy, 58 (2013) 357-363.

19. C. Ortiz-Cervantes and J. J. García, Hydrogenation of levulinic acid to γ-valerolactone using ruthenium nanoparticles, Inorganica Chim. Acta, 397 (2013) 124-128.

20. K. Yan and A. Chen, Selective hydrogenation of furfural and levulinic acid to biofuels on the ecofriendly Cu–Fe catalyst, Fuel, 115 (2014) 101-108.

21. I. Obregón, E. Corro, U. Izquierdo, J. Requies and P. L. Arias, Levulinic acid hydrogenolysis on Al_2O_3-based Ni-Cu bimetallic catalysts, CHINESE J CATAL, 35 (2014) 656-662.

22. B. Putrakumar, N. Nagaraju, V. P. Kumar and K. V. R. Chary, Hydrogenation of levulinic acid to γ-valerolactone over copper catalysts supported on γ-Al_2O_3, CATAL TODAY, 250 (2015) 209-217.

23. K. Hengst, M. Schubert, H. W. P. Carvalho, C. Lu, W. Kleist and J.-D. Grunwaldt, Synthesis of γ-valerolactone by hydrogenation of levulinic acid over supported nickel catalysts, Appl Catal A., 502 (2015) 18-26.

24. X. Long, P. Sun, Z. Li, R. Lang, C. Xia and F. Li, Magnetic Co/Al_2O_3 catalyst derived from hydrotalcite for hydrogenation of levulinic acid to γ-valerolactone, CHINESE J CATAL, 36 (2015) 1512-1518.

25. J. Fu, D. Sheng and X. Lu, Hydrogenation of levulinic acid over nickel catalysts supported on aluminum oxide to prepare γ-valerolactone, Catalysts, 6 (2016) 1-10.

26. E. I. Gürbüz, D. M. Alonso, J. Q. Bond and J. A. Dumesic, Reactive extraction of levulinate esters and conversion to γ-valerolactone for production of liquid fuels, ChemSusChem, 4 (2011) 357-361.

27. H. Zhou, J. Song, H. Fan, B. Zhang, Y. Yang, J. Hu, Q. Zhu and B. Han, Cobalt catalysts: very efficient for hydrogenation of biomass-derived ethyl levulinate to gamma-valerolactone under mild conditions, Green Chem., 16 (2014) 3870-3875.

28. Z. Yang, Y.-B. Huang, Q.-X. Guo and Y. Fu, RANEY®Ni catalyzed transfer hydrogenation of levulinate esters to γ-valerolactone at room temperature, ChemComm, 49 (2013) 5328-5330.

29. J. Geboers, X. Wang, A. B. de Carvalho and R. Rinaldi, Densification of biorefinery schemes by H-transfer with Raney Ni and 2-propanol: A case study of a potential avenue for valorization of alkyl levulinates to alkyl γ-hydroxypentanoates and γ-valerolactone, J. Mol. Catal. A: Chem., 388-389 (2014) 106-115.

30. H. Y. Luo, D. F. Consoli, W. R. Gunther and Y. Román-Leshkov, Investigation of the reaction kinetics of isolated Lewis acid sites in Beta zeolites for the Meerwein–Ponndorf–Verley reduction of methyl levulinate to γ-valerolactone, J. Catal., 320 (2014) 198-207.

31. J. He, H. Li, Y.-M. Lu, Y.-X. Liu, Z.-B. Wu, D.-Y. Hu and S. Yang, Cascade catalytic transfer hydrogenation–cyclization of ethyl levulinate to γ-valerolactone with Al–Zr mixed oxides, Appl Catal A., 510 (2016) 11-19.

32. B. Cai, X.-C. Zhou, Y.-C. Miao, J.-Y. Luo, H. Pan and Y.-B. Huang, Enhanced catalytic transfer hydrogenation of ethyl levulinate to γ-valerolactone over a robust Cu–Ni bimetallic catalyst, ACS SUSTAIN CHEM ENG, 5 (2017) 1322-1331.

33. C. Termvidchakorn, K. Faungnawakij, S. Kuboon, T. Butburee, N. Sano and T. Charinpanitkul, A novel catalyst of Ni hybridized with single-walled carbon nanohorns for converting methyl levulinate to γ-valerolactone, Appl. Surf. Sci., 474 (2019) 161-168.
34. Z. Lin, X. Cai, Y. Fu, W. Zhu and F. Zhang, Cascade catalytic hydrogenation–cyclization of methyl levulinate to form γ-valerolactone over Ru nanoparticles supported on a sulfonic acidfunctionalized UiO-66 catalyst, RSC Adv., 7 (2017) 44082–44088.
35. X. Cao, J. Wei, H. Liu, X. Lv, X. Tang, X. Zeng, Y. Sun, T. Lei, S. Liue and L. Lin, Hydrogenation of methyl levulinate to γ-valerolactone over Cu—Mgoxide using MeOH as in situ hydrogen source, J Chem Technol Biotechnol, 94 (2019) 167–177.
36. W. Ouyang, D. Zhao, Y. Wang, A. M. Balu, C. Len, and R. Luque, Continuous flow conversion of biomass-derived methyl levulinate into γ-valerolactone using functional metal organic frameworks, ACS Sustainable Chem. Eng., 6 (2018) 6746−6752.
37. M. J. Gilkey and B. Xu, Heterogeneous Catalytic transfer hydrogenation as an effective pathway in biomass upgrading, ACS Catal., 6 (2016) 1420-1436.
38. J. Ashok, M. Subrahmanyam and A. Venugopal, Hydrotalcite structure derived Ni–Cu–Al catalysts for the production of H_2 by CH_4 decomposition, Int. J. Hydrogen Energy, (33) 2008 2704-2713.
39. X. Tang, B. Zhang, Y. Li, Y. Xu, Q. Xin and W. Shen, CuO/CeO_2 catalysts: redox features and catalytic behaviors, Appl Catal A., 288 (2005) 116-125.
40. J. Sá, Y. Kayser, C. J. Milne, D. L. Abreu Fernandes and J. Szlachetko, Temperature-programmed reduction of NiO nanoparticles followed by time-resolved RIXS, PCCP, 16 (2014) 7692-7696.
41. H. Zhu, H. Dong, P. Laveille, Y. Saih, V. Caps and J.-M. Basset, Metal oxides modified NiO catalysts for oxidative dehydrogenation of ethane to ethylene, CATAL TODAY, 228 (2014) 58-64.
42. O. O. James AND S. Maity, Temperature programme reduction (TPR) studies of cobalt phases in γ-alumina supported cobalt catalysts, J. Pet. Technol. Altern. Fuels, 7 (2016) 1-12.
43. M. A. Valenzuela, P. Bosch, J. Jiménez-Becerrill, O. Quiroz and A. I. Páez, Preparation, characterization and photocatalytic activity of ZnO, Fe_2O_3 and $ZnFe_2O_4$, Photochem. Photobiol. A., 148 (2002) 177-182.
44. M. Liang, W. Kang and K. Xie, Comparison of reduction behavior of Fe_2O_3, ZnO and $ZnFe_2O_4$ by TPR technique, J. Nat. Gas Chem., 18 (2009) 110-113.
45. A. P. Amrute, C. Mondelli and J. Pérez-Ramírez, Kinetic aspects and deactivation behaviour of chromia-based catalysts in hydrogen chloride oxidation, Catal. Sci.

Technol., 2 (2012) 2057-2065.

46. G. Bai, H. Dai, Y. Liu, K. Ji, X. Li and S. Xie, Preparation and catalytic performance of cylinder- and cake-like Cr_2O_3 for toluene combustion, Catal Commun., 36 (2013) 43-47.

47. B. Wang, S. Liu, Z. Hu, Z. Li and X. Ma, Active phase of highly active Co3O4 catalyst for synthetic natural gas production, RSC Adv., 4 (2014) 57185-57191.

48. M. Chia and J. A. Dumesic, Liquid-phase catalytic transfer hydrogenation and cyclization of levulinic acid and its esters to γ-valerolactone over metal oxide catalysts, Chem. Commun., 47 (2011) 12233-12235.

49. A. E.-A. A. Said, M. M. M. Abd El-Wahab and M. N. Goda, Selective synthesis of acetone from isopropyl alcohol over active and stable CuO–NiO nanocomposites at relatively low-temperatureEgypt. j. basic appl. sci., 3 (2016) 357-365.

50. S. Song, S. Yao, J. Cao, L. Di, G. Wu, N. Guan and L. Li, Heterostructured Ni/NiO composite as a robust catalyst for the hydrogenation of levulinic acid to γ-valerolactone, Appl Catal B.: Environmental, 217 (2017) 115-124.

51. W. Tanwongwal, S. Kuboon, W. Kraithong and A. Eiad-Ua, Production of γ-Valerolactone from Methyl Levulinate via Catalytic Transfer Hydrogenation on Nickel-Copper Oxide Catalyst, Mater. Sci., 872 (2016) 187-190.

52. D. Kulkarni and I. E. Wachs, Isopropanol oxidation by pure metal oxide catalysts: number of active surface sites and turnover frequencies, Appl Catal A., 237 (2002) 121-137.

53. J. T. Richardson, R. Scates and M. V. Twigg, X-ray diffraction study of nickel oxide reduction by hydrogen, Appl Catal A., 246 (2003) 137-150.

54. X. Tang, Z. Li, X. Peng, Y. Jiang, S. Liu, T. Lei, Y. Sun, and L. Lin, In situ catalytic hydrogenation of biomass-derived methyl evulinate to γ-valerolactone in methanol, ChemSusChem, 8 (2015) 1601-1607.

Keywords (คำหลัก) : catalytic transfer hydrogenation; simultaneously activated catalysts; Cu-based metal oxides; methyl levulinate; gamma-valerolactone

Output จากโครงการวิจัยที่ได้รับทุนจาก สกว.

1. ผลงานตีพิมพ์ในวารสารวิชาการนานาชาติ (Termvidchakorn C, Faungnawakij K, Kuboon S, Butburee T, Sano N, Charinpanitkul T. A novel catalyst of Ni hybridized with single-walled carbon nanohorns for converting methyl levulinate to γ-valerolactone. Applied Surface Science. 2019; 474: 161-168
2. ผลงานตีพิมพ์ Book Chapter ทางวิชาการนานาชาติ (Kuboon S, Kraithong W, Damaurai J, Faungnawakij K. Hydro-fractionation for biomass upgrading in renewable resources and biorefineries. London: IntechOpen United Kingdom; 2018; 5: 69-84)
3. ผลงานที่อยู่ในระหว่างการพิจารณาเพื่อตีพิมพ์ในวารสารนานาชาติ (Major Revision) (Tanwongwan W, Eiad–ua A, Kraithong W, Virya–empikul N, Khomson K, Klamchuen A, Kasamechonchunga P, Khemthong P, Faungnawakij K, and Kuboon S. Simultaneous activation of copper mixed metal oxide catalysts in alcohols for gamma-valerolactone production from methyl levulinate, Applied Catalysis A: General. 2019)

Accepted Manuscript

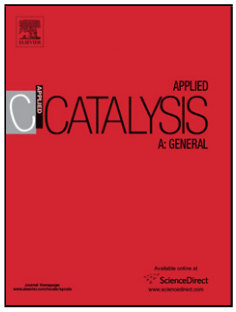

Title: Simultaneous activation of copper mixed metal oxide catalysts in alcohols for gamma-valerolactone production from methyl levulinate

Authors: Worapak Tanwongwan, Apiluck Eiad-ua, Wasawat Kraithong, Nawin Viriya-empikul, Khomson Suttisintong, Annop Klamchuen, Panita Kasamechonchung, Pongtanawat Khemthong, Kajornsak Faungnawakij, Sanchai Kuboon

PII: S0926-860X(19)30163-2
DOI: https://doi.org/10.1016/j.apcata.2019.04.011
Reference: APCATA 17043

To appear in: *Applied Catalysis A: General*

Received date: 8 February 2019
Revised date: 25 March 2019
Accepted date: 10 April 2019

Please cite this article as: Tanwongwan W, Eiad-ua A, Kraithong W, Viriya-empikul N, Suttisintong K, Klamchuen A, Kasamechonchung P, Khemthong P, Faungnawakij K, Kuboon S, Simultaneous activation of copper mixed metal oxide catalysts in alcohols for gamma-valerolactone production from methyl levulinate, *Applied Catalysis A, General* (2019), https://doi.org/10.1016/j.apcata.2019.04.011

Simultaneous activation of copper mixed metal oxide catalysts in alcohols for gamma-valerolactone production from methyl levulinate

Worapak Tanwongwan[b], Apiluck Eiad–ua[b], Wasawat Kraithong[a], Nawin Viriya–empikul[a], Khomson Suttisintong[a], Annop Klamchuen[a], Panita Kasamechonchung[a], Pongtanawat Khemthong[a], Kajornsak Faungnawakij[a], and Sanchai Kuboon*[a]

[a]National Nanotechnology Center, National Science and Technology Development Agency, 111 Phahonyothin Rd., Khlong Luang, Pathum Thani 12120, Thailand.

[b]College of Nanotechnology, King Mongkut's Institute of Technology Ladkrabang (KMITL), 1 Chalongkrung Rd., Ladkrabang, Bangkok 10520, Thailand.

**To whom correspondence should be addressed:*

E-mail: sanchai@nanotec.or.th (S. Kuboon).

Graphical abstract

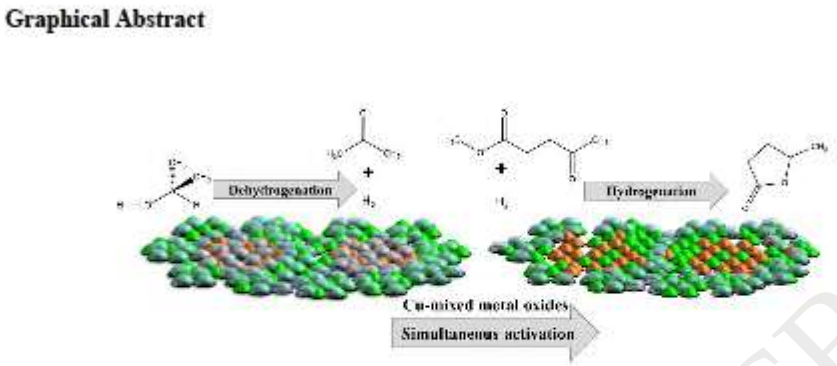

Highlights

- The formation of Cu-mixed metal oxides enhances reducibility and acid-base properties of the catalysts.
- Highly active and selective simultaneously activated dual-function catalysts, Cu- mixed metal oxides were successfully employed for GVL production.
- The catalysis concept over simultaneously activated catalysts discovered in this work could advance the catalytic transfer hydrogenation.

Abstract:

Catalytic transfer hydrogenation (CTH) of biomass-derivatives to value-added chemicals using metal-based catalysts is a promising process in biorefinery since it does not require high pressure of expensive and flammable hydrogen gas (H_2). However, an activation of these catalysts using H_2 treatment prior to the CTH process limits this advantage. Here, copper mixed metal oxides are introduced as simultaneously activated catalysts (SACs) in the presence of alcohol for a production of gamma-valerolactone (GVL) from methyl levulinate (ML) without requirement of additional H_2 gas during both catalyst pretreatment and hydrogenation steps. Different alcohols were selected to function as hydrogen sources for both catalyst activation and ML hydrogenation. All copper mixed metal oxides, especially CuNiO showed significant potential as catalysts for ML conversion to GVL at 200 ^{o}C within 3 h. While 2-propanol and 2-butanol exhibited effective roles as hydrogen sources for simultaneous reductions of the catalysts to generate metal active sites and provided hydrogen species for

hydrogenation of ML to GVL. Hydrogen temperature programmed reduction (H_2-TPR), alcohol-assisted simultaneous reaction (ASR), in situ X-ray diffraction (in situ XRD) and X-ray photoelectron spectroscopy (XPS) revealed that the complementary cooperation between secondary alcohols and catalysts is the important key for the high GVL production in this work.

Keywords: *Catalytic transfer hydrogenation; Simultaneously activated catalysts; Cu-based mixed oxides; Methyl levulinate; Gamma-valerolactone.*

1. Introduction

The consumption of fossil fuel keeps increasing with some concern of how long it would last as well as its impact on global warming.[1-5] Various renewable resources including agricultural lignocellulosic biomass becomes increasingly recognized as a valuable feedstock for biofuel and biochemical production due to its abundance and renewability.[6-10] Gamma-valerolactone (GVL), a biomass-derived chemical is a non-toxic and versatile organic compound which could be employed as a starting material or a solvent in energy and polymer industries.[11-17] Generally, GVL is produced via hydrogenation of levulinic acid (LA) or its esters.[18-33] Good number of reports have demonstrated great potential of LA as a starting material for GVL production**.** For examples, Cervantes and García showed that GVL could be produced from LA successfully after 24 h using Ru nanoparticle catalyst at 130 ^oC[19]**.** Yan and Chen found that Cu-Fe showed good activity on GVL production from LA at 200 ^oC for 10 h.[20] Moreover, a high GVL yield obtained from LA conversion over Ni–Cu/Al_2O_3 catalyst

at 250 °C after 6 h was also reported by Obregón et al.[21] However, due to the fact that levulinic acid could not be separated easily from its acid matrix that used in an extraction process from biomass feedstock, its esters were then becoming more suitable choices for GVL production.[9,27] In addition, methyl levulinate has been suggested as one of the most suitable esters for GVL production over metal catalysts.[34-36] Conventionally, H_2 gas is used directly as a hydrogen source for hydrogenation of LA or its esters which is not favorable considering its risk of explosion from exothermic heat under high reaction pressures.[18,20,21] Catalytic transfer hydrogenation (CTH), on the other hand, is more preferable because of its endothermic nature and its low reaction pressure caused by a replacement of hydrogen gas with organic compounds which could promote superior product selectivity.[28,29,31-33,35-37] Particularly, effective catalysts play the most important role in CTH for accelerating conversion of feedstock and controlling high product yield. In general, Ru-based materials were reported as efficient noble metal catalysts for conversion of LA or its esters to GVL.[19,26] Non-noble metal-based catalysts including nickel, cobalt, copper, chromium, iron or their alloys have also been reported as alternative catalysts for hydrogenation of LA or its esters to GVL as well as other related reactions.[18,20-25,27-29,31,32,50] Among many works reported recently, Song et al. demonstrated an effective Ni/NiO composite catalyst for GVL production from LA. They found that the metal/oxide active sites is the key for its high activity.[50] Another work by Ashok et al**.** suggested that a suitable loading of CuO promoted a hydrogen spillover effect which could decrease NiO reduction temperature to metallic nickel.[38] Furthermore, our previous report on methyl levulinate (ML) conversion over Ni-Cu-O catalyst indicated that the nickel and copper mixed metal oxides could be employed as catalysts for GVL production.[51] Additionally, Said et al.

had reported that CuO–NiO nanocomposites were effective catalysts for 2-propanol dehydrogenation due to enhancement of electrical conductivity and basicity.[49] This good agreement from the previous reports of copper mixed oxides or composites on their promising catalytic performance in both hydrogenation and dehydrogenation reactions is advantageous for the catalyst design in CTH.

The purpose of this work is; therefore, to integrate the hydrogen spillover effect of CuO with various alcohols as reducing agents for activation of copper mixed metal oxide catalysts and to propose their reaction mechanism for GVL production. A systematic study of catalyst reduction behaviors using Hydrogen temperature programmed reduction (H_2-TPR), alcohol-assisted simultaneous reaction (ASR), *in situ* X-ray diffraction (*in situ* XRD) reduction, and X-ray photoelectron spectroscopy (XPS) were combined with the catalytic performance of GVL production. The obtained knowledge from this work could lead us to a new catalysis concept of simultaneously activated catalysts (SACs) for advanced catalytic transfer hydrogenation (CTH).

2. Experimental

2.1 Catalyst preparation. All metal nitrate salts were purchased from Ajax Finchem Pty Ltd**.** with minimum purity of 98**%.** Metal oxide and their Cu–based mixed metal oxides were simply prepared by thermal decomposition of metal nitrate salts**.** For metal oxide preparation, a chosen nitrate salt of 0**.**042 mole of each metal was dissolved in 10 ml of DI water**.** While a mixture of 0**.**021**:**0**.**021 mole ratio of $Cu(NO_3)_2{\cdot}3H_2O$ and one of the other metal (Ni, Co, Cr, or Fe) nitrate was selected for Cu–base mixed metal oxide preparation**.** After dissolution of metal salts in DI water, the sample was dried

and calcined at 800 ^{o}C for 5 h in air and collected after cooling down at room temperature.

2.2 Catalysts Characterization. Powder X–ray diffraction (XRD) patterns of samples from both conventional and *in situ* experiments were analyzed by an X–ray diffractometer (D8 ADVANCE, Bruker, Ltd., Germany) using Cu K_{α} radiation at 40 kV and 40 mA over the 2θ range of $10 < 2\theta < 80$ degree. For the *in situ* experiment, the sample was heated with a heating rate of 12 ^{o}C /min under hydrogen atmosphere (99.99%) at the flow rate of 20 ml/min from room temperature to 600 ^{o}C on a Rh–Pt alloy substrate. Hydrogen temperature programmed reduction (H_2-TPR) was carried out using CHEMBET–Pulsar Quantachrome Instruments (Germany) equipped with a thermal conductivity detector (TCD). The catalyst (20 mg) was reduced in 5 vol% H_2 in argon at a flow rate of 30 ml/min with a heating rate of 10 ^{o}C /min from room temperature to 800 ^{o}C. X-ray photoelectron spectroscopy (XPS) was conducted using PHI 5000 Versaprobe II (ULVAC-PHI, Inc., Japan). The obtained data was fitted and interpreted using XPSPEAK4.1 program.

2.3 Evaluation of catalytic properties. All catalytic transfer hydrogenation reactions were carried out in a 130 ml stainless steel autoclave with a magnetic stirrer (500 rpm). 0.58 ml of methyl levulinate (ML), 24 ml of alcohol, and 1 g of a metal oxide or mixed metal oxide catalyst were loaded in an autoclave and heated up to 200 ^{o}C with heating

rate of 5 ºC /min. A liquid sample analyzed by gas chromatograph using a flame ionization detector or GC-FID (GC–2010, Shimadzu, Japan) and a mass spectrometry detector or GC-MS (GCMS–QP2020, Shimadzu, Japan), and a capillary column (DB–WAX, Agilent technologies, USA) with 30 m in length, 0.25 mm inner diameter, and 0.25 µm film thickness). The methyl levulinate conversion and the GVL product yield were calculated using the following equations:

$$Conversion\ (\%) = \left(\frac{mole\ of\ consumed\ ML}{mole\ of\ ininitial\ ML}\right) \times 100 \qquad (1)$$

$$Yield\ (\%) = \left(\frac{mole\ of\ produced\ GVL}{theoretical\ mole\ of\ GVL}\right) \times 100 \qquad (2)$$

The numbers of mole of ML and GVL were obtained from the peak area analysis using GC–FID while other by–products were detected by GC–MS. Hydrogen content remaining in the reaction was calculated according to the ideal gas law. In brief, the final pressure was recorded after the reactor was cooled down to room temperature. The value of remaining pressure in atm was then subjected to equation (3).

$$n = \frac{\mathrm{PV}}{RT} \qquad (3)$$

where V = 0.1 L (actual volume of the reactor), R = 0.08206 L.atm/(mol.K) and T = 298.15 K.

The gas was later analyzed using micro-GC for acquiring purity of hydrogen (CP 4900, Agilent Technologies, USA) and multiplied with the calculated total mole number of remaining gas.

3. Results and discussion

3.1 Catalytic performance. Single phase metal oxides and mixed metal oxides catalysts were compared for GVL production from ML. Initially, five single phase metal oxides including CuO, NiO, Co_3O_4, Cr_2O_3, and Fe_2O_3 were tested as catalysts for production of gamma–valerolactone (GVL) from methyl levulinate (ML) by catalytic transfer hydrogenation (CTH) in a 2–propanol (2-PrOH) system. Their crystal structure information can be found in Fig. S2 and their surface area was shown in Table S1. Catalytic evaluation results of these metal oxides showed neither catalytic behavior toward 2-propanol dehydrogenation nor GVL production at 200 ^oC during the reaction period of 3 h. These results were supported by unchanged reaction pressures caused by 2-propanol evaporation and undetectable or negligible hydrogen gas, acetone, methanol, or GVL throughout the course of the reactions. Consecutively, the four Cu–based mixed oxides were employed as catalysts giving catalytic results provided in Fig. 1a. CuNiO showed high catalytic property which was in good agreement with our previous report[51]. The order of catalytic performance in terms of ML conversion and GVL yield is as follows; CuNiO > CuCoO > CuCrO > CuFeO. The superior catalytic properties of CuNiO and CuCoO catalysts are in accordance with those nickel and cobalt catalysts reported in other studies, namely Raney-nickel[28,29], Ni/Al_2O_3[23,25], and Co-based catalysts.[24,27] The formation of H_2 was labelled as amount of remaining hydrogen in Fig. 1a. For the CuNiO catalyst, it was quite obvious that both 2-PrOH dehydrogenation and ML hydrogenation could take place effectively. CuCoO and CuCrO also showed similar behavior to CuNiO but with less catalytic activity. On the other hand, CuFeO did not show high ML conversion but gave almost the same amount of remaining H_2 as that of CuNiO. This indicated that CuFeO catalyst tended to be an active catalyst for 2-PrOH dehydrogenation but was not effective for ML hydrogenation. XRD patterns of the catalysts before and after the reaction were also shown in Fig. 1b and c. It could be seen that CuO was completely reduced to Cu metal while NiO was partially reduced to Ni metal after the reaction. As it was reported by Song et al. on their study in GVL production from LA using Ni/NiO composite catalyst. They found that the reactant was

more likely to adsorb on the NiO sites while the H_2 molecules preferred to stay on the Ni metallic sites. Therefore, the presence of Ni/NiO structure could enhance the catalytic perfamance.[50] In this work, although ML was used as a reactant instead of LA, the Ni/NiO phase with the presence of Cu metal could provide efficient GVL production. The XRD pattern of CuCoO showed complete reduction of both CuO to metallic Cu and Co_3O_4 to metallic Co, respectively. The conversion of ML over this catalyst was around 80%. Zhou et al. had used metallic Co, Ni, and Fe for conversion of ethyl levulinate (EL) to GVL. They found that metallic cobalt was the most active catalyst for GVL production.[27] The CuCrO catalyst showed moderate catalytic activity for both 2-PrOH dehydrogenation and ML conversion. According to the study of Yan and Chen, they found that Cu-Cr catalyst with the 1:2 ratio of Cu^{2+}/Cr^{3+} was an active catalyst for the conventional hydrogenation of LA to GVL using H_2 gas of 70 bar at 200 ^oC for 10 h.[18] They suggested that Cu^{2+} had an important role for H_2 dissociation where the Cu^{2+}/Cr^{3+} ratio significantly influenced the effectiveness of hydrogenation. In this work only 1:1 ratio of Cu^{2+}/Cr^{3+} was employed under the reaction pressure below 40 bar (generated from the 2-PrOH and its produced H_2) only for 3 h. It might be the unsuitable Cu^{2+}/Cr^{3+} ratio, lower reaction pressure and shorter reaction time that was responsible for its lower activity. The XRD pattern after reaction of CuCrO catalyst represented in Fig. 1c showed 2 phases of Cu metal and $CuCr_2O_4$ which was different from the spent Cu-Cr catalyst reported by Yan and Chen. The higher catalyst reduction temperature used in their work and the low reduction temperature in this work could lead to the phase difference. CuFeO catalyst did not show high activity towards GVL production but provided large amount of hydrogen gas. Yan and Chen also studied the Cu-Fe catalyst for GVL production from LA which indicated that the optimum Cu^{2+}/Fe^{3+} ratio was 1:1 under H_2 pressure of 70 bar at 200 ^oC for 10 h. Although the Cu^{2+}/Fe^{3+} ratio from this work and their work were similar but the lower reaction pressure and shorter reaction time in this work could result in its lower catalytic activity. In addition, the Cu-Fe and CuFeO catalysts after reaction showed different phases. The spent Cu-Fe had

two phases of $CuFe_2O_4$ and $CuFeO_2$ while the spent CuFeO contained Cu metal and Fe_3O_4 phases. Hence, the synergy of various oxidation states (Cu^0, Fe^{2+}, Fe^{3+} and O^{2-}) in Cu and F_3O_4 system during the dehydrogenation process should be responsible for its good H_2 production. Additionally, substrates for GVL production, besides methyl levulinate were expanded to levulinic acid, ethyl levulinate, and butyl levulinate over the NiCuO catalyst. The results shown in Table S7 suggested that conversion of other feedstocks or GVL product could barely be detected after 3 h of the reaction at 200 ^oC. This indicated that the NiCuO catalyst is highly selective toward methyl levulinate substrate.

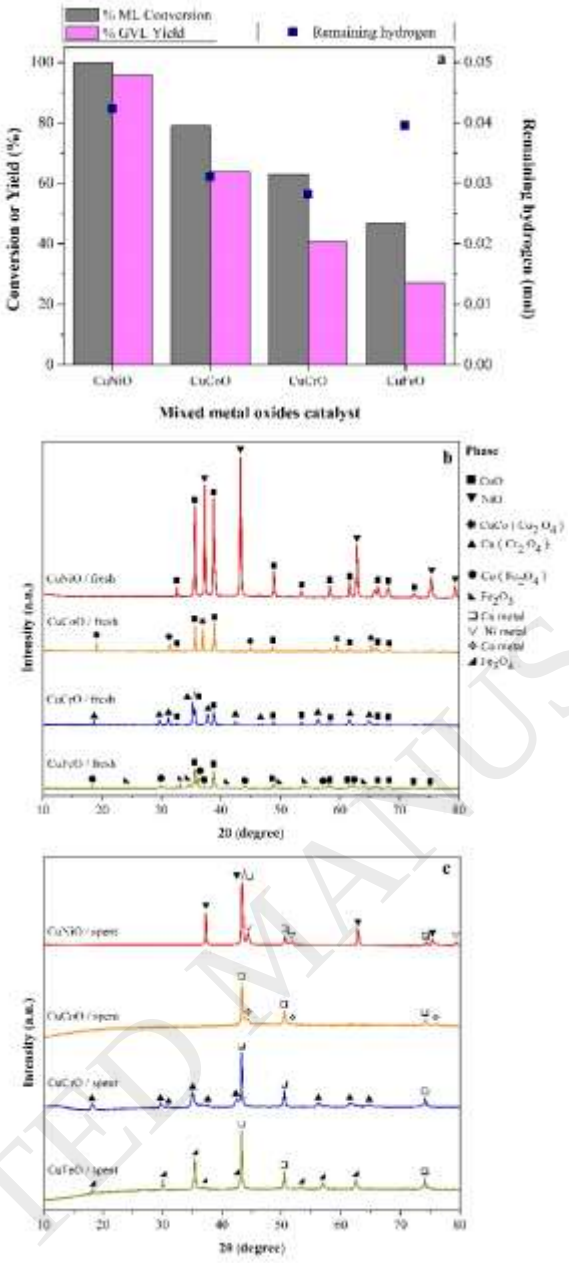

Fig. 1 (a) Catalytic performance in terms of ML conversion, GVL yield, and hydrogen production of copper mixed oxide catalysts at 200 ºC for 3 h using 0.2 M ML in 24 ml of 2-PrOH, (b) XRD patterns of (a) fresh catalysts and (c) spent catalysts.

3.2 Hydrogen temperature programmed reduction (H_2-TPR). To further elucidate the reduction behaviors associated with the catalytic performance of the Cu–based mixed oxide catalysts and their host metal oxides, the hydrogen temperature

programmed reduction (H_2–TPR) was conducted and the results were shown in Fig. 2., where their peak areas were displayed in Table S2.CuO catalyst showed a large bell peak at 439 ºC representing a complete reduction from Cu^{2+} to Cu^0 showing a good agreement with that reported by Tang et al.[39] NiO catalyst showed a major reduction peak at 500 ºC suggesting a reduction of Ni^{2+} to Ni^0 as reported by Sá et al.[40] and Zhu et al.[41] In addition, an appearance of a low intensity flat curve at around 620 ºC could be related to a difficultly reduced species of high crystalline NiO (Fig. S2). Co_3O_4 catalyst showed only one broadly asymmetric reduction peak at 514 ºC which was similar to that reported by James and Maity.[42] Fe_2O_3 catalyst was reduced at two different temperatures of 506 and 665 ºC, in accordance with studies by Valenzuela et al.[43] and Liang et al.[44] In contrast, there was a small peak observed at around 380 ºC in Cr_2O_3 catalyst. This result was different from Cr_2O_3 reduction behavior reported by Amrute et al.[45] and Bai et al.[46] They mentioned that the reduction process of Cr_2O_3 underwent two steps including Cr^{6+} to Cr^{3+} at lower temperature and Cr^{3+} to Cr^{2+} at higher temperature. Hence, a very small reduction peak found in this work of the Cr_2O_3 catalyst could be attributed to the reduction of small portion of Cr^{6+} presented in Cr_2O_3 to Cr^{3+}. Moreover, it was clear that all five single phase metal oxides catalysts prepared in this work showed smaller degree of reduction or appeared at higher reduction temperature compared to the similar metal oxides synthesized at lower calcination temperatures in other reports. The inferior reduction behavior of all metal oxides which resulted in a lack of their active metallic sites lead to their poor catalytic performance towards GVL production. Further investigation in the H_2-TPR study of the copper mixed oxide catalysts indicated that each catalyst had at least two reduction peaks as shown in Fig. 2b. The CuNiO catalyst showed two main reduction peaks at 408 and 440 ºC with a very broadly flat curve at around 700 ºC. As it could be observed in the corresponding XRD pattern (Fig. 1b), two phases of CuO and NiO were presented in the CuNiO catalyst.

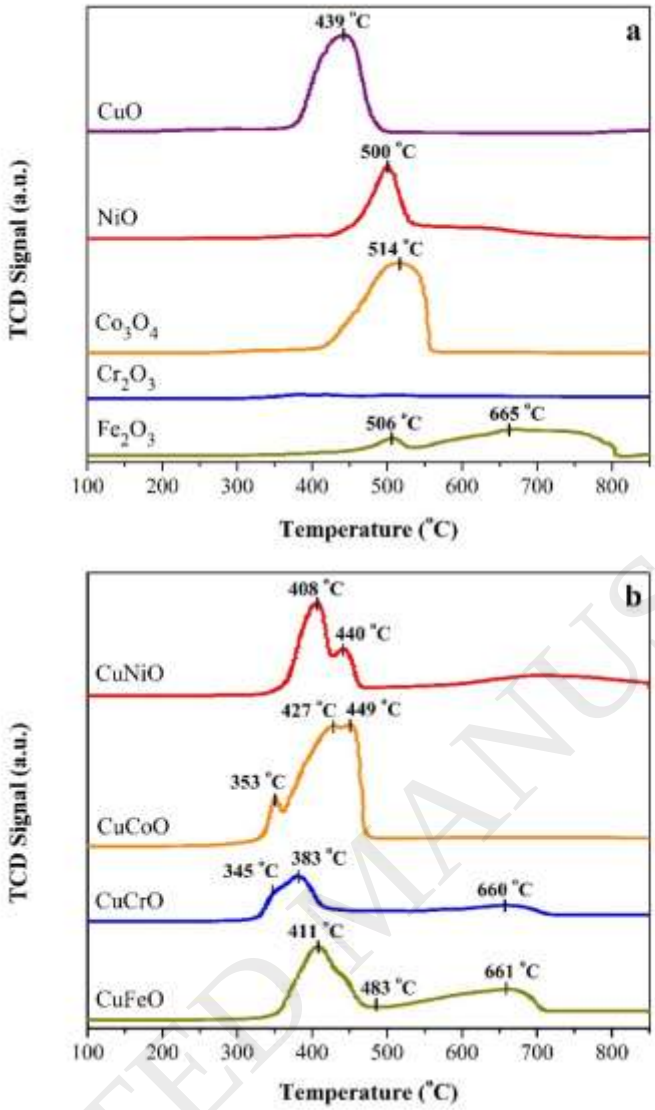

Fig. 2 H_2-TPR profiles of (a) single phase metal oxide (b) mixed metal oxides catalysts.

The first reduction peak belonged to the reduction of CuO to metallic copper (Cu^0) while the second peak was assigned to the reduction of NiO to metallic nickel (Ni^0). CuCoO showed three reduction peaks at 353, 427, and 449 ^oC**.** Based on the XRD pattern of CuCoO catalyst shown in Fig. 1b, this catalyst had two major phases of CuO and CuCo(Co_2O_4) spinel. Therefore, the first small peak at the lowest temperature should be assigned to the easily reduced CuO phase while the peak at 427 ^oC should

correspond to the reduction of Cu^{2+} to Cu^0 and Co^{3+} to Co^{2+} in the spinel structure. The highest reduction peak at 449 ^oC belonged to the reduction of Co^{2+} to metallic Co.[47] Interestingly, XRD pattern of CuCrO showed two different phases of CuO and $Cu(Cr_2O_4)$ spinel without the presence of Cr_2O_3 phase. This meant that the formation of copper oxide and chromium oxide could alter the oxidation states of chromium. In addition, TPR profile of CuCrO displayed two overlapped peaks at 345 and 383 ^oC as well as another broad peak at 660 ^oC**.** The first peak at 345 ^oC was attributed to the reduction of Cu^{2+} in CuO to Cu^0. The second peak at 383 ^oC was a reduction of Cu^{2+} in the $Cu(Cr_2O_4)$ spinel to Cu^0 and the last peak at 660 ^oC was attributed to the reduction of Cr^{3+} in $Cu(Cr_2O_4)$ spinel to Cr^{2+}. Lastly, CuFeO also showed three reduction peaks at 411, 483, and 661 ^oC while its XRD pattern in Fig. 1b showed three phases of CuO, $Cu(Fe_2O_4)$ and Fe_2O_3. The first peak at 411 ^oC indicated the reduction of Cu^{2+} in CuO to Cu^0. A shoulder appeared at around 450 ^oC could be assigned to the reduction of Fe^{3+} in Fe_2O_3 to Fe^{2+} in a spinel Fe_3O_4. A very small peak shown at 483 ^oC could represent the reduction of Cu^{2+} in $Cu(Fe_2O_4)$. Finally, the broad asymmetric peak at 661 ^oC could both be attributed to the partial reduction of Fe^{3+} in $Cu(Fe_2O_4)$ to Fe^{2+} in $(CuFe)(Fe_2O_4)$ spinel and the complete reduction from Fe^{3+} in both rhombohedral and spinel structures to FeO and/or Fe^0. In brief, the CuNiO was composed of two separated phases of CuO and NiO; however, the reduction temperature of both CuO and NiO were lower than their host metal oxides. On the other hand, the addition of copper oxide to the cobalt oxide (CuCoO) created the new phase of $CuCo(Co_2O_4)$ spinel structure while maintaining the CuO phase but without the presence of pure the Co_3O_4 phase. The reduction profile of CuCoO indicated that CuO could be reduced at low temperature. The formation of copper oxide and chromium oxide created the more reducible phase of $Cu(Cr_2O_4)$. Finally, the formation of copper and iron mixed metal oxides (CuFeO) could create the new $CuFe_2O_4$ phase but still maintained their host metal oxides of CuO and Fe_2O_3. All reductions of Cu^{2+} and Fe^{3+} were shifted to lower temperatures. In all cases, the reducibility of metal ions were improved after the mixed oxide formation

with copper oxide. The alteration of catalyst redox behaviors was strongly related to the enhanced catalytic performance.

3.3 Alcohols-assisted simultaneous reaction evaluation (ASR). With the consistent results among XRD, H_2-TPR, and catalytic performance evaluation, it could be confirmed that the CuNiO was the most effective catalyst for GVL production from ML. Subsequently, various alcohols including aliphatic primary alcohols (ethanol, EtOH and 1-propanol, 1-PrOH), aliphatic secondary alcohols (2-propanol, 2-PrOH and 2-butanol, 2-BuOH), and a cyclic secondary alcohol (cyclohexanol, CyOH) were selected for catalytic testing to verify effect of alcohol types on GVL production over the CuNiO catalyst. Catalytic results presented in Fig**.** 3a showed that the secondary alcohols were more suitable than primary alcohols in this reaction. EtOH and 1–PrOH gave about 30**%** of ML conversion and less than 10**%** of GVL yield**.** Formation of a stronger bond between the catalyst active sites and alkoxide species generated from the primary alcohol compared to that of the secondary alcohol could support the ineffectiveness of the primary alcohols.[30] On the other hand, the aliphatic secondary alcohols (2-PrOH and 2-BuOH) showed drastically better catalytic activity than the cyclic secondary alcohol (CyOH)**.** This was due to a high adsorption tendency of CyOH over the catalyst surface.[30] In addition, its high viscosity (Table S4) could also affect ML dispersion in the solution which lowered ML conversion. In addition, the efficiency of CyOH in GVL production from ML reported here was different from the GVL production from EL reported by Cai et al.[32] Although similar CuNi-based catalysts were employed in both studies, alcohol had additional role in facilitating metal oxide reduction in our investigation.

A very low amount of H_2 generated after reaction as shown in Fig. 3a indicated that CyOH has low tendency for hydrogen production. Both 2–PrOH and 2–BuOH provided

high ML conversion and more than 95**%** of GVL yield which is in good agreement with the previous reports.[28-32] In addition, the highest remaining hydrogen amount was obtained in the 2–PrOH system. As mentioned above, generated hydrogen species from alcohol could perform as a reducing agent for the activation of metal oxide catalyst to generate metal active sites**.** Phase alteration of CuNiO catalyst after reactions in various alcohols was determined by XRD technique as shown in Fig**.** 3b. In the primary alcohol system, Cu metal phase was formed with the presence of CuO and NiO**.** Aliphatic secondary alcohols; on the other hand, showed higher degree of catalyst reduction where metallic nickel was also observed**.** Surprisingly, although low ML conversion, low GVL yield, and low H_2 production were observed in CyOH system (Fig. 3a) both metallic Cu and Ni were generated after the reaction**.** This means that the CyOH could reduce CuNiO catalyst**.** However, its strong adsorption on the catalyst as well as its high viscosity could be the reasons for its ineffective role in GVL production.

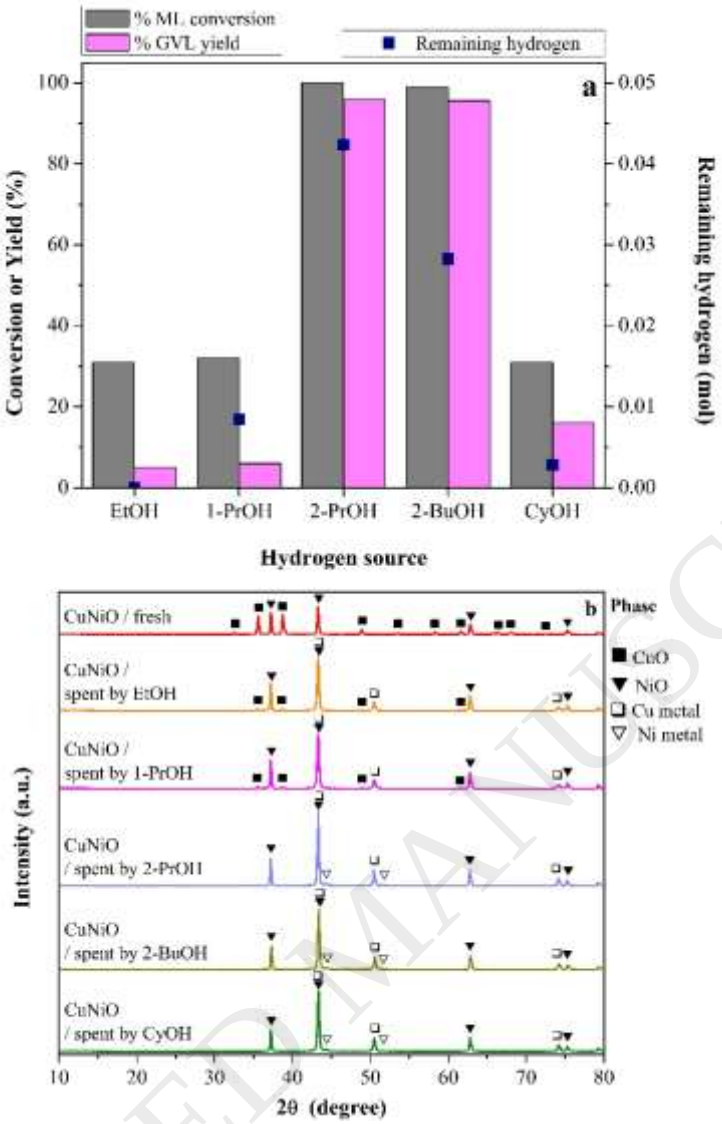

Fig. 3 (a) Catalytic performance in terms of ML conversion, GVL yield, and hydrogen production of CuNiO catalyst at 200 °C for 3 h using 0.2 M ML in 24 ml of various alcohols and (b) XRD patterns of fresh and spent CuNiO catalyst after the reaction.

3.4 *In situ* XRD reduction: Role of CuO in copper mixed metal oxide catalysts. To confirm and gain more insight information on the reducibility enhancement of CuO addition in the copper mixed oxide catalysts, the CuNiO was further selected for an *in situ* XRD reduction experiment in comparison with the CuO and NiO catalysts.[53] Phase

transformation of each catalyst was recorded while the catalyst was reduced under pure hydrogen atmosphere at elevated temperature**.** The *in situ* reduction of CuNiO result shown in Fig. 4a indicated that CuO was reduced to form metallic copper at around 150 ^{o}C, following by NiO reduction to form metallic nickel at around 155 ^{o}C**.** While the reduction profile of CuO shown in Fig. 4b indicated that Cu metal was created when the temperature reached 130 ^{o}C**.** The reduction behavior of NiO was displayed in Fig. 4c where Ni metal was generated at 200 ^{o}C**.** It can be seen that CuO phase in the CuO catalyst was reduced to Cu metal at lower temperature than CuO in CuNiO while NiO phase in the NiO catalyst was reduced at higher temperature than that of the CuNiO catalyst**.** The shift of CuO reduction temperature to higher temperature (from 130 to 150 ^{o}C) and the shift of NiO reduction temperature to lower temperature (from 200 to 155 ^{o}C) was an important evidence of the complementary reduction between CuO and NiO in this catalyst. In addition, the occurrence of CuO and NiO reduction temperatures in the CuNiO catalyst at a very close values (150 and 155 ^{o}C, respectively) could support that there was a good interaction between these two oxides in the structure. In brief, the *in situ* XRD results obtained here could confirm the spillover effect of hydrogen species from the created Cu metal to its neighboring NiO for generating nickel metal active sites at lower temperature.

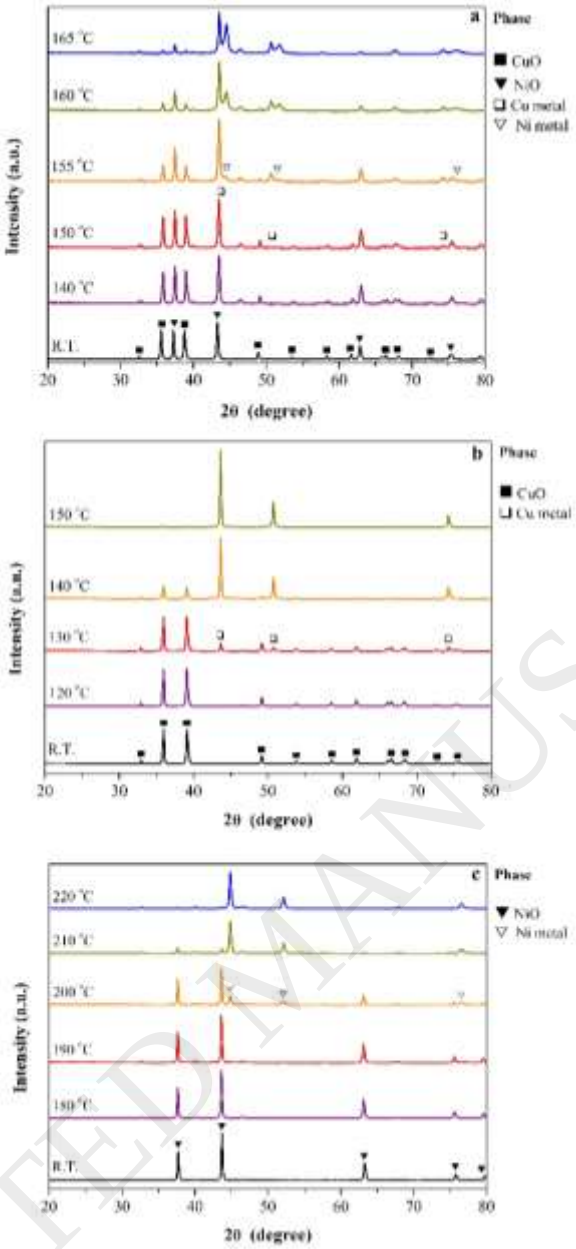

Fig. 4 *In situ* XRD patterns during reduction of (a) CuNiO, (b) CuO, and (c) NiO catalysts under pure H_2 gas flow of 20 ml/min.

3.5 Reusability and versatility of the catalyst. The spent CuNiO catalyst was employed for four more times for the GVL production. The results depicted in Fig. 5a revealed that this catalyst showed only a small decrease in terms of ML conversion and

GVL yield after the fourth time. The XRD patterns of the fresh and the 4th reuse of the catalyst were shown in Fig. 5b. It indicated that the spent catalyst still had the same three phases including Cu metal, Ni metal, and NiO as it was reported earlier in Fig. 1c. The small decrease of the catalytic activity might be resulted from the fact that some metallic sites became agglomerated (Fig. S5). The number of phases existed in the CuNiO catalyst before and after the reaction led to a further challenge to find out whether the catalytic performance of the mechanically mixed CuO and NiO would be similar or different from that of the CuNiO catalyst as well as its completely reduced form (alloy). The comparative results of the three scenarios were shown in Fig. 5c. The mechanically mixed CuO+NiO catalyst gave 17% of ML conversion with negligible GVL yield and H_2 production. The improvement in terms of ML conversion compared with the inactive CuO and NiO suggested that the presence of both CuO and NiO in the same system promoted the catalytic activity. The similar XRD patterns of the catalyst before and after reaction without the presence of reduced species (Cu or Ni metal) indicated that the oxide phases in the mechanically mixed metal oxide catalyst might have some capability to accelerate ML conversion; however, metallic sites were required for producing GVL (Fig. 5d). On the other hand, a completely reduced CuNiO labelled as CuNi_alloy showed only one single phase of CuNi alloy. Surprisingly, this alloy catalyst showed comparable ML conversion and GVL yield to those of the pristine CuNiO catalyst. These results suggested that the ML could be converted either on mixed metal oxides or metal/alloy active sites, however, the high selectivity of GVL product preferred the suitable ratio of metal oxides/metallic active sites. In addition, in terms of H_2 production, the alloy catalyst was not comparable to the CuNiO catalyst suggesting that the 2-PrOH dehydrogenation preferably took place over the mixed

metal oxide catalysts. Comparative H_2-TPR results of the mechanically mixed CuO + NiO, CuNiO, CuO, and NiO catalysts were shown in Fig. S3. Higher reduction peaks of the mechanically mixed catalyst than that of the CuNiO could explain why there was no metal phase generated after the catalyst utilization. As it was described above, CuNiO showed its impressive catalytic activity in all forms namely, pristine mixed metal oxides (CuNiO), partially reduced composite (Cu + Ni/NiO), and completely reduced solid solution (CuNi alloy). This is the important proof to confirm that CuNiO was a versatile catalyst for GVL production.

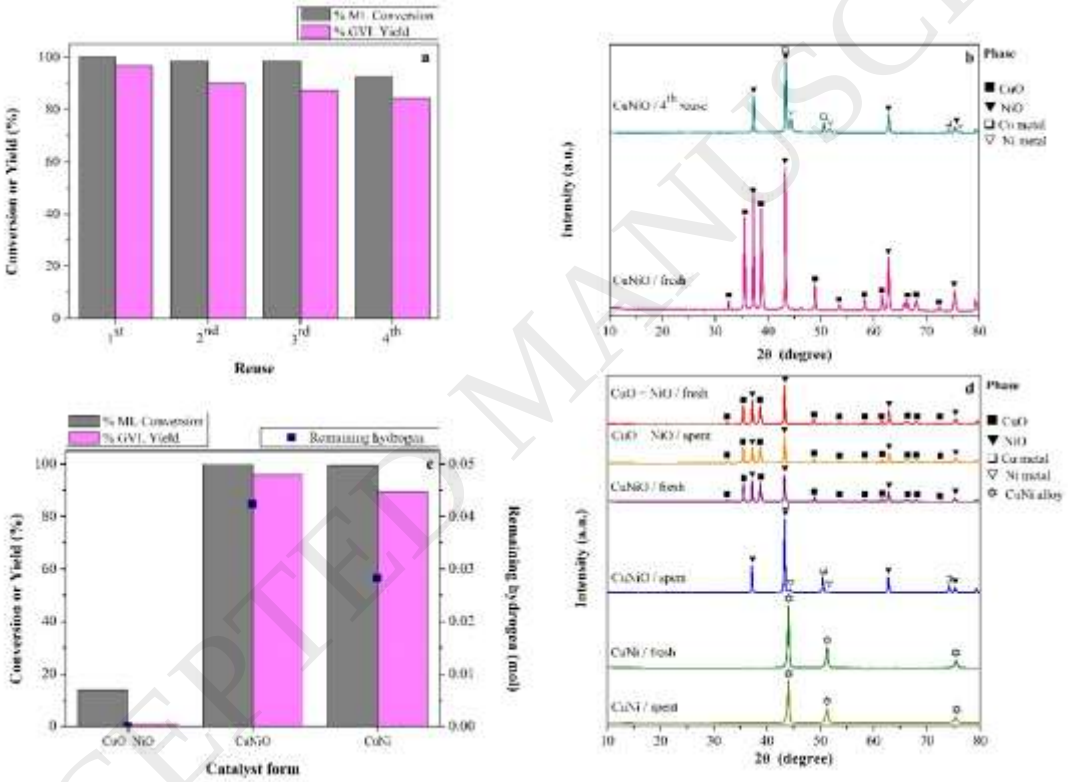

Fig. 5 (a) Catalytic performance of reused CuNiO catalyst up to 4 times at 200 °C for 3 h using 0.2 M ML in 24 ml of 2-PrOH, (b) XRD patterns of fresh CuNiO and after its 4th reuse, (c) catalytic performance of mechanically mixed CuO+NiO, CuNiO, and CuNi at 200 °C after 3 h using 0.2 M ML in 24 ml of 2-PrOH, and (d) XRD patterns of mechanically mixed CuO+NiO, CuNiO, and CuNi after reaction at 200 °C for 3 h in 2-PrOH.

3.6 Metal valences and surface species. To gain more understanding about good performance of the mixed metal oxide catalyst, the Cu/Ni molar ratio of 1.00 and 1.03 were observed in the pristine CuNiO and CuNi_alloy catalysts by using XRF method, respectively (Table S6). Surface analysis results using XPS technique of the pristine CuNiO, spent CuNiO, and CuNiO after 4th reuse were compared in Fig. 6. According to the Cu2p spectra (Fig. 6a, b, c), the pristine CuNiO was originally composed of CuO and $Cu(OH)_2$. After its first use, CuO was completely transformed to Cu metal, while the $Cu(OH)_2$ was still existed. The 4th reuse catalyst also showed these two species but with higher Cu metal/$Cu(OH)_2$ peak ratio. Ni2p spectra (Fig. 6d, e, f) also showed two species of NiO and $Ni(OH)_2$ in the pristine catalyst while the Ni metal was observed along with these two species both in the spent and 4th reuse catalysts. The O1s spectra (Fig. 6 g, h, i) showed good agreement with the Cu2p and Ni2p results on their surface metal oxides and metal hydroxides formation. Additionally the high binding energy at around 532.6 – 532.7 eV in the spent catalyst and the 4th reuse samples indicated the physically adsorbed water and/or organic compounds (i.e. ML, GVL, 2-PrOH) over NiO species. This could be implied that the NiO was an important site for ML or 2-PrOH adsorption during the ML conversion to GVL. The XPS results revealed various types of surface species including Cu, Ni, CuO, NiO, $Cu(OH)_2$, and $Ni(OH)_2$. While the CuO was found in the pristine catalyst but disappeared after its first use in the reaction. The role of CuO was consistent with the *in situ* XRD results stated above for facilitating NiO reduction at low temperature. The mutual presence of Cu, Ni, NiO, $Cu(OH)_2$, and $Ni(OH)_2$ on the surface were responsible for high catalytic performance of CuNiO catalyst. There was a report by Tang et al. that CuO in form of nanostructure could be also employed as catalysts for GVL production from ML in the presence of

methanol directly without catalyst pretreatment[54]. An investigation by combining the findings of their work and the current study to prepare nanostructured mixed metal oxides catalysts for more effective GVL production could be an interesting aspect to conduct in the future.

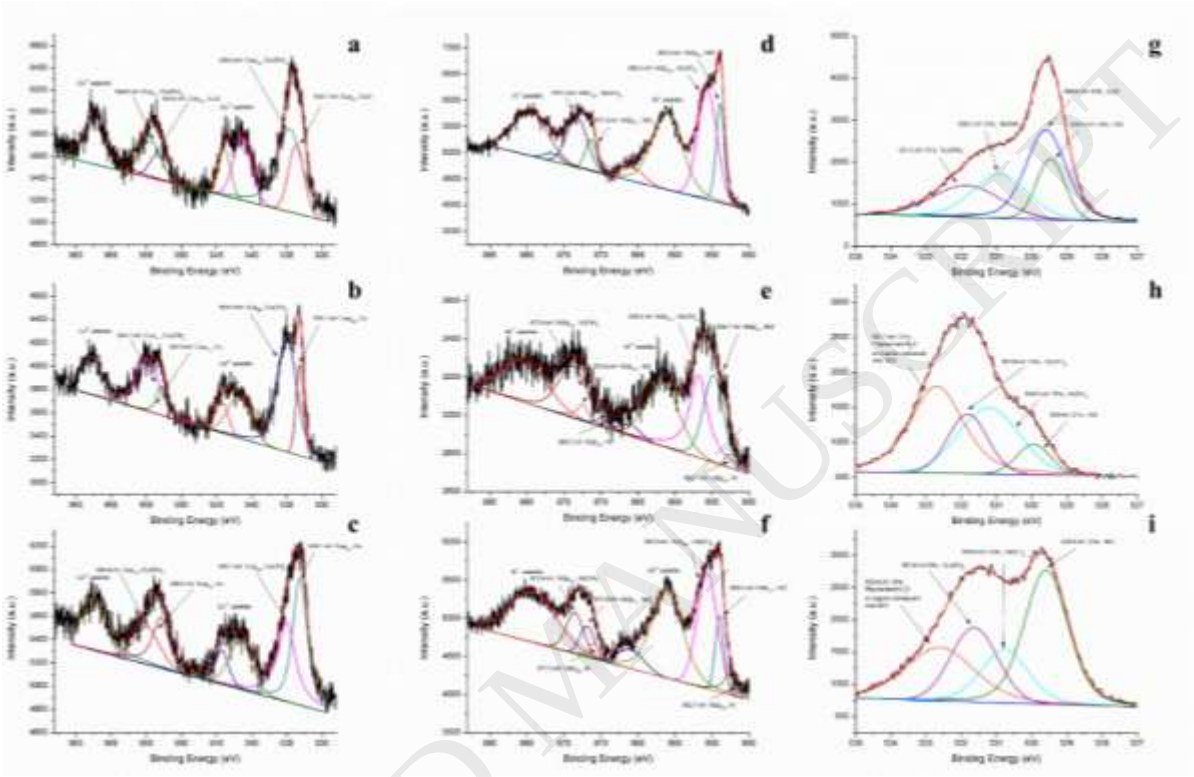

Fig. 6 XPS spectra of CuNiO (a, d, and g); spent CuNiO (b, e, and h); and CuNiO after 4th reuse (c, f, and i) in terms of Cu2p, Ni2p, and O1s, respectively

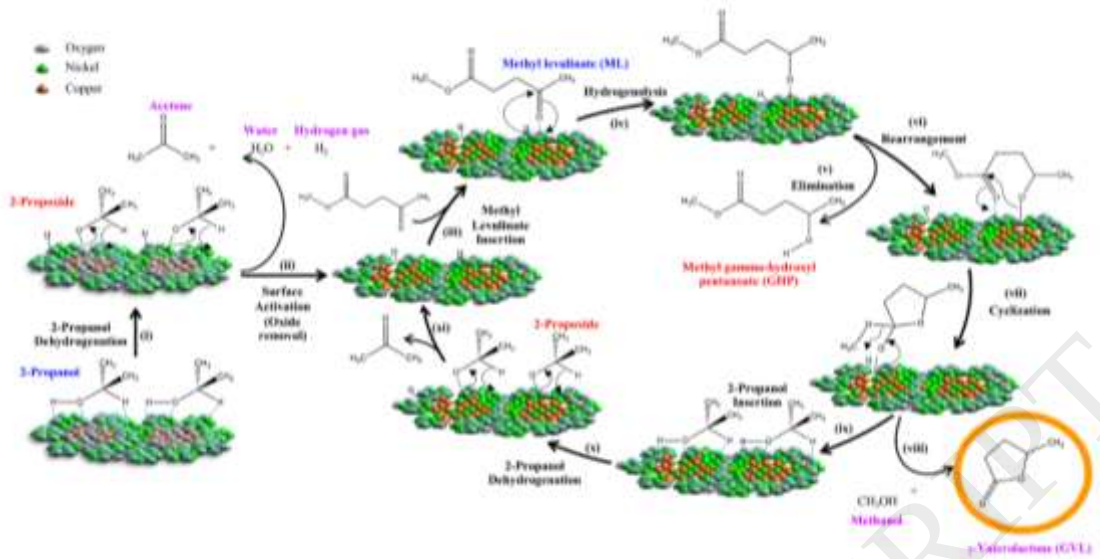

Scheme 1 Proposed reaction mechanism

3.6 Proposed mechanism of alcohol-assisted simultaneous activated copper mixed oxide catalysts for GVL production. Generally, catalytic transfer hydrogenation mechanism over heterogeneous catalysts can take place either through direct catalytic transfer (MPV) or metal hydride mechanism depending on catalyst active sites.[29-31,37] If both Lewis acid and Brønsted basic sites are presented next to each other on the catalyst, the reaction would undergo via MPV mechanism. On the other hand, the reaction would proceed through the metal hydride mechanism if only a Lewis acid or the metal active site is presented. Therefore, in this work, it is worth proposing a reaction mechanism of ML to GVL conversion over the CuNiO catalyst to clarify its simultaneous reduction behavior and promising catalytic performance under 2-PrOH system (Scheme 1). As it was shown in Fig. S4, CuNiO showed the highest acidity compared with other mixed metal oxide catalysts while the acidity could be doubled after the reduction of CuNiO to form CuNi alloy. Moreover, the CO_2-TPD results (Fig. S4c and d) also confirmed that the CuNi alloy has the highest basicity (Table S3). This data could strongly support that the catalytic performance of ML conversion to GVL is

not only dependent on catalysts' reducibility but also their acid and base properties. Typically, two major steps including (1) alcohol dehydrogenation to activate surface of the catalyst and (2) hydrogenation of ML followed by simultaneous cyclization to produce GVL. In the first major step, 2-propanol was oxidized over a mixed metal oxide catalyst (containing both Lewis acid and Brønsted base sites) to form 2-propoxide on the catalyst surface[52] (step i). This dehydrogenated intermediate generated hydrogen species and acetone via direct catalytic transfer or MPV mechanism (step ii). Then, the hydrogen species reduced metal oxides surface simultaneously to form metal active sites (Lewis acid) and this process generated water (Table S5) which could partially reoxidize the metals to metal hydroxides. After ML was inserted to the active metal sites (step iii) under adequate reaction pressure resulted from generated hydrogen gas and alcohol vapor at 200 ^{o}C, ML could then spontaneously react with adsorbed hydrogen species on the catalyst surface to form methyl gamma-hydroxypentanoate (GHP) adsorbed on the surface (step iv).[29-31,37] Some of this intermediate could be eliminated from the surface (step v) while the others underwent cyclization (step vii) leading to GVL production as well as methanol (MeOH) formation (step viii). The vacant active sites were then filled with 2-propanol (step ix) to generate active hydrogen species after 2-propanol dehydrogenation (step x) and acetone elimination (step xi). This led to an active site ready for the next cycle of GVL production. Due to the fact that there were less number of Lewis acid (metal or alloy) than Brønsted base (species on the catalyst active sites at the beginning of the reaction, both alcohol dehydrogenation and GVL production preferably underwent trough MPV mechanism.[37] However, after the first cycle of reaction both MPV and metal hydride are crucial pathways for 2-PrOH dehydrogenation and ML hydrogenation.

4. Conclusions

The catalytic transfer hydrogenation was successfully employed in both activation of copper mixed oxide catalysts and production of GVL consecutively. By using H_2-TPR technique, alcohol-assisted reduction evaluation (ASR), *in-situ* XRD reduction, and XPS analysis, it was evident that the good synergistic behaviour between the secondary alcohols and the H_2 spillover effect in copper mixed oxide catalysts is the key for the superior catalytic performance. All catalysts showed potential performance for GVL production from ML in the 2-PrOH system at 200 ^oC within 3 h. The most efficient catalyst, CuNiO could be recycled up to four times with only slight decrease of GVL yield. The reaction mechanism in alcohol dehydrogenation and ML hydrogenation underwent through both MPV and metal hydride routes. The discovery in this work could pave the way for a new sustainable concept in catalysis over simultaneously activated mixed metal oxide catalysts.

Acknowledgements

The financial support from Thailand Research Fund (TRF), project no. TRG6080004 is acknowledged. The authors are grateful to the Collaboration Hubs for International Program (CHIRP) of Strategic International Collaborative Research Program (SICORP), Japan Science and Technology Agency (JST) and the JASTIP program–WP2 (NSTDA-Kyoto University collaboration). Also kind advice during manuscript preparation from Prof. Dr. Supapan Seraphin, Senior Advisor from National Nanotechnology (NANOTEC) is greatly appreciated.

References

1. M. Hoel and S. Kverndokk, Depletion of fossil fuels and the impacts of global warming, Resour. Energy Econ., 18 (1996) 115-136.

2. J. Hansen, M. Sato, R. Ruedy, A. Lacis and V. Oinas, Global warming in the twenty-first century: An alternative scenario, Proc. Natl. Acad. Sci., 97 (2000) 9875-9880.

3. A. Midilli and I. Dincer, Hydrogen as a renewable and sustainable solution in reducing global fossil fuel consumption, Int. J. Hydrog. Energy, 33 (2008), 4209-4222.

4. A. Zecca and L. Chiari, Fossil-fuel constraints on global warming, Energy Policy, 38 (2010) 1-3.

5. C. McGlade and P. Ekins, The geographical distribution of fossil fuels unused when limiting global warming to 2 °C, Nature, 517 (2015), 187-190.

6. D. M. Alonso, J. Q. Bond and J. A. Dumesic, Catalytic conversion of biomass to biofuels, Green Chem., 12 (2010) 1493-1513.

7. D. M. Alonso, S. G. Wettstein and J. A. Dumesic, Bimetallic catalysts for upgrading of biomass to fuels and chemicals, Chem. Soc. Rev., 41 (2012) 8075-8098.

8. Y. Liu, L. Chen, T. Wang, Q. Zhang, C. Wang, J. Yan and L. Ma, One-Pot Catalytic conversion of raw lignocellulosic biomass into gasoline alkanes and chemicals over $LiTaMoO_6$ and Ru/C in aqueous phosphoric acid, ACS Sustain. Chem. Eng., 3 (2015) 1745-1755.

9. D. Ding, J. Xi, J. Wang, X. Liu, G. Lu and Y. Wang, Production of methyl levulinate from cellulose: selectivity and mechanism study, Green Chem., 17 (2015) 4037-4044.

10. M. J. Biddy, R. Davis, D. Humbird, L. Tao, N. Dowe, M. T. Guarnieri, J. G. Linger, E. M. Karp, D. Salvachúa, D. R. Vardon and G. T. Beckham, The techno-economic basis for coproduct manufacturing To enable hydrocarbon fuel production from lignocellulosic biomass, ACS Sustain. Chem. Eng., 4 (2016) 3196-3211.

11. I. T. Horváth, H. Mehdi, V. Fábos, L. Boda and L. T. Mika, γ-Valerolactone-a sustainable liquid for energy and carbon-based chemicals, Green Chem., 10 (2008) 238-

242.

12. D. Fegyverneki, L. Orha, G. Láng and I. T. Horváth, Gamma-valerolactone-based solvents, Tetrahedron, 66 (2010) 1078-1081.

13. J. Q. Bond, D. M. Alonso, D. Wang, R. M. West and J. A. Dumesic, Integrated catalytic conversion of γ-valerolactone to liquid alkenes for transportation fuels, Science, 327 (2010) 1110-1114.

14. Y. Zhao, Y. Fu and Q.-X. Guo, Production of aromatic hydrocarbons through catalytic pyrolysis of γ-valerolactone from biomass, Bioresource Technology, 114 (2012) 740-744.

15. J. C. Serrano-Ruiz, D. J. Braden, R. M. West and J. A. Dumesic, Conversion of cellulose to hydrocarbon fuels by progressive removal of oxygen, Appl. Catal. B., 100 (2010) 184-189.

16. D. M. Alonso, S. G. Wettstein and J. A. Dumesic, Gamma-valerolactone, a sustainable platform molecule derived from lignocellulosic biomass, Green Chem., 15 (2013) 584-595.

17. A. Kumar, Y. E. Jad, J. M. Collins, F. Albericio and B. G. de la Torre, Microwave-assisted green solid-hhase peptide synthesis using γ-valerolactone (GVL) as solvent, ACS Sustain. Chem. Eng., 6 (2018) 8034-8039.

18. K. Yan and A. Chen, Efficient hydrogenation of biomass-derived furfural and levulinic acid on the facilely synthesized noble-metal-free Cu-Cr catalyst, Energy, 58 (2013) 357-363.

19. C. Ortiz-Cervantes and J. J. García, Hydrogenation of levulinic acid to γ-valerolactone using ruthenium nanoparticles, Inorganica Chim. Acta, 397 (2013) 124-128.

20. K. Yan and A. Chen, Selective hydrogenation of furfural and levulinic acid to biofuels on the ecofriendly Cu-Fe catalyst, Fuel, 115 (2014) 101-108.

21. I. Obregón, E. Corro, U. Izquierdo, J. Requies and P. L. Arias, Levulinic acid hydrogenolysis on Al_2O_3-based Ni-Cu bimetallic catalysts, Chin. J. Catal., 35 (2014)

656-662.

22. B. Putrakumar, N. Nagaraju, V. P. Kumar and K. V. R. Chary, Hydrogenation of levulinic acid to γ-valerolactone over copper catalysts supported on γ-Al_2O_3, Catal. Today., 250 (2015) 209-217.

23. K. Hengst, M. Schubert, H. W. P. Carvalho, C. Lu, W. Kleist and J.-D. Grunwaldt, Synthesis of γ-valerolactone by hydrogenation of levulinic acid over supported nickel catalysts, Appl. Catal. A., 502 (2015) 18-26.

24. X. Long, P. Sun, Z. Li, R. Lang, C. Xia and F. Li, Magnetic Co/Al_2O_3 catalyst derived from hydrotalcite for hydrogenation of levulinic acid to γ-valerolactone, Chin. J. Catal., 36 (2015) 1512-1518.

25. J. Fu, D. Sheng and X. Lu, Hydrogenation of levulinic acid over nickel catalysts supported on aluminum oxide to prepare γ-valerolactone, Catalysts, 6 (2016) 1-10.

26. E. I. Gürbüz, D. M. Alonso, J. Q. Bond and J. A. Dumesic, Reactive extraction of levulinate esters and conversion to γ-valerolactone for production of liquid fuels, ChemSusChem, 4 (2011) 357-361.

27. H. Zhou, J. Song, H. Fan, B. Zhang, Y. Yang, J. Hu, Q. Zhu and B. Han, Cobalt catalysts: very efficient for hydrogenation of biomass-derived ethyl levulinate to gamma-valerolactone under mild conditions, Green Chem., 16 (2014) 3870-3875.

28. Z. Yang, Y.-B. Huang, Q.-X. Guo and Y. Fu, RANEY®Ni catalyzed transfer hydrogenation of levulinate esters to γ-valerolactone at room temperature, Chem. Commun., 49 (2013) 5328-5330.

29. J. Geboers, X. Wang, A. B. de Carvalho and R. Rinaldi, Densification of biorefinery schemes by H-transfer with Raney Ni and 2-propanol: A case study of a potential avenue for valorization of alkyl levulinates to alkyl γ-hydroxypentanoates and γ-valerolactone, J. Mol. Catal. A: Chem., 388-389 (2014) 106-115.

30. H. Y. Luo, D. F. Consoli, W. R. Gunther and Y. Román-Leshkov, Investigation of the reaction kinetics of isolated Lewis acid sites in Beta zeolites for the Meerwein-Ponndorf-Verley reduction of methyl levulinate to γ-valerolactone, J. Catal., 320 (2014)

198-207.

31. J. He, H. Li, Y.-M. Lu, Y.-X. Liu, Z.-B. Wu, D.-Y. Hu and S. Yang, Cascade catalytic transfer hydrogenation–cyclization of ethyl levulinate to γ-valerolactone with Al-Zr mixed oxides, Appl. Catal. A., 510 (2016) 11-19.

32. B. Cai, X.-C. Zhou, Y.-C. Miao, J.-Y. Luo, H. Pan and Y.-B. Huang, Enhanced catalytic transfer hydrogenation of ethyl levulinate to γ-valerolactone over a robust Cu-Ni bimetallic catalyst, ACS Sustain. Chem. Eng., 5 (2017) 1322-1331.

33. C. Termvidchakorn, K. Faungnawakij, S. Kuboon, T. Butburee, N. Sano and T. Charinpanitkul, A novel catalyst of Ni hybridized with single-walled carbon nanohorns for converting methyl levulinate to γ-valerolactone, Appl. Surf. Sci., 474 (2019) 161-168.

34. Z. Lin, X. Cai, Y. Fu, W. Zhu and F. Zhang, Cascade catalytic hydrogenation-cyclization of methyl levulinate to form γ-valerolactone over Ru nanoparticles supported on a sulfonic acidfunctionalized UiO-66 catalyst, RSC Adv., 7 (2017) 44082-44088.

35. X. Cao, J. Wei, H. Liu, X. Lv, X. Tang, X. Zeng, Y. Sun, T. Lei, S. Liue and L. Lin, Hydrogenation of methyl levulinate to γ-valerolactone over Cu-Mgoxide using MeOH as in situ hydrogen source, J. Chem. Technol. Biotechnol., 94 (2019) 167-177.

36. W. Ouyang, D. Zhao, Y. Wang, A. M. Balu, C. Len, and R. Luque, Continuous flow conversion of biomass-derived methyl levulinate into γ‑ valerolactone using functional metal organic frameworks, ACS Sustainable Chem. Eng., 6 (2018) 6746-6752.

37. M. J. Gilkey and B. Xu, Heterogeneous Catalytic transfer hydrogenation as an effective pathway in biomass upgrading, ACS Catal., 6 (2016) 1420-1436.

38. J. Ashok, M. Subrahmanyam and A. Venugopal, Hydrotalcite structure derived Ni-Cu-Al catalysts for the production of H_2 by CH_4 decomposition, Int. J. Hydrogen Energy, 33 (2008) 2704-2713.

39. X. Tang, B. Zhang, Y. Li, Y. Xu, Q. Xin and W. Shen, CuO/CeO_2 catalysts: redox features and catalytic behaviors, Appl. Catal. A., 288 (2005) 116-125.

40. J. Sá, Y. Kayser, C. J. Milne, D. L. Abreu Fernandes and J. Szlachetko, Temperature-programmed reduction of NiO nanoparticles followed by time-resolved RIXS, PCCP, 16 (2014) 7692-7696.

41. H. Zhu, H. Dong, P. Laveille, Y. Saih, V. Caps and J.-M. Basset, Metal oxides modified NiO catalysts for oxidative dehydrogenation of ethane to ethylene, Catal Today, 228 (2014) 58-64.

42. O. O. James AND S. Maity, Temperature programme reduction (TPR) studies of cobalt phases in γ-alumina supported cobalt catalysts, J. Pet. Technol. Altern. Fuels, 7 (2016) 1-12.

43. M. A. Valenzuela, P. Bosch, J. Jiménez-Becerrill, O. Quiroz and A. I. Páez, Preparation, characterization and photocatalytic activity of ZnO, Fe_2O_3 and $ZnFe_2O_4$, Photochem. Photobiol. A., 148 (2002) 177-182.

44. M. Liang, W. Kang and K. Xie, Comparison of reduction behavior of Fe_2O_3, ZnO and $ZnFe_2O_4$ by TPR technique, J. Nat. Gas Chem., 18 (2009) 110-113.

45. A. P. Amrute, C. Mondelli and J. Pérez-Ramírez, Kinetic aspects and deactivation behaviour of chromia-based catalysts in hydrogen chloride oxidation, Catal. Sci. Technol., 2 (2012) 2057-2065.

46. G. Bai, H. Dai, Y. Liu, K. Ji, X. Li and S. Xie, Preparation and catalytic performance of cylinder- and cake-like Cr_2O_3 for toluene combustion, Catal. Commun., 36 (2013) 43-47.

47. B. Wang, S. Liu, Z. Hu, Z. Li and X. Ma, Active phase of highly active Co_3O_4 catalyst for synthetic natural gas production, RSC Adv., 4 (2014) 57185-57191.

48. M. Chia and J. A. Dumesic, Liquid-phase catalytic transfer hydrogenation and cyclization of levulinic acid and its esters to γ-valerolactone over metal oxide catalysts, Chem. Commun., 47 (2011) 12233-12235.

49. A. E.-A. A. Said, M. M. M. Abd El-Wahab and M. N. Goda, Selective synthesis of acetone from isopropyl alcohol over active and stable CuO-NiO nanocomposites at relatively low-temperature, Egypt. J. Basic Appl. Sci., 3 (2016) 357-365.

50. S. Song, S. Yao, J. Cao, L. Di, G. Wu, N. Guan and L. Li, Heterostructured Ni/NiO composite as a robust catalyst for the hydrogenation of levulinic acid to γ-valerolactone, Appl. Catal. B.: Environmental, 217 (2017) 115-124.

51. W. Tanwongwal, S. Kuboon, W. Kraithong and A. Eiad-Ua, Production of γ-Valerolactone from Methyl Levulinate via Catalytic Transfer Hydrogenation on Nickel-Copper Oxide Catalyst, Mater. Sci., 872 (2016) 187-190.

52. D. Kulkarni and I. E. Wachs, Isopropanol oxidation by pure metal oxide catalysts: number of active surface sites and turnover frequencies, Appl. Catal. A., 237 (2002) 121-137.

53. J. T. Richardson, R. Scates and M. V. Twigg, X-ray diffraction study of nickel oxide reduction by hydrogen, Appl. Catal. A., 246 (2003) 137-150.

54. X. Tang, Z. Li, X. Peng, Y. Jiang, S. Liu, T. Lei, Y. Sun, and L. Lin, In situ catalytic hydrogenation of biomass-derived methyl evulinate to γ-valerolactone in methanol, ChemSusChem, 8 (2015) 1601-1607.

Available online at www.sciencedirect.com

ScienceDirect

journal homepage: www.elsevier.com/locate/he

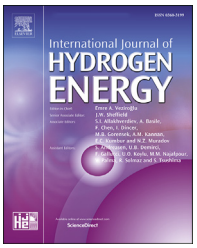

Highly dispersed Ni–Cu nanoparticles on SBA-15 for selective hydrogenation of methyl levulinate to γ-valerolactone

Cheng Fang [a], *Sanchai Kuboon* [a], *Pongtanawat Khemthong* [a], *Teera Butburee* [a], *Pongkarn Chakthranont* [a], *Vorranutch Itthibenchapong* [a], *Panita Kasamechonchung* [a], *Thongthai Witoon* [b,c], *Kajornsak Faungnawakij* [a,c,*]

[a] *National Nanotechnology Center (NANOTEC), National Science and Technology Development Agency, 111 Thailand Science Park, Phahonyothin, Khlong Luang, Pathum Thani, 12120, Thailand*

[b] *Center of Excellence on Petrochemical and Materials Technology, Department of Chemical Engineering, Faculty of Engineering, Kasetsart University, Bangkok, 10900, Thailand*

[c] *Research Network of NANOTEC–KU on NanoCatalysts and NanoMaterials for Sustainable Energy and Environment, Kasetsart University, Bangkok, 10900, Thailand*

ARTICLE INFO

Article history:
Received 17 September 2018
Received in revised form
24 January 2019
Accepted 28 March 2019
Available online xxx

Keywords:
Highly dispersed Ni and Cu
γ-valerolactone
Hydrogenation
Methyl levulinate

ABSTRACT

Copper and nickel nanoparticles highly dispersed on an ordered mesoporous silica support (SBA-15) were prepared by a glycol-assisted impregnation method and tested for the catalytic transfer hydrogenation reaction of methyl levulinate to γ-valerolactone (GVL). Characterizations by high resolution transmission electron microscopy, X-ray diffraction, N_2 sorption, H_2 temperature-programmed reduction and X-ray absorption spectroscopy confirm that the highly dispersed nanoparticles were well-anchored to the mesopores of SBA-15 with the strong interaction. Comparing to a catalyst synthesized by a conventional aqueous impregnation method, our catalyst shows a higher conversion and greater selectivity towards GVL of reaction at 140–170 °C using 2-propanol as a solvent and a hydrogen donor. Results showed that Ni–Cu/SBA-15 (EG) had much better activity, providing 91.3% conversion of ML with 89.7% selectivity towards GVL in 3 h at 140 °C. The high compositional homogeneity, uniform distribution of the nanoparticles in the mesoporous channels and the strong interaction between the metal nanoparticles and SBA-15 contribute to the superior catalytic performance. This catalyst also demonstrates superb stability over the course of 5 reaction cycles without significant loss in catalytic activity and selectivity towards GVL formation.

* *Corresponding author*. National Nanotechnology Center (NANOTEC), National Science and Technology Development Agency, 111 Thailand Science Park, Phahonyothin, Khlong Luang, Pathum Thani, 12120, Thailand.
E-mail address: kajornsak@nanotec.or.th (K. Faungnawakij).

https://doi.org/10.1016/j.ijhydene.2019.03.272
0360-3199/

Introduction

The depletion of non-renewable fossil sources is a major drive for the development of alternative methods for fuel and chemical production. One of the viable solutions is the utilization of biomass and/or biomass derivatives to produce biofuels and value-added platform molecules [1–4]. Among these molecules, γ-valerolactone (GVL) is an attractive target as it is widely used in fuel production as a precursor and an additive [5–7], as well as in various chemical industries, e.g. perfume, solvent, coupling agent, brake fluid, insecticide, and adhesive [8–10].

Generally, the GVL is synthesized by the hydrogenation of levulinate esters and levulinic acid (LA) under reducing conditions [11–14]. It was previously reported that the hydrogenation of levulinate esters offers great yields of GVL product which can be simply separated from the reaction media [15]. Various levulinate esters, for instance, methyl levulinate (ML), ethyl levulinate (EL), and butyl levulinate (BL) have been reported as feedstocks for the GVL production [16–18]. Apart from a type of feedstocks, hydrogen donor is another critical component for the catalytic transfer hydrogenation (CTH) process for GVL production. It was demonstrated that the primary alcohols (such as methanol and ethanol) were not positive hydrogen donors in CTH reaction, while the secondary alcohols (e.g. isopropanol, sec-butyl alcohol) exhibited better performances for CTH processes [15,19]. Overall, the CTH process of levulinate ester and secondary alcohols is a promising reaction route for GVL production. Yet, for large-scale production of GVL, highly efficient catalyst is required to minimize the energy intensity of the process.

Noble metals have been reported to be active catalysts for GVL synthesis [20–24]. However, the low stability, high cost, and harsh process conditions limit their application for the large-scale production. Recently, various non-noble metal catalysts have been proposed for the CTH [25,26], such as RANEY®Ni [15,27], Ni supported on various supports (Al_2O_3, ZnO, SiO_2, H-ZSM-5, montmorillonoid, TiO_2 and MgO) [28–31], Cu–ZnO supported on carbon nanotubes [32], $FeZrO_x$ nanoparticles [33], etc. Ni–Cu catalysts have been developed and explored as candidates for the conversion of LA to GVL [34–36]. However, high hydrogen pressure and reaction temperature as well as long reaction time are commonly needed for the efficient production of GVL. Besides, the systems suffer from leaching and sintering of metal particles at high temperatures. Therefore, it is a challenge to develop active and stable catalysts for producing GVL by catalytic hydrogenation under mild reaction conditions.

Nowadays, ordered mesoporous materials with uniform porous structure, high chemical and thermal stability, and high surface area, have aroused considerable attention due to their potential applications in storage, adsorption, sensing, and catalysis [37–39]. In catalysis applications, mesoporous materials are often used as supports for metal and/or metal oxides nanoparticles to enhance the catalytic performance, especially when the nanoparticles are evenly distributed on the support [40–42]. However, to the best of our knowledge, highly dispersed Ni and Cu nanoparticles supported on ordered mesoporous silica have not been reported for the catalytic transfer hydrogenation reaction of methyl levulinate to GVL.

In this paper, we present a glycol-assisted impregnation route to synthesize highly dispersed Ni and Cu nanoparticles on an ordered mesoporous silica. Comparing to a catalyst synthesized by a conventional aqueous impregnation method, our catalyst demonstrates superior activity and stability for the production of GVL from methyl levulinate via CTH reaction using 2-propanol as both solvent and H-donor without using any H_2 gas. In this glycol-assisted impregnation method, ethylene glycol acts as a carrier for the transfer of metal species into the mesoporous channels of SBA-15 by capillary force. Subsequently, the polyol decomposes to carbon, which restricts the location of metal particles, and then is completely removed by stepwise calcination in inert and air atmosphere. Therefore, highly dispersed metal nanoparticles can be distributed on SBA-15.

Experimental

Catalyst preparation

SBA-15 silica was synthesized via a hydrothermal process as reported by Zhao et al. [43]. 4.0 g of Pluronic P123 (Sigma-Aldrich Chemical Co.) was dissolved in 150 mL of 1.6 mol/L HCl (Carlo Erba Reagents) solution. The resulting mixture was stirred for about 1 h until the solution became transparent. Then, 8.50 g of tetraethyl orthosilicate (TEOS, 98%, Sigma-Aldrich Chemical Co.) was added dropwise under continuous stirring at 40 °C. After stirring for 24 h, the mixture was transferred into an autoclave for a reaction at 100 °C for next 24 h. The precipitate product was collected by filtration and washed with water and followed by ethanol (Sigma-Aldrich Chemical Co.) for 3 times each. The sample was subsequently dried at 100 °C and then calcined at 550 °C for 6 h to remove the surfactant.

The Ni–Cu/SBA-15 catalysts were prepared by a glycol-assisted impregnation route. A typical catalyst, 5 wt % Ni and 5 wt % Cu on SBA-15, was synthesized by dispersing 0.11 g of $Ni(NO_3)_2 \cdot 6H_2O$ (Ajax Finchem Pty Ltd), 0.08 g of $Cu(NO_3)_2 \cdot 3H_2O$ (Ajax Finchem Pty Ltd), and 0.5 g of SBA-15 into 10 mL of ethylene glycol (Sigma-Aldrich Chemical Co.) and then the mixture was stirred overnight under vacuum. Subsequently, the samples were dried in a vacuum oven at 80 °C until the solvent was completely evaporated. Then the sample was calcined at 550 °C for 4 h in N_2, followed by another 2 h in air. Finally, we obtained the product via reduction at 500 °C for 4 h in 5% H_2/Ar. This sample was denoted as Ni–Cu/SBA-15 (EG).

For comparison, Ni–Cu/SBA-15 catalysts were also prepared by a conventional impregnation method using water as a solvent. The impregnation procedure consists of dissolving the aforementioned amount of $Ni(NO_3)_2 \cdot 6H_2O$ and $Cu(NO_3)_2 \cdot 3H_2O$ in 10 mL of deionized water and added the solution to the beaker containing 0.5 g of SBA-15. The mixture was stirred overnight and then dried in an ambient pressure at 80 °C for 12 h. After that, the sample was calcined at 550 °C for 6 h in air and reduced at 500 °C for 4 h in 5% H_2/Ar. The obtained sample was denoted as Ni–Cu/SBA-15(IM).

Please cite this article as: Fang C et al., Highly dispersed Ni–Cu nanoparticles on SBA-15 for selective hydrogenation of methyl levulinate to γ-valerolactone, International Journal of Hydrogen Energy, https://doi.org/10.1016/j.ijhydene.2019.03.272

Characterization

Phase identity and crystallinity of the samples were assessed by X-ray diffraction (XRD) using an X-ray diffractometer (D8 ADVANCE, Bruker, Ltd., Germany). The radiation source was Cu Kα and the measurement was operated at 40 kV and 40 mA over a 2θ range of 15°–80° with a step of 0.02° s^{-1} and 0.5 s per step. The size, morphology, and elemental composition of the catalyst particles were examined by transmission electron microscopy (TEM) equipped with an energy dispersive spectrometer (EDS), which was operated at 200 kV (JEOL JEM-2100Plus).

The specific surface area as well as details on pore volume and diameter of the samples was measured by a N_2 sorption technique (Nova 2000e, Quantachrome Instruments) at −196 °C. Prior to the measurements, the samples underwent a degas process at 150 °C for 3 h under vacuum. The calculation for the specific surface area was done using the Brunauer-Emmett-Teller (BET) method. Pore size distribution was determined using the Barrett-Joyner-Halenda (BJH) method from the desorption branch. The reduction temperature profiles as well as the catalyst reduction process prior to experiments were obtained by the hydrogen temperature-programmed reduction (H_2-TPR) method in a CHEMBET-Pulsar (Quantachrome Instruments). The sample amount of 150 mg was pretreated at 120 °C for 0.5 h in a He flow. The reduction was performed in a range of 50–500 °C (10 °C min^{-1}) in a H_2/Ar flow (5 vol %) at 30 cm^3 min^{-1}.

The information on the local structure, geometry, and oxidation state during the reduction process was obtained by an X-ray absorption near edge structure (XANES) analysis at Cu K-edge (8979 eV) and Ni K-edge (8333 eV) at the XAS Beamline (BL-5.2) of the Synchrotron Light Research Institute (Public Organization), Thailand, employing a double monochromator. A pressed thin pellet of sample was used in the experiment and inserted in the *in situ* XAS cell [44]. The measurement was performed starting at room temperature under a N_2 flow (20 cm^3 min^{-1}) and then heated to 500 °C at a rate of 2 °C min^{-1} in a H_2/N_2 flow (33 vol%). Afterward, the cooling process was conducted in a N_2 atmosphere. The data were collected in transmission mode at varying temperatures during the heating and cooling cycles. Bulk Cu foil, Cu_2O, CuO, $Cu(NO_3)_2$, Ni foil, and NiO were used as reference compounds. The linear combination fitting (LCF) and EXAFS curve fitting were done on the Athena and EXAFSPAK programs, respectively [45,46]. Metal leaching into the reaction solution was quantified by inductively coupled plasma–atomic emission spectroscopy (ICP-AES, VISTA-MPX).

Catalytic activity measurements

Activity testing was conducted in a 120 mL stainless steel reactor. 59.4 μL methyl levulinate (Sigma-Aldrich Chemical Co.), 24 mL of 2-propanol (Fisher Scientific UK), and 0.1 g of the catalyst were used in each catalytic run and the mixture was stirred at 300 rpm. The reactor was purged 5 times with N_2 before the reaction tests, otherwise stated. In general, the autogenous pressure of the reactor varies from 1 to 18 bar during the reaction. The product mixture was collected in an ice cold trap and analyzed by gas chromatography (GC-2010, Shimadzu) with a flame ionization detector at 300 °C using DB-WAX (30 m in length, 0.25 mm i.d., and 0.25 μm film thickness) with the oven temperature ramping from 50 to 210 °C. The results were further confirmed by GC-MS at detector temperature of 400 °C (QP-5050, Shimadzu). The methyl levulinate conversion and the GVL product selectivity and yield were calculated using the following equations:

$$Conversion(\%) = \left(\frac{mole\ of\ consumed\ ML}{mole\ of\ initial\ ML}\right) \times 100 \quad (1)$$

$$Selectivity(\%) = \left(\frac{mole\ of\ produced\ GVL}{mole\ of\ consumed\ ML}\right) \times 100 \quad (2)$$

$$Yield(\%) = \left(\frac{Convesion\ of\ ML \times Selectivity\ of\ GVL}{100}\right) \quad (3)$$

The numbers of mole of ML and GVL were obtained from the peak area analysis using GC-FID.

Results and discussion

Catalyst characterization

XRD analysis

The XRD was conducted to determine the chemical compositions and phases of all samples as shown in Fig. 1. Fig. 1a depicts the XRD patterns of the calcined NiO–CuO/SBA-15 catalysts. The broad diffraction peak at around 23° in all patterns can be assigned to amorphous silica, which is a component of the SBA-15 support. On the XRD pattern of NiO–CuO/SBA-15(IM), sharp peaks were observed and the peak positions match these following ICDD references: CuO from PDF 01-080-1916 and $Ni_{0.75}Cu_{0.25}O$ from PDF 01-078-0648. The strong peak intensity suggests large crystallite size of oxides in NiO–CuO/SBA-15(IM). In the case of the NiO–CuO/SBA-15 (EG), only the characteristic feature of SBA-15 and three extremely weak and broad XRD peaks of $Ni_{0.9}Cu_{0.1}O$ (PDF 01-078-0645) can be observed. This behavior could cause by the small crystallite sizes of the oxides, implying that the metal oxide species disperse well on the support. Fig. 1b shows the XRD patterns of the reduced Ni–Cu/SBA-15. The metallic Cu (PDF 00-004-0838) and NiCu (PDF 03-065-7246) phases are highly apparent in the XRD pattern of Ni–Cu/SBA-15(IM). While for Ni–Cu/SBA-15 (EG), no prominent characteristic peak of metal phase was observed, suggesting the presence of very small Ni and Cu nanoparticles on the SBA-15 support. The XRD results indicates that the glycol-assisted impregnation method is an appropriate way for preparing highly dispersed metal species on an ordered mesoporous silica.

TEM analysis

Fig. 2a shows the TEM image of the Ni–Cu/SBA-15 (EG) catalyst and homogenous dispersion of nanoparticles can be clearly observed. Particularly, small nanoparticles uniformly distributed in the mesoporous channels and are isolated from each other. Fig. 2b shows the metal particle size distribution of the Ni–Cu/SBA-15 (EG) catalyst. The particles on SBA-15 are in the range of 2–16 nm with the average particle size of 7 nm. The high-angle annular dark field-scanning transmission electron

Please cite this article as: Fang C et al., Highly dispersed Ni–Cu nanoparticles on SBA-15 for selective hydrogenation of methyl levulinate to γ-valerolactone, International Journal of Hydrogen Energy, https://doi.org/10.1016/j.ijhydene.2019.03.272

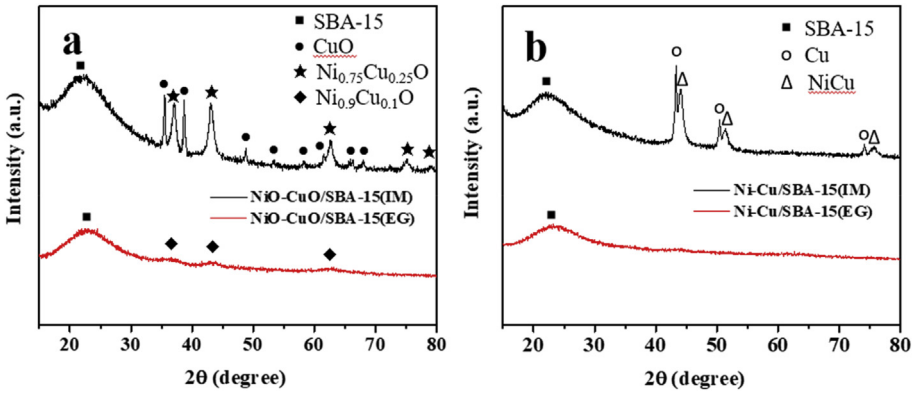

Fig. 1 – XRD patterns of (a) calcined NiO–CuO/SBA-15 and (b) reduced Ni–Cu/SBA-15 samples.

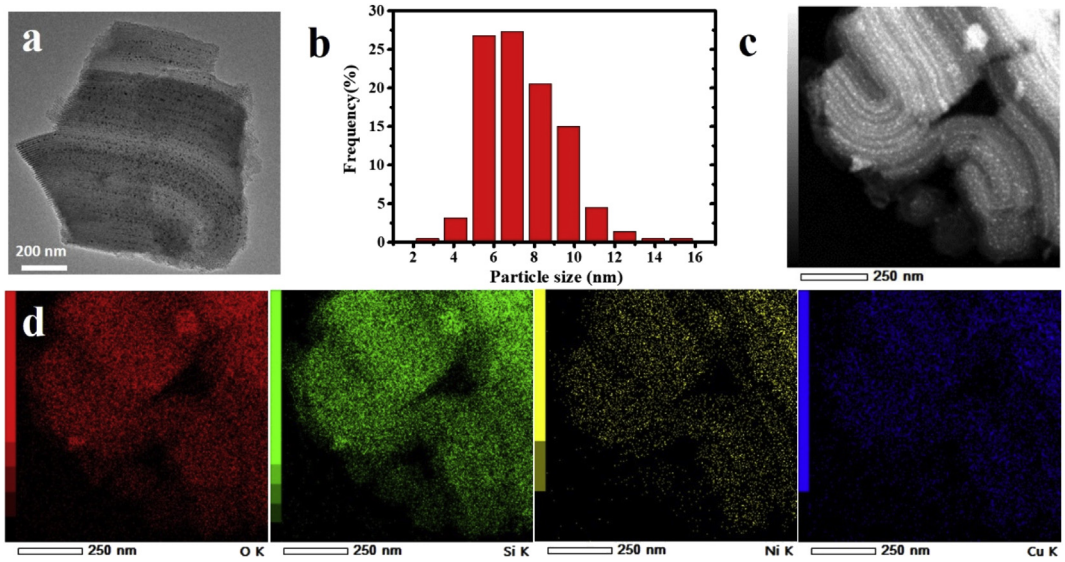

Fig. 2 – (a) TEM image, (b) metal particle size distribution, (c) HAADF-STEM image and (d) elemental mapping of the Ni–Cu/SBA-15 (EG).

microscopy (HAADF-STEM) image (Fig. 2c) demonstrates highly ordered arrays of nanoparticles located in the long-range ordered mesoporous silica. The corresponding elemental mapping images for the different elements in this selected area are presented in Fig. 2d, which exhibits the homogenous dispersion of nanoparticles on the silica matrix. Moreover, the mapping shapes of Ni and Cu elements are following the tunnel arrays of SBA-15, implying that both metals were located inside the mesoporous channels. The strong association of Ni and Cu species in the X-ray images suggested the formation of NiCu alloy structures.

Fig. 3a is the TEM image of the Ni–Cu/SBA-15(IM). It reveals that majority of the particles (average particle size around 35 nm) are deposited on the outside of SBA-15 framework and fewer numbers of particles are found inside the channels of the mesoporous silica support. The image also shows that many small particles are located very close to one another and some of them agglomerate into big clusters. The particle size distribution of metals in the Ni–Cu/SBA-15(IM) (Fig. 3b) ranges from 10 to 80 nm, which are much larger than those on Ni–Cu/SBA-15 (EG). Fig. 3c exhibits the HAADF-STEM image of Ni–Cu/SBA-15(IM), which shows plenty of accumulated nanoparticles on the SBA-15 surface. The elemental mapping images in Fig. 3d show that the deposition of nickel and copper species *via* impregnation method is uneven and the element composition is not as uniform as that on Ni–Cu/SBA-15 (EG).

N_2 *sorption analysis*

N_2 adsorption-desorption was performed to evaluate the texture and porosity of the catalysts, and the results are shown in Fig. 4. The N_2 adsorption-desorption isotherms of both catalyst samples reveal a typical type IV(a) curve with type H1 hysteresis loops, a characteristic feature of a mesoporous material with uniform porosity according to the IUPAC definition [47]. In the inset of Fig. 4, the pore size distribution of both catalysts show a sharp peak at around 6 nm, corresponding to the internal cavity of SBA-15. Additionally, the Ni–Cu/SBA-15 (EG) shows a multi-model pore distribution in the range of 3–8 nm originates from the presence of metal nanoparticles inside the mesoporous channels. By deriving the N_2 adsorption-desorption isotherms, the pore structural parameters are given in Table 1 and the information of SBA-15

Please cite this article as: Fang C et al., Highly dispersed Ni–Cu nanoparticles on SBA-15 for selective hydrogenation of methyl levulinate to γ-valerolactone, International Journal of Hydrogen Energy, https://doi.org/10.1016/j.ijhydene.2019.03.272

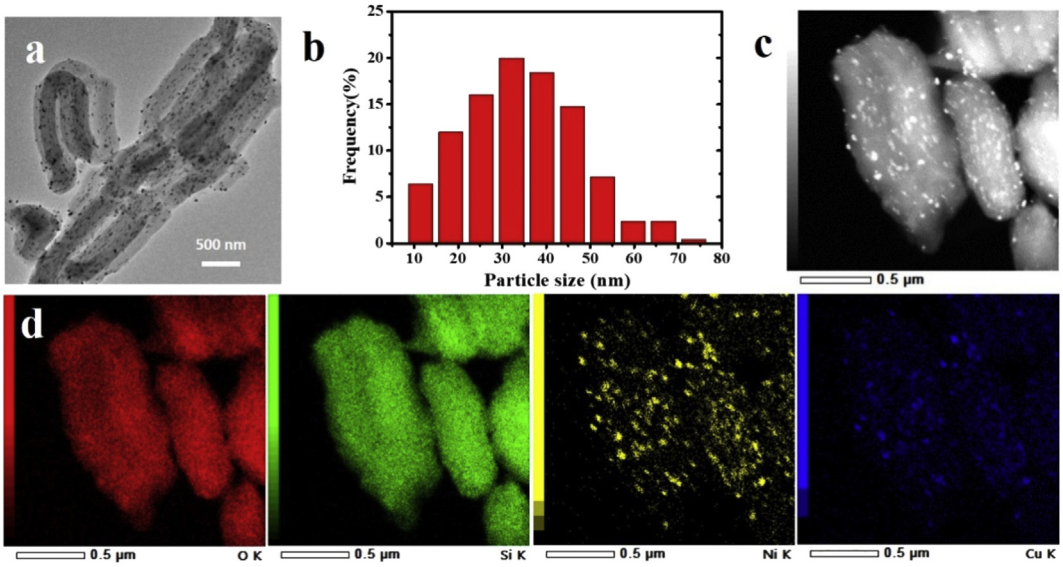

Fig. 3 – (a) TEM image, (b) metal particle size distribution, (c) HAADF-STEM image and (d) elemental mapping of the Ni–Cu/SBA-15(IM).

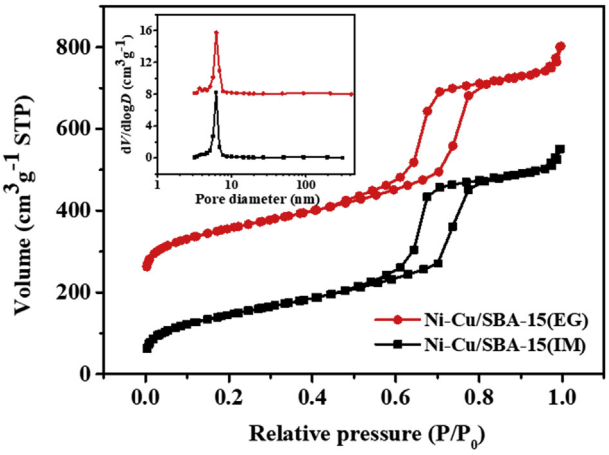

Fig. 4 – N_2 adsorption-desorption isotherms and pore size distributions (inset) of the catalysts.

is shown as a reference. The calculated BET surface areas and pore volumes of the Ni–Cu/SBA-15 (EG) and Ni–Cu/SBA-15(IM) catalysts are 559 m^2 g^{-1}, 520 m^2 g^{-1} and 0.89 cm^3 g^{-1}, 0.81 cm^3 g^{-1}, respectively. The surface area and pore volume of both Ni–Cu/SBA-15 (EG) and Ni–Cu/SBA-15(IM) are smaller than those of SBA-15 (724 m^2 g^{-1} and 0.96 cm^3 g^{-1}). The results suggest that metal nanoparticles could fill in or block the pores of SBA-15, resulting in the reduction of the surface area and pore volume. Furthermore, the Ni–Cu/SBA-15 (EG) presents larger specific surface area and pore volume than those of Ni–Cu/SBA-15(IM), which can be arise from the better dispersion of nanoparticles.

Table 1 – The physical characteristics of the catalysts.

Samples	S_{BET}[a] (m^2 g^{-1})	V_{BIH}[b] (cm^3 g^{-1})	D_{BJH}[c] (nm)
SBA-15	724	0.96	6.9
Ni–Cu/SBA-15 (EG)	559	0.89	6.2
Ni–Cu/SBA-15(IM)	520	0.81	6.2

[a] BET surface area.
[b] BJH desorption pore volume.
[c] Average pore diameter.

H_2-TPR analysis

The H_2-TPR profiles (Fig. 5) show the reduction behaviors of these two catalysts. Previous studies have demonstrated that the reduction of bulk CuO generally occurs below 300 °C and the reduction peaks of NiO on silica take place above 370 °C [34,48]. It was also reported that the presence of Ni and Cu lowers the reduction temperature of their corresponding oxides [49]. The XRD result of NiO–CuO/SBA-15(IM) shows the presence of CuO and $Ni_{0.75}Cu_{0.25}O$ phases. The reduction curves of NiO–CuO/SBA-15(IM) possesses three peaks (Fig. 5). The peaks located at 286 °C and 304 °C can be assigned to the

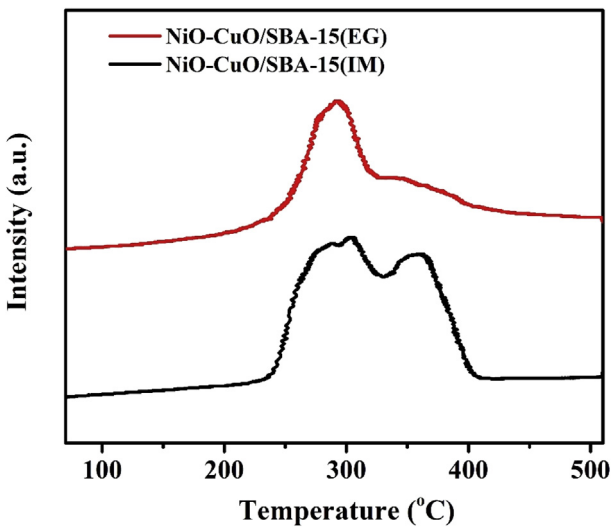

Fig. 5 – H_2-TPR profiles of the catalysts.

Please cite this article as: Fang C et al., Highly dispersed Ni–Cu nanoparticles on SBA-15 for selective hydrogenation of methyl levulinate to γ-valerolactone, International Journal of Hydrogen Energy, https://doi.org/10.1016/j.ijhydene.2019.03.272

reduction of CuO and $Ni_{0.75}Cu_{0.25}O$ species having a weak or negligible interaction with the silica [50,51]. The third H_2 consumption peak centered at 357 °C is ascribable to the reduction of $Ni_{0.75}Cu_{0.25}O$ which strongly interact with the silica [52,53]. The observed shift of reduction peaks to lower temperature can be describable to formation of $Ni_xCu_{1-x}O$ solid solution [34,52,54]. Next, the reduction profile of NiO–CuO/SBA-15 (EG) is composed of one reduction peak situated at 290 °C with a weak shoulder peak centered at 335 °C, corresponding to the reduction of the well dispersed $Ni_xCu_{1-x}O$ species which have weak and enhanced interaction, respectively. In H_2-TPR, the area of the reduction peak, corresponding to the consumption of H_2, directly reveals the amount of the reducible species [55,56]. The area of the reduction peak of NiO–CuO/SBA-15(IM) is larger than that of NiO–CuO/SBA-15 (EG), implying more surface reducible oxides on NiO–CuO/SBA-15(IM).

XAS analysis

XAS measurements were performed at the K-edge of copper and nickel to obtain information on the geometry and oxidation state changes during the in-situ reduction process. Fig. 6a1 and Fig. 6b1 depict the normalized K-edge XANES spectra of the reference materials, while Fig. 6a2-3 and Fig. 6b2-3 show the *in situ* XANES spectra of different NiO–CuO/SBA-15 samples. With the increasing of temperature during the reduction process, decreased white line intensity and increased edge of all the NiO–CuO/SBA-15 samples are observed, indicating that Ni^{2+} and Cu^{2+} are gradually reduced to metallic Ni and Cu. Linear combination fittings (insets) reveal that the Ni^{2+} and Cu^{2+} species in NiO–CuO/SBA-15 (EG) were both partially reduced under H_2 atmosphere even when the reduction temperature was raised to 500 °C, while the Ni^{2+} and Cu^{2+} species in NiO–CuO/SBA-15(IM) were almost fully reduced. Combining TEM and H_2-TPR results, it is reasonable

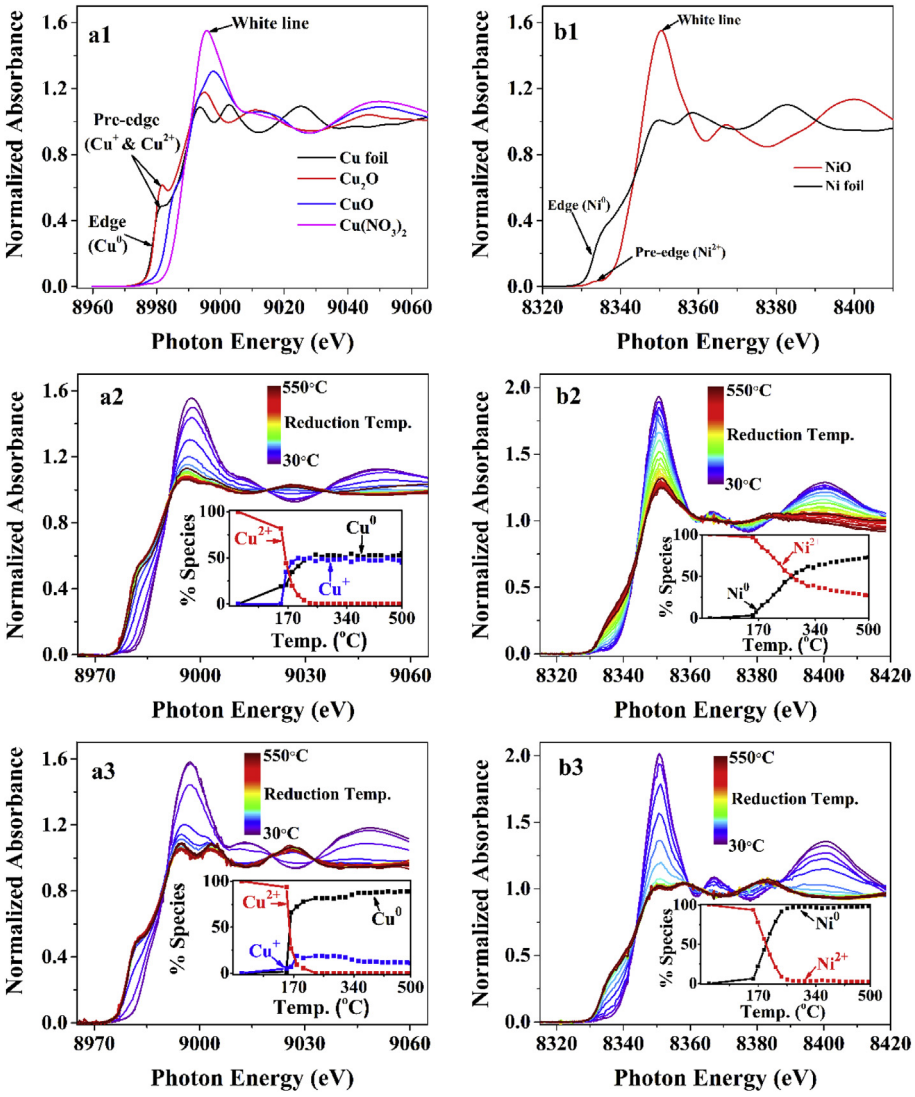

Fig. 6 – Normalized K-edge *in situ* XANES spectra of different samples: a-Cu K-edge; b-Ni K-edge; 1-reference materials; 2-NiO–CuO/SBA-15 (EG); 3-NiO–CuO/SBA-15(IM). (Inset: enlarged spectra and linear combination fitting result.)

Please cite this article as: Fang C et al., Highly dispersed Ni–Cu nanoparticles on SBA-15 for selective hydrogenation of methyl levulinate to γ-valerolactone, International Journal of Hydrogen Energy, https://doi.org/10.1016/j.ijhydene.2019.03.272

to deduce that the unreduced Ni^{2+} and Cu^{2+} species in NiO–CuO/SBA-15 (EG) should arise from the small $Ni_xCu_{1-x}O$ nanoparticles immobilized in the mesoporous channels with an intimate contact to the support.

Fig. 7 demonstrates the Cu K-edge and Ni K-edge magnitude of Fourier transform (FT) of the reduced NiO–CuO/SBA-15 catalysts measured at room temperature and Table 2 shows the local coordination structures and the fits of the k^2-weighted FT data of the reduced catalysts. The coordination number of metal atoms and bond distances between metal-oxygen atoms were only found in Cu K-edge indicated that copper ions were not completely reduced, as evidence by the XANES results. It is clear from the FT EXAFS oscillation that NiO–CuO/SBA-15 (EG) exhibited longer distance as well as smaller coordination number than NiO–CuO/SBA-15(IM), representing a smaller metal cluster. This could be ascribed that the NiO–CuO/SBA-15 (EG) contains well dispersed nanoparticles on the SBA-15 support.

All the characterizations: XRD, TEM, *in situ* XAS, N_2 sorption analysis, and H_2-TPR, confirm that the metal nanoparticles on Ni–Cu/SBA-15 (EG) are smaller, more homogeneously mixed, and well-dispersed throughout the entire SBA-15 support when compared to the nanoparticles on Ni–Cu/SBA-15(IM). These superior characteristics were achieved by using glycol-assisted impregnation process instead of a conventional aqueous impregnation process. During the glycol-assisted impregnation process, ethylene glycol coordinates with the metal species and transports them into the mesopores by capillary force [41,57]. Then by heat treating the sample in an inert condition, the polyol is decomposed to carbon, providing a spacer between metal species and immobilizing the metal species to the wall of mesoporous silica support. Lastly, the calcination in air completely removes the carbon and oxidizes the metal species to oxide nanoparticles. Hence, these metal oxide particles on NiO–CuO/SBA-15 (EG) are small, located further apart from each other, and mainly exist inside the pore network. On the contrary, in the NiO–CuO/SBA-15(IM) sample which utilized water as a solvent, the CuO and $Ni_xCu_{1-x}O$ particles are much larger and mostly appear on the outside of the silica pores. Different preparation methods lead to the variation in dispersion and particle size distribution of the active metal components, which might result in the disparity of hydrogenation performance.

Table 2 – EXAFS fits on different *in situ*-reduced NiO–CuO/SBA-15 catalysts.

Sample	Scatter	CN	R (Å)	σ^2 (Å^2)	E_0 (eV)
in situ-reduced	Cu–O	1.36	1.96	0.009	10.94
NiO–CuO/SBA-15 (EG)	Cu–Cu	7.95	2.60	0.008	
	Ni–Ni	10.3	2.49	0.011	−2.92
in situ-reduced	Cu–O	1.84	1.84	0.017	−2.59
NiO–CuO/SBA-15(IM)	Cu–Cu	10.50	2.50	0.025	
	Ni–Ni	11.3	2.48	0.009	−4.47

CN = coordination numbers, R = interatomic distances, σ^2 = Debye-Waller factors, E_0 = energy shifts.

Catalytic results of ML hydrogenation

The catalytic transfer hydrogenation activities of methyl levulinate to γ-valerolactone on Ni–Cu/SBA-15 (EG) and Ni–Cu/SBA-15(IM) catalysts are shown in Fig. 8. It was reported that the hydrogenation activity could be dependent on the reaction temperature – the higher temperature gave higher conversion, but lower selectivity [17,31,58]. Interestingly, the reaction temperature did not dramatically affect the hydrogenation activities of methyl levulinate over Ni–Cu/SBA-15 (EG). The ML conversion and GVL yield reached 94.2% and 87.3% within 3 h at 170 °C. At the lower temperature of 140 °C, the ML conversion and GVL yield still reached 91.3% and 81.8% (only 5.5% decline in GVL yield). When the reaction temperature dropped from 170 to 140 °C, the selectivity of GVL decreased by

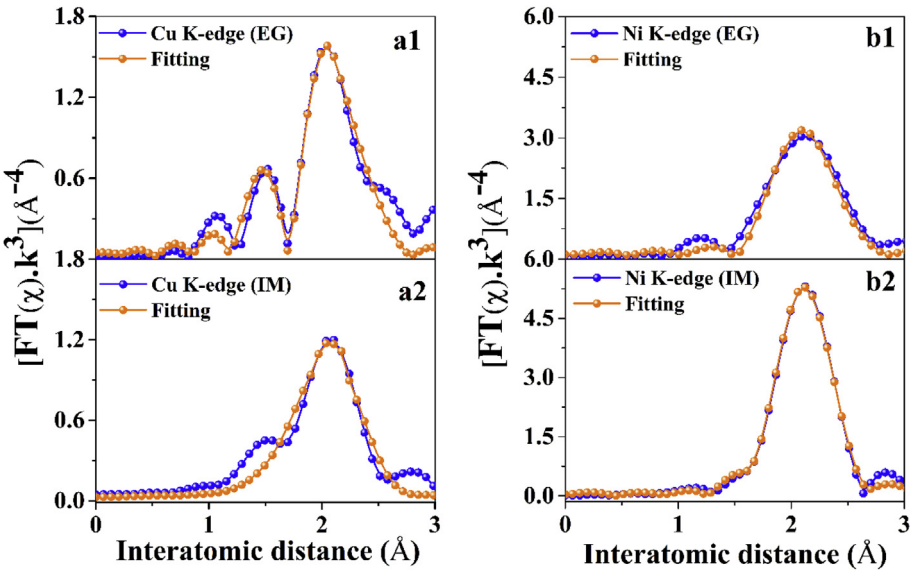

Fig. 7 – (a1-a2) Cu K-edge and (b1-b2) Ni K-edge magnitude of Fourier transform of *in situ* reduced NiO–CuO/SBA-15 catalysts after cooling down to room temperature.

Please cite this article as: Fang C et al., Highly dispersed Ni–Cu nanoparticles on SBA-15 for selective hydrogenation of methyl levulinate to γ-valerolactone, International Journal of Hydrogen Energy, https://doi.org/10.1016/j.ijhydene.2019.03.272

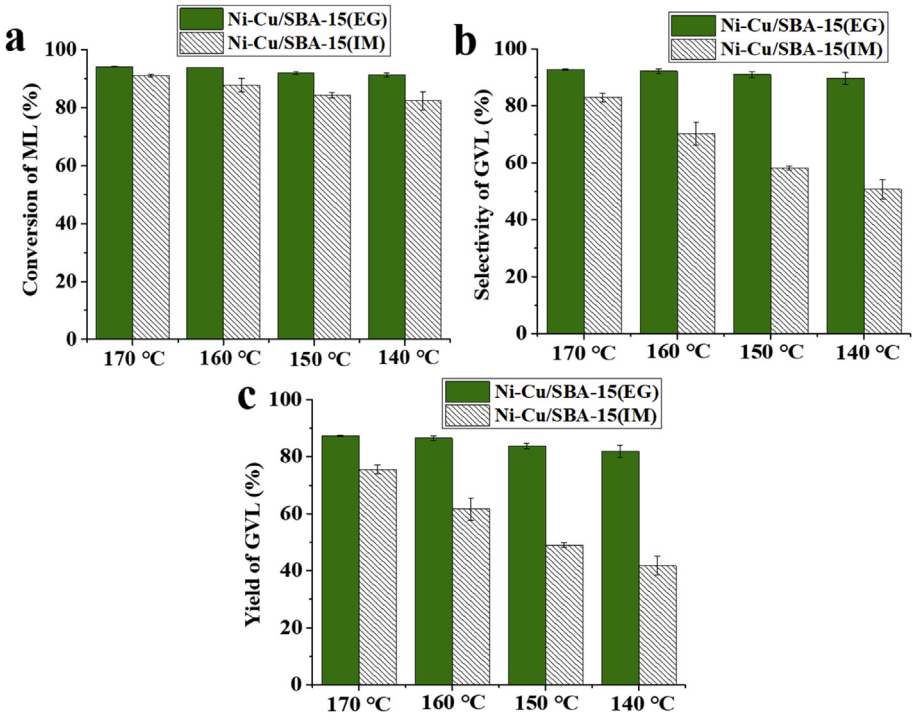

Fig. 8 – Catalytic activity of Ni–Cu/SBA-15 (EG) and Ni–Cu/SBA-15(IM) catalysts for catalytic transfer hydrogenation of ML at different reaction temperature. Reaction conditions: catalyst, 0.1 g; 2-propanol 24 mL; methyl levulinate/2-propanol = 0.02 mol/L; reaction time, 3 h.

only 3% with value remained around 90%. These results indicate that decreasing the temperature does not significantly reduce the catalytic activity of Ni–Cu/SBA-15 (EG). This catalyst shows excellent catalytic efficiency in shorter time at lower temperature compared to other catalysts reported in the previous literature [34,36]. In contrast, the hydrogenation performance of Ni–Cu/SBA-15(IM) is highly sensitive to reaction temperature. The Ni–Cu/SBA-15(IM) provided lower ML conversion and GVL yield than that of Ni–Cu/SBA-15 (EG) in the range of 140–170 °C. The ML conversion of Ni–Cu/SBA-15(IM) decreased drastically with respect to the decrease in reaction temperature from 91.1% at 170 °C to 82.4% at 140 °C. As the reaction temperature decreased, the selectivity of GVL severely dropped 32%. The corresponding GVL yield dropped from 75.6% to 41.8%, which means about 24% of the GVL yield was lost when the temperature is reduced by 30 °C. This result showed that more side-reactions would proceed over the Ni–Cu/SBA-15(IM) at lower temperatures which presumably due to the larger particle side of Ni–Cu species located outside the pore structures. The result suggested that Ni–Cu alloy species might be more selective towards GVL than individual species of Ni or Cu. In addition, it was considered that the confinement effect of alloy nanoparticles in the silica channel reactor would help suppress the side reactions. It was reported that the single metal particles of Ni or Cu gave lower activity and selectivity towards GVL as compared to Cu–Ni alloy species [59]. Clearly, Ni–Cu/SBA-15 (EG) catalyst exhibited higher and more stable ML conversion and GVL yield than Ni–Cu/SBA-15(IM) in the low temperature range. The highly dispersed Ni–Cu nanoparticle apparently leads to a superior performance for the production of γ-valerolactone at low reaction temperature.

As it is shown in Scheme 1, the catalytic transfer hydrogenation of ML in 2-propanol could yield GVL and give methanol as a byproduct. Moreover, 2-propanol was partially dehydrogenated to form acetone during the reaction.

It could be obviously observed in Table 3 that the Ni–Cu/SBA-15 (EG) requires lower reaction temperature as well as shorter reaction time to provide comparable catalytic behaviors as other previously reported catalysts for GVL production. Our catalyst showed high GVL yield of 81.9% even at low reaction temperature of 140 °C and 3 h. It could also see that the Cu/SBA-15 (EG), Ni/SAB-15 (EG), and Ni–Cu/SAB-15 (EG) showed slight difference in catalytic properties. Both Ni/SAB-15 (EG), and Ni–Cu/SAB-15 (EG) showed higher ML conversion than Cu/SBA-15 (EG) while Ni–Cu/SAB-15 (EG) seemed to be

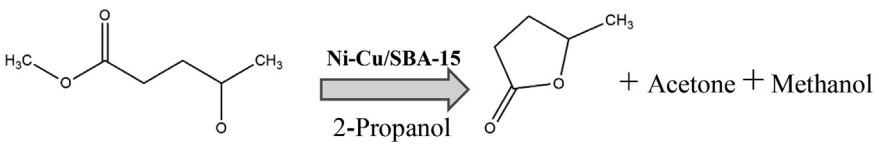

Scheme 1 – Reaction scheme of ML conversion to GVL over Ni–Cu/SBA-15 [60].

Please cite this article as: Fang C et al., Highly dispersed Ni–Cu nanoparticles on SBA-15 for selective hydrogenation of methyl levulinate to γ-valerolactone, International Journal of Hydrogen Energy, https://doi.org/10.1016/j.ijhydene.2019.03.272

Table 3 – Comparative catalytic properties of Ni–Cu/SBA-15 (EG) and Ni–Cu/SBA-15(IM) catalysts with previously reported catalysts.

Catalysts	ML/EL/LA Conversion (%)	GVL Selectivity (%)	GVL Yield (%)	Reaction temperature (°C)	Reaction time (h)	Reference
Ni–Cu/SBA-15(IM)	91.1	82.9	75.6	170	3	This work
Ni–Cu/SBA-15 (EG)	94.2	92.7	87.3	170	3	This work
Ni/SBA-15 (EG)	94.4	90.4	85.4	170	3	This work
Cu/SBA-15 (EG)	87.0	90.6	78.8	170	3	This work
Ni–Cu/SBA-15 (EG)	91.3	89.7	81.9	140	3	This work
Ni–Cu/Al_2O_3(WI)	100	–	~90	250	2	[61]
Ni(23%)-Cu(12%)/ Al_2O_3	100	–	77	250	1	[62]
10Cu–5Ni/Al_2O_3	100	–	97	150	12	[59]
CuNi@SiO_2–B	–	–	66.3	120	9	[63]
10Cu–5Ni/SiO_2	0	–	0	150	12	[59]

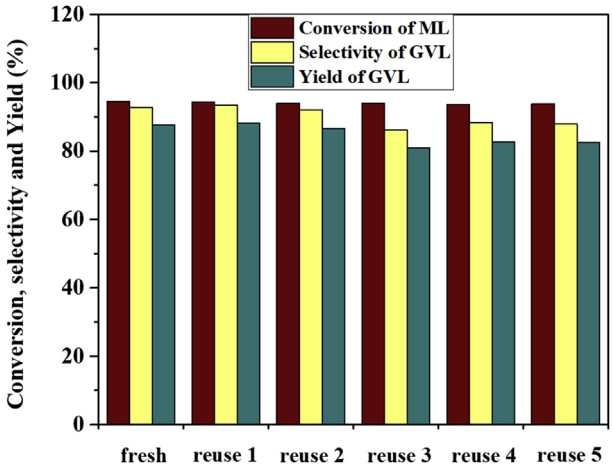

Fig. 9 – Reusability of Ni–Cu/SBA-15 (EG) catalyst. Reaction conditions: catalyst, 0.1 g; 2-propanol 24 mL; methyl levulinate/2-propanol = 0.02 mol/L; reaction temperature, 170 °C; reaction time, 3 h.

the most selective catalyst for GVL production. This could imply that Cu, Ni, and Ni–Cu could act as active centers for ML conversion but the presence of Ni is more preferable. On the other hand the presence of Cu could enhance the GVL selectivity in the Ni–Cu/SAB-15 (EG). It was reported that the alumina-supported Ni–Cu catalysts showed GVL yield of 77% [62] and 90% [61] at high reaction temperature of 250 °C. The product yield of 97% was reported over the 10Cu–5Ni/Al_2O_3 with much longer reaction time of 12 h as compared to our catalyst system [59]. The silica-supported Ni–Cu catalysts typically showed lower activity than the alumina-supported ones, while the structural property of silica and the catalyst preparation methods seemed to have considerable effects on the CTH reaction [59,63].

Reusability of the catalyst

The reusability of Ni–Cu/SBA-15 (EG) catalyst was also studied in view of its excellent performance in the CTH reaction, and the results are shown in Fig. 9. The spent catalyst was separated from the product by centrifugation and then used for the next run without further activation. ML conversion around 94% was achieved in all the runs. Moreover, Ni–Cu/SBA-15 (EG) exhibited very stable selectivity and yield of GVL in the first 3 cycles and declined slightly in the next 3 runs. GVL yield can be maintained at 82.5% even in the 6th run. The data shows that the Ni–Cu/SBA-15 (EG) catalyst did not suffer from severe deactivation under the relatively harsh conditions, demonstrating great stability during the hydrogenation process. During the catalytic transfer hydrogenation of ML, two-dimensional hexagonal mesoporous channels restricted the diffusion of the metal nanoparticles in the channel, repressing the agglomeration as well as leaching of metal nanoparticles into the reaction solution. This could be the possible reason that the Ni–Cu/SBA-15 (EG) catalyst exhibited excellent stability during the hydrogenation process. Cai et al. [59] reported that the Cu–Ni catalyst system exhibited excellent stability than the Cu or Ni single element due to the lower sintering rate or carbon formation. The Cu–Ni combined species showed good stability toward oxidation.

The metal leaching of Ni–Cu/SBA-15 (EG) catalyst during the reactions was investigated by determining the concentration of Ni and Cu in the reaction solutions via ICP, and the results are depicted in Table 4. It turned out that the concentration of both Ni and Cu in the reaction solutions was extremely low during all the recycling times. The maximum value of metal leaching is less than 250 ppb, which is much lower than the results of non-noble metal catalysts that were used in a similar condition reported previously [16,29,64–67]. The low metal leaching rate might be due to the confinement

Table 4 – ICP-AES analysis of reaction solution after reusability tests of Ni–Cu/SBA-15 (EG) catalyst.

Solution after reaction	Fresh	Reuse 1	Reuse 2	Reuse 3	Reuse 4	Reuse 5
Ni leaching (ppb)	3.5	3.5	5.4	4.7	33.3	193.3
Cu leaching (ppb)	15.8	25.4	27.1	17.0	46.3	237.8

Please cite this article as: Fang C et al., Highly dispersed Ni–Cu nanoparticles on SBA-15 for selective hydrogenation of methyl levulinate to γ-valerolactone, International Journal of Hydrogen Energy, https://doi.org/10.1016/j.ijhydene.2019.03.272

effect of the ordered mesoporous silica support and the formation of $Ni_xCu_{1-x}O$ solid solution, leading to a low deactivation rate of Ni–Cu/SBA-15 (EG). Hence, only slight decrease in GVL yield was observed in Fig. 9 which could arise from catalyst loss between runs and/or mild aggregation of metal nanoparticles.

Conclusions

In summary, our work presents a practical glycol-assisted impregnation method for the synthesis of well dispersed Ni–Cu nanoparticles on SBA-15. A highly efficient Ni–Cu/SBA-15 (EG) catalyst was successfully prepared and found to exhibit much better catalytic activity in the CTH reaction by using 2-propanol as the H-donor at 140–170 °C than the Ni–Cu/SBA-15 synthesized by conventional aqueous impregnation method, providing higher ML conversion of 91.3% with greater GVL selectivity of 89.7% at 140 °C for 3 h. Characterization of the catalysts showed that small particle size, high homogeneity in metal composition, and even distribution of the metal nanoparticles on the mesoporous substrate were responsible for the high reactivity of the Ni–Cu/SBA-15 (EG) catalyst. Our catalyst retained fairly high reaction efficiency during the recycling test and can be reused at least 5 times without drastic loss in catalytic activity and yield towards GVL formation. The excellent stability could be ascribed to the restricted diffusion of the metal nanoparticles in the channel, repressed agglomeration as well as leaching of metal nanoparticles into the reaction solution. Therefore, the developed Ni–Cu/SBA-15 catalyst is a promising candidate for selective hydrogenation of ML to GVL under mild conditions without using external H_2.

Acknowledgements

The authors acknowledge the financial support from the Thailand Research Fund, the National Nanotechnology Center (NANOTEC), and the Synchrotron Light Research Institute (SLRI) (BRG6080015 and TRG6080004). Also, this work has been partially supported by the Research Network NANOTEC (RNN) program of the National Nanotechnology Center (NANOTEC), NSTDA, Ministry of Science and Technology, Thailand.

REFERENCES

[1] Ragauskas AJ, Williams CK, Davison BH, Britovsek G, Cairney J, Eckert CA, Frederick WJ, Hallett JP, Leak DJ, Liotta CL, Mielenz JR, Murphy R, Templer R, Tschaplinski T. The path forward for biofuels and biomaterials. Science 2006;311:484–9.
[2] Huber GW, Corma A. Synergies between bio- and oil refineries for the production of fuels from biomass. Angew Chem Int Ed 2007;46:7184–201.
[3] Huang YB, Yang T, Luo YJ, Liu AF, Zhou YH, Pan H, Wang F. Simple and efficient conversion of cellulose to γ-valerolactone through an integrated alcoholysis/transfer hydrogenation system using Ru and aluminium sulfate catalysts. Catal Sci Technol 2018;8:6252–62.
[4] Wachała M, Grams J, Kwapinski W, Ruppert AM. Influence of ZrO_2 on catalytic performance of Ru catalyst in hydrolytic hydrogenation of cellulose towards γ-valerolactone. Int J Hydrogen Energy 2016;41:8688–95.
[5] Liguori F, Moreno-Marrodan C, Barbaro P. Environmentally friendly synthesis of γ-valerolactone by direct catalytic conversion of renewable sources. ACS Catal 2015;5:1882–94.
[6] Bond JQ, Alonso DM, Wang D, West RM, Dumesic JA. Integrated catalytic conversion of γ-valerolactone to liquid alkenes for transportation fuels. Science 2010;327:1110–4.
[7] Lange JP, Price R, Ayoub PM, Louis J, Petrus L, Clarke L, Gosselink H. Valeric biofuels: a platform of cellulosic transportation fuels. Angew Chem Int Ed 2010;49:4479–83.
[8] Du XL, Bi QY, Liu YM, Cao Y, He HY, Fan KN. Tunable copper-catalyzed chemoselective hydrogenolysis of biomass-derived [gamma]-valerolactone into 1,4-pentanediol or 2-methyltetrahydrofuran. Green Chem 2012;14:935–9.
[9] Horvath IT, Mehdi H, Fabos V, Boda L, Mika LT. [gamma]-Valerolactone-a sustainable liquid for energy and carbon-based chemicals. Green Chem 2008;10:238–42.
[10] Jessop PG. Searching for green solvents. Green Chem 2011;13:1391–8.
[11] Upare PP, Lee JM, Hwang DW, Halligudi SB, Hwang YK, Chang JS. Selective hydrogenation of levulinic acid to γ-valerolactone over carbon-supported noble metal catalysts. J Ind Eng Chem 2011;17:287–92.
[12] Unlu D, Hilmioglu ND. Applicability of a TSA/ZrO_2 catalytic membrane for the production of ethyl levulinate as raw material of gamma-valerolactone. Int J Hydrogen Energy 2017;42:21487–94.
[13] Zhang R, Ma Y, You F, Peng T, He Z, Li K. Exploring to direct the reaction pathway for hydrogenation of levulinic acid into γ-valerolactone for future Clean-Energy Vehicles over a magnetic Cu-Ni catalyst. Int J Hydrogen Energy 2017;42:25185–94.
[14] Kasar GB, Date NS, Bhosale PN, Rode CV. Steering the ester and γ-valerolactone selectivities in levulinic acid hydrogenation. Energy Fuels 2018;32:6887–900.
[15] Yang Z, Huang YB, Guo QX, Fu Y. RANEY(R) Ni catalyzed transfer hydrogenation of levulinate esters to gamma-valerolactone at room temperature. Chem Commun 2013;49:5328–30.
[16] Hengne AM, Rode CV. Cu-ZrO_2 nanocomposite catalyst for selective hydrogenation of levulinic acid and its ester to [gamma]-valerolactone. Green Chem 2012;14:1064–72.
[17] Zhou H, Song J, Fan H, Zhang B, Yang Y, Hu J, Zhu Q, Han B. Cobalt catalysts: very efficient for hydrogenation of biomass-derived ethyl levulinate to gamma-valerolactone under mild conditions. Green Chem 2014;16:3870–5.
[18] Du XL, Bi QY, Liu YM, Cao Y, Fan KN. Conversion of biomass-derived levulinate and formate esters into γ-valerolactone over supported gold catalysts. ChemSusChem 2011;4:1838–43.
[19] Wang X, Rinaldi R. Exploiting H-transfer reactions with RANEY Ni for upgrade of phenolic and aromatic biorefinery feeds under unusual, low-severity conditions. Energy Environ Sci 2012;5:8244–60.
[20] Braden DJ, Henao CA, Heltzel J, Maravelias CC, Dumesic JA. Production of liquid hydrocarbon fuels by catalytic conversion of biomass-derived levulinic acid. Green Chem 2011;13:1755–65.
[21] Molleti J, Tiwari MS, Yadav GD. Novel synthesis of Ru/OMS catalyst by solvent-free method: selective hydrogenation of levulinic acid to γ-valerolactone in aqueous medium and kinetic modelling. Chem Eng J 2018;334:2488–99.

Please cite this article as: Fang C et al., Highly dispersed Ni–Cu nanoparticles on SBA-15 for selective hydrogenation of methyl levulinate to γ-valerolactone, International Journal of Hydrogen Energy, https://doi.org/10.1016/j.ijhydene.2019.03.272

[22] Nemanashi M, Noh J, Meijboom R. Hydrogenation of biomass-derived levulinic acid to γ-valerolactone catalyzed by mesoporous supported dendrimer-derived Ru and Pt catalysts: an alternative method for the production of renewable biofuels. Appl Catal A Gen 2018;550:77–89.
[23] Lin Z, Luo M, Zhang Y, Wu X, Fu Y, Zhang F, Zhu W. Coupling Ru nanoparticles and sulfonic acid moieties on single MIL-101 microcrystals for upgrading methyl levulinate into γ-valerolactone. Appl Catal A Gen 2018;563:54–63.
[24] Moustani C, Anagnostopoulou E, Krommyda K, Panopoulou C, Koukoulakis KG, Bakeas EB, Papadogianakis G. Novel aqueous-phase hydrogenation reaction of the key biorefinery platform chemical levulinic acid into γ-valerolactone employing highly active, selective and stable water-soluble ruthenium catalysts modified with nitrogen-containing ligands. Appl Catal B Environ 2018;238:82–92.
[25] Cao XJ, Wei JN, Liu H, Lv XY, Tang X, Zeng XH, Sun Y, Lei TZ, Liu SJ, Lin L. Hydrogenation of methyl levulinate to γ-valerolactone over Cu—Mg oxide using MeOH as in situ hydrogen source. J Chem Technol Biotechnol 2019;94:167–77.
[26] Zhang CT, Huo ZB, Ren DZ, Song ZY, Liu YJ, Jin FM, Zhou WN. Catalytic transfer hydrogenation of levulinate ester into γ-valerolactone over ternary Cu/ZnO/Al_2O_3 catalyst. J Energy Chem 2018;000:1–9.
[27] Geboers J, Wang X, Carvalho AB, Rinaldi R. Densification of biorefinery schemes by H-transfer with Raney Ni and 2-propanol: a case study of a potential avenue for valorization of alkyl levulinates to alkyl γ-hydroxypentanoates and γ-valerolactone. J Mol Catal A Chem 2014;388–389:106–15.
[28] Mohan V, Raghavendra C, Pramod CV, Raju BD, Rama Rao KS. Ni/H-ZSM-5 as a promising catalyst for vapour phase hydrogenation of levulinic acid at atmospheric pressure. RSC Adv 2014;4:9660–8.
[29] Hengne AM, Kadu BS, Biradar NS, Chikate RC, Rode CV. Transfer hydrogenation of biomass-derived levulinic acid to γ-valerolactone over supported Ni catalysts. RSC Adv 2016;6:59753–61.
[30] Mohan V, Venkateshwarlu V, Pramod CV, Raju BD, Rao KSR. Vapour phase hydrocyclisation of levulinic acid to γ-valerolactone over supported Ni catalysts. Catal Sci Technol 2014;4:1253–9.
[31] Grilc M, Likozar B. Levulinic acid hydrodeoxygenation, decarboxylation and oligmerization over NiMo/Al_2O_3 catalyst to bio-based value-added chemicals: modelling of mass transfer, thermodynamics and micro-kinetics. Chem Eng J 2017;330:383–97.
[32] Zhang B, Chen Y, Li J, Pippel E, Yang H, Gao Z, Qin Y. High Efficiency Cu-ZnO Hydrogenation Catalyst: the tailoring of Cu-ZnO interface sites by molecular layer deposition. ACS Catal 2015;5:5567–73.
[33] Li H, Fang Z, Yang S. Direct conversion of sugars and ethyl levulinate into γ-valerolactone with superparamagnetic acid-base bifunctional $ZrFeO_x$ nanocatalysts. ACS Sustain Chem Eng 2016;4:236–46.
[34] Upare PP, Jeong MG, Hwang YK, Kim DH, Kim YD, Hwang DW, Lee UH, Chang J-S. Nickel-promoted copper–silica nanocomposite catalysts for hydrogenation of levulinic acid to lactones using formic acid as a hydrogen feeder. Appl Catal A Gen 2015;491:127–35.
[35] Gupta SSR, Kantam ML. Selective hydrogenation of levulinic acid into γ-valerolactone over Cu/Ni hydrotalcite-derived catalyst. Catal Today 2018;309:189–94.
[36] Zhu J, Tang Y, Tang K. Enhanced hydrogenation of ethyl-levulinate to γ-valerolactone over Ni_8O_x stabilized Cu^+ surface sites. RSC Adv 2016;6:87294–8.
[37] Ren Y, Ma Z, Bruce PG. Ordered mesoporous metal oxides: synthesis and applications. Chem Soc Rev 2012;41:4909–27.
[38] De Vos DE, Dams M, Sels BF, Jacobs PA. Ordered mesoporous and microporous molecular sieves functionalized with transition metal complexes as catalysts for selective organic transformations. Chem Rev 2002;102:3615–40.
[39] Wang L, Han YX, Gao SS, Luo Y, Liu L. Promoted catalytic performance of Ni-SBA-15 catalysts by modifying with Fe and Cu for hydrogenation of levulinic acid to gamma-valerolactone. Reac Kinet Mech Cat 2018;124:389–99.
[40] Fang C, Shi L, Li H, Huang L, Zhang J, Zhang D. Creating hierarchically macro-/mesoporous Sn/CeO_2 for the selective catalytic reduction of NO with NH_3. RSC Adv 2016:78727–36.
[41] Xie T, Shi L, Zhang J, Zhang D. Immobilizing Ni nanoparticles to mesoporous silica with size and location control via a polyol-assisted route for coking- and sintering-resistant dry reforming of methane. Chem Commun 2014;50:7250–3.
[42] Xie T, Zhao X, Zhang J, Shi L, Zhang D. Ni nanoparticles immobilized Ce-modified mesoporous silica via a novel sublimation-deposition strategy for catalytic reforming of methane with carbon dioxide. Int J Hydrogen Energy 2015;40:9685–95.
[43] Zhao DY, Feng JL, Huo QS, Melosh N, Fredrickson GH, Chmelka BF, Stucky GD. Triblock copolymer syntheses of mesoporous silica with periodic 50 to 300 angstrom pores. Science 1998;279:548–52.
[44] Khemthong P, Kongmak C, Faungnawakij K. TH patent, TH1501001426. 2017.
[45] Ravel B, Newville M. ATHENA, ARTEMIS, HEPHAESTUS: data analysis for X-ray absorption spectroscopy using IFEFFIT. J Synchrotron Radiat 2005;12:537–41.
[46] Newville M. EXAFS analysis using FEFF and FEFFIT. J Synchrotron Radiat 2001;8:96–100.
[47] Thommes M, Kaneko K, Neimark AV, Olivier JP, Rodriguez-Reinoso F, Rouquerol J, Sing KSW. Physisorption of gases, with special reference to the evaluation of surface area and pore size distribution (IUPAC Technical Report). Pure Appl Chem 2015;87:9–10.
[48] Varkolu M, Velpula V, Ganji S, Burri DR, Rao Kamaraju SR. Ni nanoparticles supported on mesoporous silica (2D, 3D) architectures: highly efficient catalysts for the hydrocyclization of biomass-derived levulinic acid. RSC Adv 2015;5:57201–10.
[49] Ang ML, Miller JT, Cui Y, Mo L, Kawi S. Bimetallic Ni-Cu alloy nanoparticles supported on silica for the water-gas shift reaction: activating surface hydroxyls via enhanced CO adsorption. Catal Sci Technol 2016;6:3394–409.
[50] Putrakumar B, Nagaraju N, Kumar VP, Chary KVR. Hydrogenation of levulinic acid to γ-valerolactone over copper catalysts supported on γ-Al_2O_3. Catal Today 2015;250:209–17.
[51] Liu Z, Zhou J, Cao K, Yang W, Gao H, Wang Y, Li H. Highly dispersed nickel loaded on mesoporous silica: one-spot synthesis strategy and high performance as catalysts for methane reforming with carbon dioxide. Appl Catal B Environ 2012;125:324–30.
[52] Yin A, Wen C, Guo X, Dai WL, Fan K. Influence of Ni species on the structural evolution of Cu/SiO_2 catalyst for the chemoselective hydrogenation of dimethyl oxalate. J Catal 2011;280:77–88.
[53] Khromova SA, Smirnov AA, Bulavchenko OA, Saraev AA, Kaichev VV, Reshetnikov SI, Yakovlev VA. Anisole hydrodeoxygenation over Ni–Cu bimetallic catalysts: the effect of Ni/Cu ratio on selectivity. Appl Catal A Gen 2014;470:261–70.
[54] De Rogatis L, Montini T, Lorenzut B, Fornasiero P. Ni_xCu_y/Al_2O_3 based catalysts for hydrogen production. Energy Environ Sci 2008;1:501–9.
[55] Fang C, Zhang DS, Cai SX, Zhang L, Huang L, Li HR, Maitarad P, Shi LY, Gao RH, Zhang JP. Low-temperature

Please cite this article as: Fang C et al., Highly dispersed Ni–Cu nanoparticles on SBA-15 for selective hydrogenation of methyl levulinate to γ-valerolactone, International Journal of Hydrogen Energy, https://doi.org/10.1016/j.ijhydene.2019.03.272

selective catalytic reduction of NO with NH_3 over nanoflaky MnO_x on carbon nanotubes in situ prepared via a chemical bath deposition route. Nanoscale 2013;5:9199–207.
[56] Ali S, Chen L, Yuan F, Li R, Zhang T, Bakhtiar SUH, Leng X, Niu X, Zhu Y. Synergistic effect between copper and cerium on the performance of Cu_x-$Ce_{0.5-x}$-$Zr_{0.5}$ (x=0.1-0.5) oxides catalysts for selective catalytic reduction of NO with ammonia. Appl Catal B Environ 2017;210:223–34.
[57] Park JH, Kim SK, Kim HS, Cho YJ, Park J, Lee KE, Yoon CW, Nam SW, Kang SO. Convenient metal embedment into mesoporous silica channels for high catalytic performance in AB dehydrogenation. Chem Commun 2013;49:10832–4.
[58] Wettstein SG, Alonso DM, Chong Y, Dumesic JA. Production of levulinic acid and gamma-valerolactone (GVL) from cellulose using GVL as a solvent in biphasic systems. Energy Environ Sci 2012;5:8199–203.
[59] Cai B, Zhou XC, Miao YC, Luo JY, Pan H, Huang YB. Enhanced catalytic transfer hydrogenation of ethyl levulinate to γ-valerolactone over a robust Cu–Ni bimetallic catalyst. ACS Sustain Chem Eng 2017;5:1322–31.
[60] Chompoopitch T, Kajornsak F, Sanchai K, Teera B, Noriaki S, Tawatchai C. A novel catalyst of Ni hybridized with single-walled carbon nanohorns for converting methyl levulinate to γ-valerolactone. Appl Surf Sci 2018. https://doi.org/10.1016/j.apsusc.2018.04.054.
[61] Obregón I, Corro E, Izquierdo U, Requies J, Arias PL. Levulinic acid hydrogenolysis on Al_2O_3-based Ni-Cu bimetallic catalysts. Chin J Catal 2014;35:656–62.
[62] Obregon I, Gandarias I, Al-Shaal MG, Mevissen C, Arias PL, Palkovits R. The role of the hydrogen source on the selective production of γ-valerolactone and 2-methyltetrahydrofuran from levulinic acid. ChemSusChem 2016;9:1–9.
[63] Pendem S, Mondal I, Shrotri A, Rao BS, Lingaiah N, Mondal J. Unraveling the structural properties and reactivity trends of Cu–Ni bimetallic nanoalloy catalysts for biomass-derived levulinic acid hydrogenation. Sustain Energy Fuels 2018;2:1516–29.
[64] Upare PP, Lee JM, Hwang YK, Hwang DW, Lee JH, Halligudi SB, Hwang JS, Chang JS. Direct hydrocyclization of biomass-derived levulinic acid to 2-methyltetrahydrofuran over nanocomposite copper/silica catalysts. ChemSusChem 2011;4:1749–52.
[65] Al-Shaal MG, Wright WRH, Palkovits R. Exploring the ruthenium catalysed synthesis of [gamma]-valerolactone in alcohols and utilisation of mild solvent-free reaction conditions. Green Chem 2012;14:1260–3.
[66] Li W, Xie JH, Lin H, Zhou QL. Highly efficient hydrogenation of biomass-derived levulinic acid to [gamma]-valerolactone catalyzed by iridium pincer complexes. Green Chem 2012;14:2388–90.
[67] Menon PG. Diagnosis of industrial catalyst deactivation by surface characterization techniques. Chem Rev 1994;94:1021–46.

Please cite this article as: Fang C et al., Highly dispersed Ni–Cu nanoparticles on SBA-15 for selective hydrogenation of methyl levulinate to γ-valerolactone, International Journal of Hydrogen Energy, https://doi.org/10.1016/j.ijhydene.2019.03.272

Chapter 5

Hydro-Fractionation for Biomass Upgrading

Sanchai Kuboon, Wasawat Kraithong,
Jaruwan Damaurai and Kajornsak Faungnawakij

Additional information is available at the end of the chapter

http://dx.doi.org/10.5772/intechopen.79396

Abstract

Lignocellulosic biomass is mainly composed of three components including cellulose, hemicellulose, and lignin. A fractionation step is considered as one of the most important preliminary processes for the separation of these three components before their further utilization. Among different separation techniques, water-based pretreatments or hydro-fractionations including (a) subcritical water extraction, (b) supercritical water extraction, and (c) steam explosion have shown their promising advantages both in terms of separation efficiency and in terms of environmental friendliness. Several hydro-fractionation technologies have been developed during the last decade in which each fractionation process has different impacts on the compositional and structural features of biomass. The fractionation principle, current status, and their potential uses in the biorefinery for sugar-based chemical platform production are mainly discussed.

Keywords: lignocellulosic biomass, hydro-fractionation, subcritical water extraction, supercritical water extraction, steam explosion, bio-based product

1. Introduction

The fossil fuel demand from industrialization and domestic utilization has been continually rising, which is in contrast to the depleting supply of petroleum resources that leads to public concerns for the adequacy of long-term energy supply and also environmental issues due to greenhouse gases being drastically released. In addition, the expanding consumption of natural resources also drives the global community to force with economic problems. The replacement of supplies from fossil fuels, which is one of the challenging tasks, has been of intense concern. The use of alternative energy from renewable resources is a promising solution not only for long-term environment sustainability but also in economic aspects. Plant biomass including agricultural, forestry, herbaceous,

and residue, which is a sufficiently abundant natural renewable resource, has been considered as a suitable alternative carbon source that can be converted into useful sustainable products and varieties of chemicals. Among these, the exploitation and utilization of biomass energy have motivated and attracted a great deal of interest from around the world due to a power opportunity to improve energy security, reduce the trade deficit, dramatically lower greenhouse gas emissions, and improve price stability [1]. Besides the advantages mentioned above, agricultural biomass such as crop residues are generated with large quantity annually, making them promising sources for further utilization due to their abundance, diversity, and low-cost. Therefore these potential biomass residues can play important roles as sustainable carbon sources.

The term "lignocellulosic agricultural residues" is used for describing all organic materials which are produced as by-products from harvesting and processing agricultural crops. Chemically, lignocellulosic agricultural residue can be generally regarded as being composed of three polymers including 40–50% of cellulose, which is a major component, 25–30% of hemicellulose, and 15–20% of lignin along with smaller amounts of pectin, protein, nitrogen compounds, and inorganic ingredients [1]. Crystalline and amorphous bundles of cellulose form a skeleton surrounded by the covalently linked matrix of hemicellulose and lignin [2]. These polymers are associated with each other in a hetero-matrix and varying relative compositions depending on the system, type, species, age, stage of growth, and even source of biomass, and they can be in the form of liquids, slurries, or solids. **Figure 1** displays three main components of lignocellulosic biomass.

According to **Figure 1**, each component of lignocellulosic biomass is described below.

Cellulose: the most enormously bountiful biopolymer in the world and the main source of the C6 sugar unit is a linear homo-polysaccharide of D-glucose linked together by β-(1, 4) glycosidic linkages, with cellobiose as the smallest repetitive unit. The long cellulose chains linked together with β-(1, 4) orientation results in the formation of intermolecular and intramolecular hydrogen and van der Waals bonds, which cause cellulose to be packed into microfibrils; they are fine structures bundled up together to form cellulose fibers with highly crystalline structure causing its stable properties, insoluble in water unless at high temperatures or with the presence of a catalyst, and are resistant to enzyme attacks [1, 3].

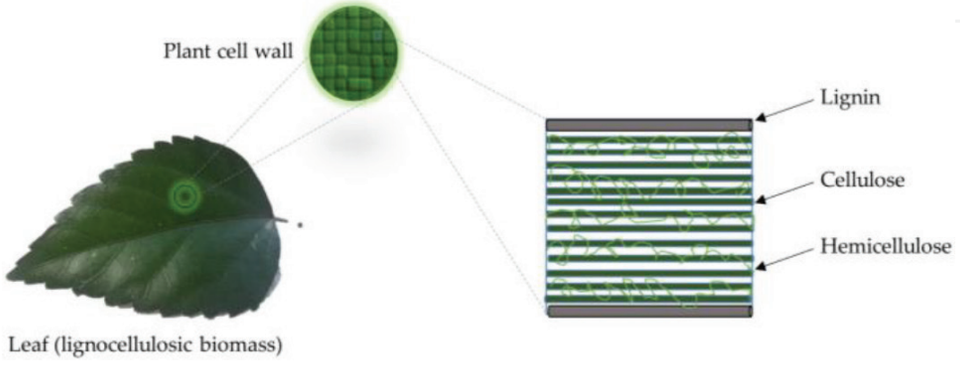

Figure 1. Lignocellulosic biomass composed of cellulose, hemicellulose, and lignin.

http://dx.doi.org/10.5772/intechopen.79396

Hemicellulose: the second most abundant polymer is a complex, random, and amorphous branched carbohydrate comprising of different polysaccharides, including hexoses (D-glucose, D-mannose, D-galactose), pentoses (L-arabinose, D-xylose), and uronic acid with 50–200 units. The backbone of hemicellulose is either a homopolymer or a heteropolymer with short branches linked by β-(1, 4) glycosidic linkage or β-(1, 3) glycosidic linkage and groups of acetates were randomly attached with ester linkages to the hydroxyl groups of the sugar rings [3]. Hemicellulose has a lower molecular weight when compared to cellulose. Moreover, hemicellulose has short lateral chains, which provide linkage between cellulose and lignin, making hemicellulose easier to hydrolyze and degrade into monosaccharides than cellulose [4]. This allows hemicellulose to be removed under mild reaction conditions.

Lignin: it is a complex hydrophobic, large molecular structure containing cross-linked heteropolymers of three different main phenolic components which are trans-p-coumaryl alcohol, trans-coniferyl alcohol, and trans-sinapyl alcohol, which shield the polysaccharide fibers from external environment stress, microbial attacks, and oxidative stress. Lignin is recognized as the cellular glue and encrusting material due to the existence of strong carbon—carbon bond connection (C—C) and ether linkages (C—O—C), which together provide compressive strength to different compositions and individual fibers of lignocellulosic biomass (**Figure 2**).

The high crystallization region, high degree of polymerization, different connection forces between each composition, the protection effect from hemicellulose, and lignin of the lignocellulosic agricultural residue cell wall are stable and make it hard to be degraded for utilization in a further step; therefore, to convert lignocellulosic agricultural residue to biofuels, energy, or chemical platforms, a large number of pretreatment approaches have been investigated on a wide variety of feedstocks to deconstruct and fractionate the complex network structure to its simpler molecules in order to increase the efficiency of biomass composition utilization. Several fractionation technologies have been developed during the last decades. Those methods are usually classified into physical, biological, chemical, and physicochemical pretreatments. The several key properties to take into consideration for low-cost and advanced pretreatment processes are (a) the large amount of yield and harvesting time of feedstock, (b) the large volume of accessible pretreated substrate, (c) less sugar degradation, (d) a minimum number of inhibitors generated after the reaction, (e) a reasonable size and cost of reactor, (f) less solid waste production, (g) effectiveness at low moisture content, and (h) the minimum heat and power requirement [5].

Considering the concerns above, the most cost-effective processes in the biomass upgrading in the industry utilize the dispensable pretreatment and fractionation process where water most

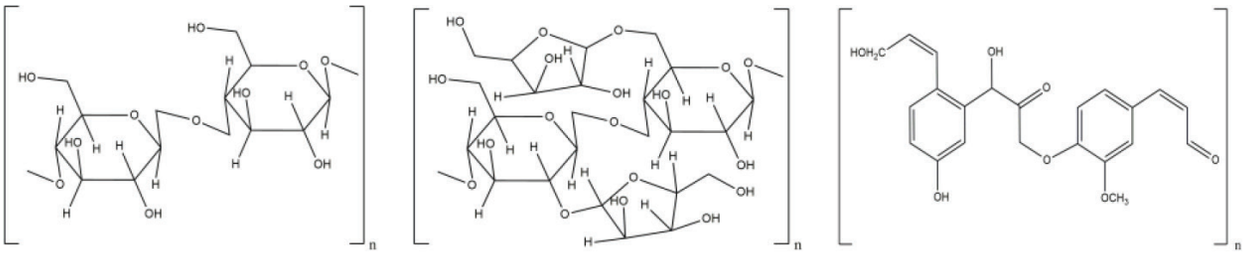

Figure 2. Examples of cellulose (left) hemicellulose (middle) and lignin (right) structures.

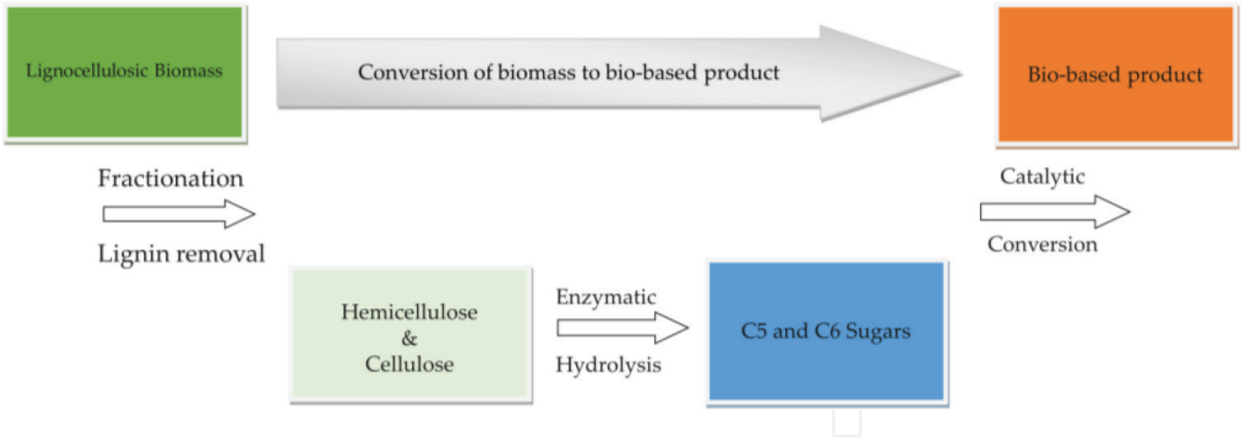

Figure 3. Process for sugar-based chemical platform production from biomass.

certainly takes great effects. The essential function of water in common fractionation includes the following: (a) it acts as a mass transfer medium, (b) it plays as a reactant constructing a mild acidic state due to the mitigation of pKw at an increased temperature, (c) it performs as a heat transfer medium, and (d) it represents as an explosion medium for explosion pretreatment to tear biomass into small pieces. Due to the advantages of water-lignocellulose interaction and efficacy, many attempts have practically focused on applying water into the fractionation process to separate the mixture of lignocellulosic biomass into an individual composition called aqueous fractionation, hydro-based fractionation, or "hydro-fractionation." The overall process of bio-based product production from lignocellulosic biomass is shown in **Figure 3**.

Hydro-fractionations or the processes utilizing water as a medium, reactant, or catalyst for separating mixture compositions including subcritical extraction, supercritical extraction, and steam explosion are mainly discussed in terms of their fractionation principle, current status and potential uses, life cycle and bioeconomy.

2. Principle of hydro-fractionation

2.1. Subcritical and supercritical water extraction

Subcritical and supercritical water extractions have been employed extensively in biomass utilization due to the tunable physical and chemical properties of water, potentially valuable products, and environmental friendliness. Furthermore, these two fractionation methods are known as the promising methods to make the biorefinery concept more practical with sufficient and sustainable profit.

Typically, subcritical water is defined as the use of water at a temperature between the boiling point and critical temperature (373–647 K) under pressure, which is high enough to maintain its liquid state. Supercritical water occurs at a temperature and pressure higher than its critical point (22.1 MPa and 647 K). In the supercritical region, the properties of liquid and vapor fuse [6, 7]. The behavior of subcritical and supercritical water near critical point mainly depends on pressure and temperature; therefore, some important properties of water could be tuned

http://dx.doi.org/10.5772/intechopen.79396

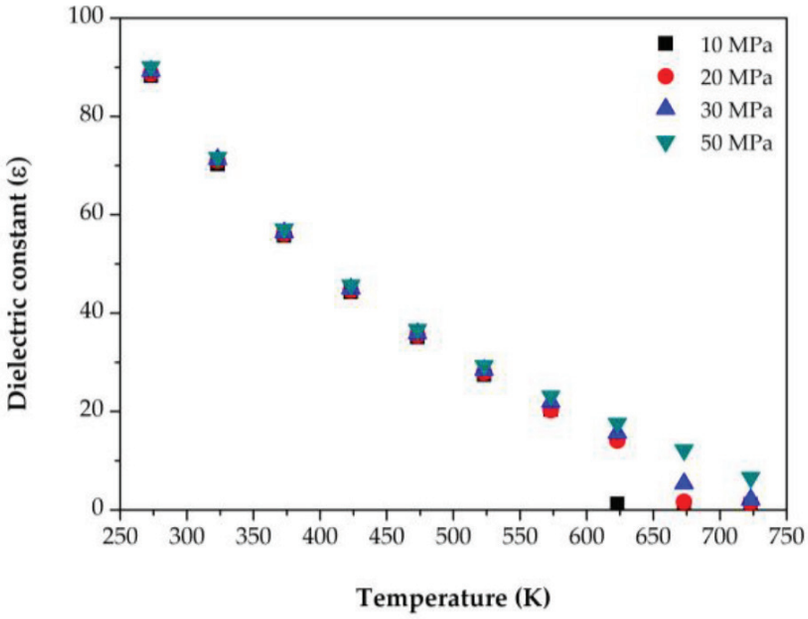

Figure 4. Static dielectric constant of water at various temperatures and pressures [14].

by varying the temperature and pressure for particular conditions of biomass fractionation. In this section, the important properties of water at the subcritical and supercritical state related to biomass fractionation including dielectric constant, ionization constant, density, and viscosity are demonstrated and discussed. A better understanding of water properties under various temperatures and pressures can allow an appropriate experimental design and suitable operating conditions for some specific proposes.

Dielectric constant is a dimensionless value showing the relative permittivity of a material compared with the permittivity of free space. Typically, the high dielectric constant of a solvent means that it has high polarity and vice versa. **Figure 4** shows the influence of temperature and pressure on the dielectric constant. The value of the dielectric constant tends to decrease with the increasing temperatures while it is slightly affected by pressure around the critical point. This phenomenon hints that the polarity of water can be reduced by increasing the temperature which indicated that the solubility of hydrophobic organic compounds and low molecular biopolymers in biomass could be enhanced by using low polarity of water generated at elevated temperatures [8–10]. It is worth mentioning that low polarity of water also reduces the solubility of salt in the process, especially type 2 salts (classified by solubility behavior) such as Na_2SO_4, Na_2CO_3, and K_2SO_4 [11], and the participation of salt might cause fouling that diminishes the efficiency of the process or even terminates the process. Therefore, the water supply should be treated to eliminate type 2 salts before its use in the process; also, a special design of a reactor might be required in case of raw material containing high contents of type 2 salts [12, 13].

The ionization constant of water is the ratio between the concentration of ionic ($[H_3O]^+$ and $[OH]^-$) products and the reactant at the equilibrium condition. The influence of temperature and pressure on the ionization constant is shown in **Figure 5**. In the subcritical region, the ionization constant increases with the raising of temperature and is slightly affected by the increase of pressure. On the other hand, beyond critical temperature, the ionic constant

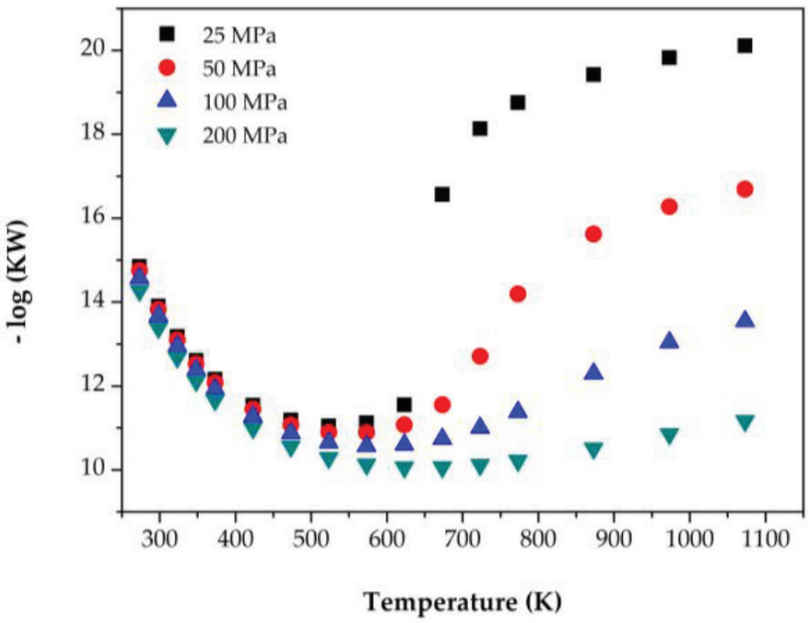

Figure 5. Negative log (base 10) of ionization constant of water at various temperatures and pressures [19].

declines with the increase of reaction temperature and dramatically drops with the reduction of pressure. Therefore, the reaction of biomass degradation takes place in ionic media for subcritical water extraction. On the other hand, the supercritical water extraction provided a radical-oriented environment for biomass fractionation [15–18].

Density of water is defined as the ratio between the mass and volume of water at a specific temperature and pressure. The density of water is decreased with the increase of temperature due to the expansion of the volume. With the increase of pressure, the density of water increases. The higher density of water at specific conditions provides a better chance to penetrate the biomass structure [20].

The viscosity of water is the resistance of water from the external stress such as tensile strength and shear strength. It refers to the resistivity of the water over movement or deformity. The viscosity of water decreased with the increase of temperature but only a slight change was observed when the pressure increased in the subcritical region. However, a more effect of higher pressure was found in the supercritical region on the higher value of viscosity. The viscosity has a direct effect on biomass fractionation. Since the small value of water viscosity provides better wettability of the biomass, the penetration of water to destroy the biomass structure increases (**Figure 6**).

2.2. Steam explosion

Steam explosion, one of the most widely employed hydrothermal technologies for pretreating lignocellulose in industrial applications to convert biomass into useful chemicals, has been recognized as an environmental friendly pretreatment method that can effectively enhance subsequent enzymatic hydrolysis without the necessity of using chemicals, except water, which can lower environmental impact, lower capital investment, bring more potential for energy efficiency, and give rise to less hazardous process chemicals and conditions; this offers several attractive features when compared to hydrolytic acid and oxidative processes. Steam explosion involves exposing wet lignocellulosic biomass to high-pressure saturated steam (0.69–4.83 MPa) and temperature

http://dx.doi.org/10.5772/intechopen.79396

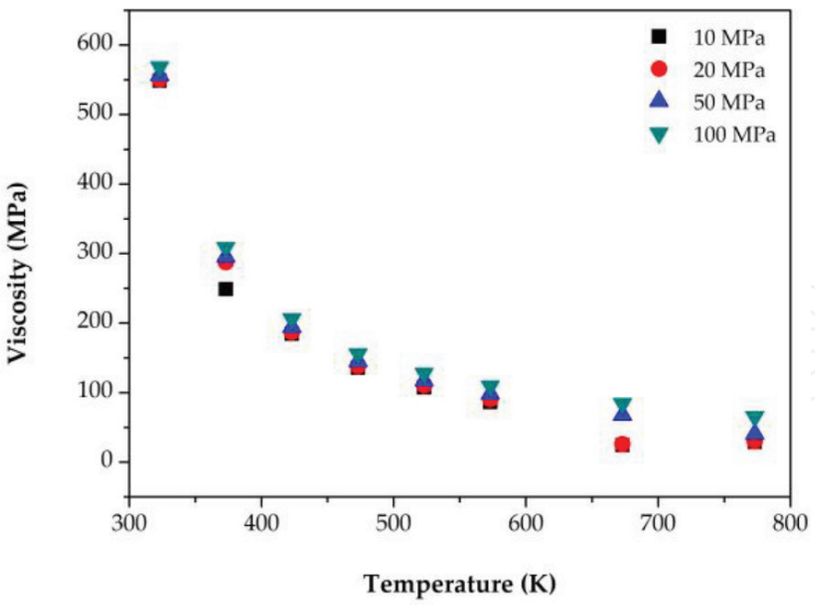

Figure 6. Viscosity of water at various temperatures and pressures [21].

(433–533 K) for a period ranging from seconds to several minutes and then suddenly depressurizing it to atmospheric pressure, making the biomass undergo an explosive decompression. This pretreatment is the combination of mechanical forces and chemical effects due to autohydrolysis of the acetyl group in hemicellulose. Autohydrolysis takes place from the formation of acetic acid from the acetyl group in the hemicellulose structure at high temperature where water acts as an acid at high temperature. The hemicellulose and lignin bonds are cleaved during the explosion, allowing the hemicellulose become water soluble; water-soluble lignin from plant cell wall is also released from the cleavage action into water phase. The mechanical effect is caused by explosive decompression that occurred from suddenly dropped pressure at the termination of the pretreatment, which induced the cell walls in biomass to undergo structural disruption and expansion. Because of these effects, a part of hemicellulose hydrolyzed and solubilized; lignin was redistributed, lignocellulosic matrix polymer was broken down, particle size was decreased, the degree of polymerization was reduced, and porosity was increased; moreover, cellulose was slightly depolymerized, which led to the improvement of lignocellulose digestibility [22–24].

Supercritical extraction in terms of operating conditions, reaction mechanism, and preferred biomass is shown in **Table 1**.

Hydro-fractionation method	Temperature range (K)	Pressure range (MPa)	Fractionation route	Application
Subcritical water extraction	373–647	>0.001 (maintain liquid phase)	Liquid ionic reaction	Extract desired product
Supercritical water extraction	>647	>22.1	Radical reaction	Extract desired product
Steam explosion	433–533	0.69–4.83	Rapid volume expansion of water	Reduce crystallinity of biopolymer

Table 1. Comparison of different hydro-fractionation methods.

3. Current status of hydro-fractionation

3.1. Patent filing of hydro-fractionation technologies

In **Figure 7**, it showed that numbers of filed patents in fields of subcritical and supercritical water extraction and steam explosion technologies have increased from 2007 to 2015. The trend of patent filing of subcritical water extraction decreased in 2016 and was the same number until 2017. On the other hand, more patents were filed in supercritical water extraction and steam explosion after 2015. Quantitatively, it can be seen that the number of filed patents for supercritical water extraction is a lot greater than that of steam explosion and subcritical water extraction. This could be explained by the fact that supercritical water extraction has more versatile applications than the other two technologies. Since this method is not only employed in biomass fractionation, it could be used in coal, oil, polymer, organic and inorganic compounds, nanomaterial, and waste-recycle applications [25].

3.2. Subcritical and supercritical water extraction

With the adjustable properties of water regarding operating temperatures and pressures described earlier, subcritical and supercritical water extraction were applied in many studies to resolve the complexity of the biomass structure. To achieve the maximum benefit from the utilization of biomass in the biorefinery, the conditions of the selective pretreatment of subcritical and supercritical water extraction were tuned. Therefore, several kinetics of selective products

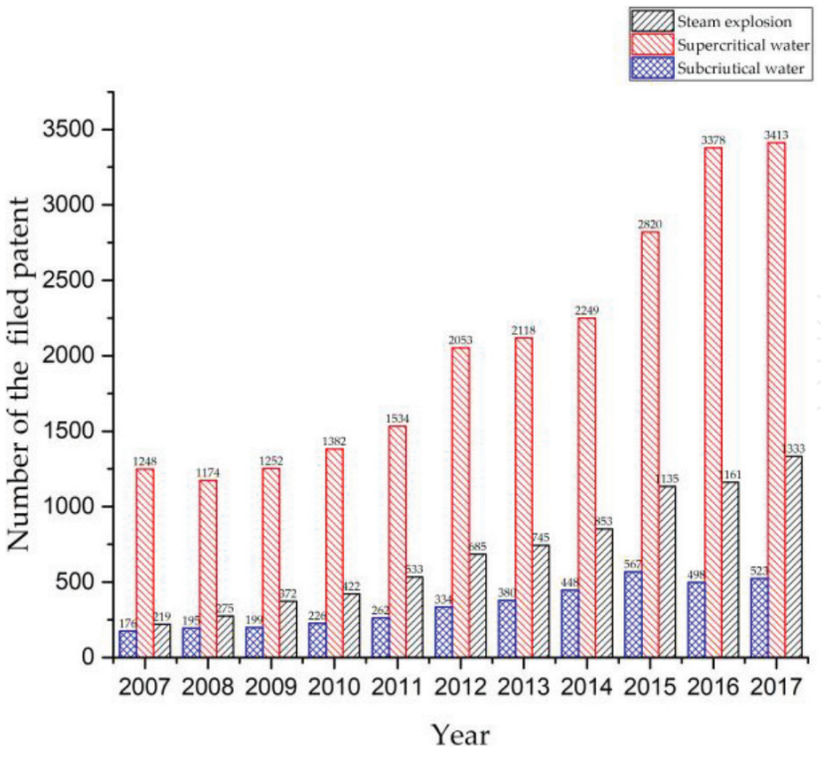

Figure 7. Numbers of filed patents in hydro-fractionation technology.

from the model compounds and the fine conditions including temperature, pressure, heating rate, and residence time were published [26–29]. It is worth mentioning that in subcritical extraction, temperature, heating rate, and residue time enormously affected the reaction behavior and desired products, while the role of pressure is to maintain water in a liquid state and increases the rate of reaction. On the other hand, the effect of pressure on the reaction and kinetics was gained at the supercritical water state [30]. The first component after the degradation of biomass under hot compressed water is hemicellulose at a temperature above 453 K. Typically, at a suitable temperature, a random cleavage between monomeric sugar bonds took place and hemicellulose oligomers were extracted when the chain was cleaved until shorter chains were obtained. And if the reaction time is high enough, another reaction called deacetylation occurred and gave acetic acid. With higher temperature, the product yield was increased but the selectivity dropped [31, 32]. Moreover, if the temperature was raised above 513 K, the oligomer of cellulose from the amorphous part in cellulose was generated, leading to the reduction of the solid yield [33]. After the temperature reached 553 K, the products derived from the hydrolysis reaction of cellulose were 5-hydroxymethylfurfural, levulinic acid, formic acid, and lactic acid [34–36]. For the extraction of lignin, there was a handful of evidence that indicated that the decomposition temperature of lignin without the addition of a catalyst was above 623 K and provided phenols, cresols, guaiacol, catechol, and methyl dehydroabietate as its degrading products [37, 38].

3.3. Steam explosion

The steam explosion process offers several attractive features for biomass fractionation technologies. Obviously, this process has low environmental impacts and mild operating reaction conditions, no chemical is required except water, and moist biomass can be used as feedstock; the higher the moisture content, the longer the steam pretreatment time [39]; it provides high sugar yield and small amounts of by-products and offers low capital investment. However, some unwanted degradation compounds occur when the operating condition is excessive (high temperature and pressure). For example, xylose obtained from hemicellulose could be degraded to furfural, and glucose obtained from cellulose could be degraded to 5-hydroxymethyl furfural, respectively. These two by-products are undesirable compounds since they could inhibit some microbial activities. Therefore, some detoxification methods should be determined prior to enzymatic hydrolysis. During the process, heat transfer can generate the issue of overcooking at the surface of the larger biomass particles and an incomplete pretreatment of the interior region [39], so optimization size of the feedstock is also a crucial step to achieve high sugar conversion and low production cost.

Steam explosion can be performed as a process either in a batch or as a continuous reaction with the most important operational conditions as residence time, temperature, and particle size; a combination effect of these parameters that depend upon feedstocks has been operational for steam explosion such as Salix [40], orange peel [41], wheat straw [42] and barley straw [39]. In recent years, there have been a good number of researchers who gained interest in the underlying work of water responsibility. Boluda-Aguilar et al. studied the steam explosion pretreatment of lemon (*Citrus limon* L.) citrus peel wastes to obtain bioethanol, galacturonic acid, and other coproducts [43]. The steam explosion pretreatment showed an interesting effect on lemon peel wastes for obtaining ethanol and galacturonic acid. The simultaneous saccharification and fermentation (SSF) processing of steam-exploded lemon citrus peel wastes with low enzymatic

concentration produced more than 60 L ethanol/1000 kg of fresh lemon citrus peel wastes. In addition, it has been discussed that the minimum inhibitory concentration of lemon citrus essential oils on yeast is lower than that obtained from orange and mandarin citrus essential oils. Singh et al. [44] reported the steam explosion of sugarcane bagasse, which eventually showed the enzymatic hydrolysis efficiency of 100% after 24 h of incubation by using the cellulases from Penicillium pinophilum with an enzyme loading of 10 FPU/g. To compare its potential use with commercially available cellulose (Accellerase™ 1000), the results indicated that using Penicillium cellulase and Accellerase™ 1000 showed that the saccharification potentials are comparable to the treated substrates such as steam-exploded sugarcane bagasse and ball-milled cellulose powder.

In our recent report on sugar production from sugarcane bagasse, the batch-type steam explosion system was developed for lignin removal to increase sugar yield. The sugarcane bagasse was first impregnated in a diluted alkaline solution and subjected to the steam explosion experiment at the temperature range of 433–493 K with the pressure below 2 MPa for a maximum reaction time of 10 min. The study showed good synergy on the combination of diluted alkaline impregnation and steam explosion for enhancing the purity of obtained bagasse leading to the higher yield of sugar production after the enzymatic hydrolysis process [45]. This could be a good evidence to show that the combination of the steam explosion technique and diluted base solution treatment could fractionate the lignin content into the water phase and provide the nonsoluble solid product of cellulose and hemicellulose for sugar production.

4. Life cycle assessment and bioeconomy of biomass upgrading

4.1. Life cycle of biomass hydro-fractionation

For the conversion of the lignocellulosic biomass feedstock to bio-based products, there are several processes involved. Firstly, the agricultural plants are grown and harvested in which the agricultural residues and wastes could then be collected and transported for storage. The pretreatment and fractionation of the biomass are performed to prepare the material for some particular manufacturing processes. The obtained bio-based products are later on distributed to marketplaces and delivered to customers. The life cycle assessment (LCA) is known as a systematic method for evaluating the environmental impact of a product's entire life, starting from growing its feedstock to its disposal process [46]. For example, in case of the bio-based product, lignocellulosic biomass feedstock was generated from agricultural crops which require soil, fertilizers, water, and sunlight for its growth, while water, electricity, and heat are necessary for its manufacturing process. However, to make this chapter concise, only the pretreatment and fractionation process of the feedstock is emphasized.

In a study, Prasad and his team evaluated the life cycle of four different pretreatment methods including liquid hot water (or subcritical) extraction, organosolve extraction, dilute acid extraction, and steam explosion of milled corn stover [47]. The four environmental impacts in terms of climate change, eutrophication, water depletion, and acidification potential were predicted and compared among the four methods. For climate change, the CO_2 emission was reported whereas subcritical water extraction gave the smallest amount of CO_2 emission while almost 15 times of CO_2

could be released from steam explosion due to higher energy consumption which required more electricity during the fractionation process. The second parameter, eutrophication or the nutrition enrichment of the Earth's surface, was determined by comparing nitrogen gas and phosphorus equivalents. The eutrophication took place mostly on the feedstock growth step; therefore, the efficiency of the fractionation process plays important roles on this part. Subcritical water extraction was found to show the smallest impact on eutrophication since less amount of feedstock is required for producing the same amount of the desired product. The subcritical water extraction also showed the smallest impact toward water depletion. In addition, the study indicated more than 90% of water in all four processes that was used in the feedstock growth step. The last parameter is acidification potential, where organosolve extraction and steam explosion showed smallest effects while diluted acid extraction had the highest impact on acidification potential.

4.2. Bioeconomy of bio-based product manufacturing from biomass

Besides the environmental impact, an economic aspect is very important for product development. The term bioeconomy or bio-based economy refers to an economy employing renewable bioresources such as microorganisms, agricultural crops or residues, and livestock to produce food, pharmaceuticals, energy, plastics, and other bio-based materials. In this context the utilization of lignocellulosic biomass from agricultural residues for the production of various bio-based products was explained. As shown in **Figure 8**, promising products from biomass feedstock upgrading are biogas, biofuels, biochemicals, bioplastics, carbon fiber, nanofiber,

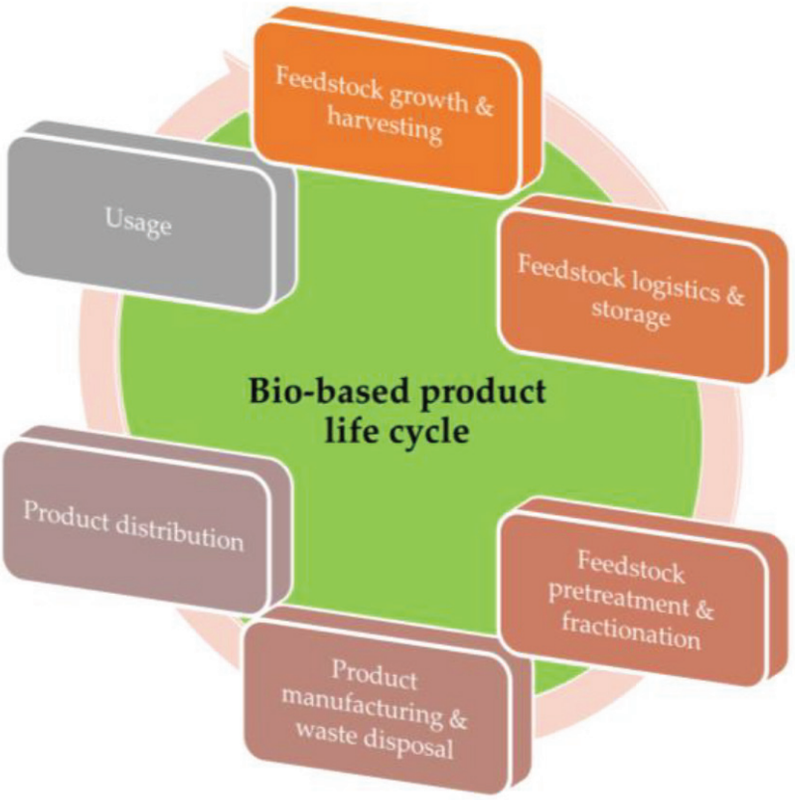

Figure 8. Life cycle of bio-based product upgraded from lignocellulosic biomass.

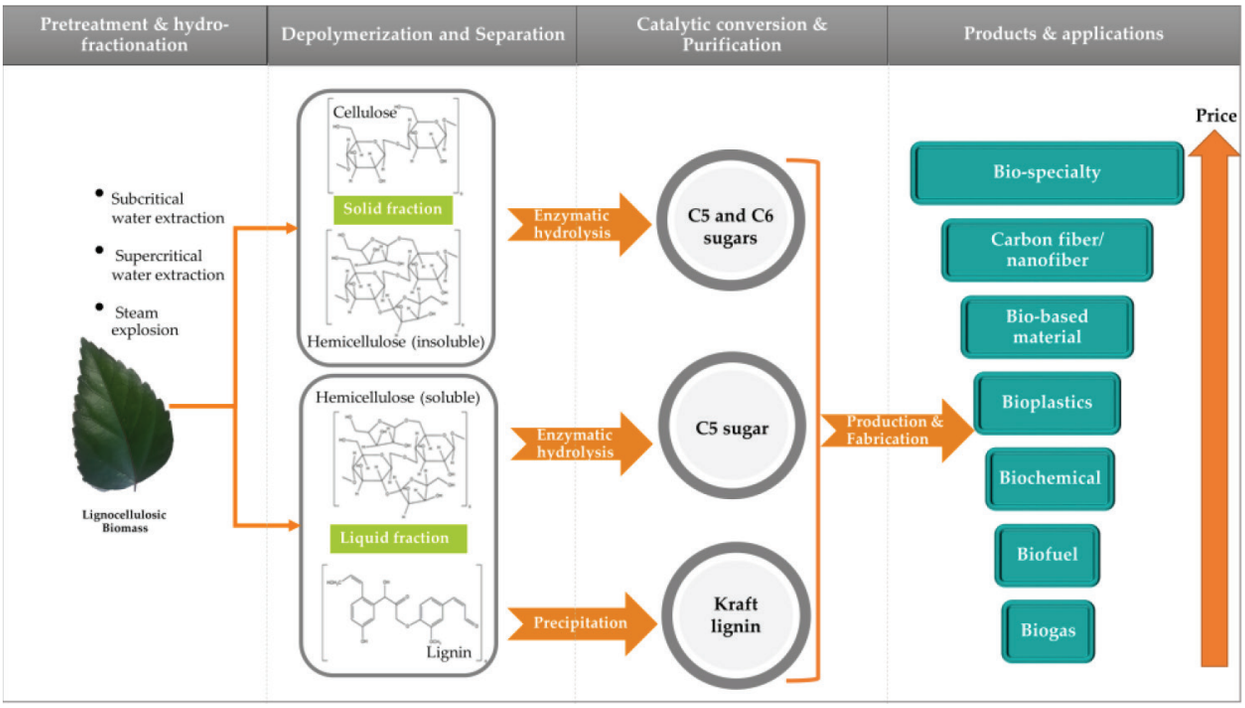

Figure 9. Bioeconomy of biomass upgrading.

and bio-specialty (a unique high-value product derived from bioresources for a specific customer group). In general, the feedstock undergoes pretreatment or hydro-fractionation to prepare the material for some particular applications. Then, the material is manufactured to produce a targeted product (**Figure 9**).

5. Conclusions

Hydro-fractionation enhanced lignin removal and provided a higher yield of sugar-based chemical platform production from biomass. The three green processes including subcritical water extraction, supercritical water extraction, and steam explosion are practical for biomass treatment. With the adjustable water properties, subcritical and supercritical water extractions are attractive tunable techniques for various bio-based compound extractions while the rapid volume expansion of water in steam explosion can destroy the high crystallinity of biopolymers. In addition, some technical feasibility in terms of energy consumption and reactor system as well as economic feasibility should be taken into consideration for future advancement.

Acknowledgements

The financial support from the National Nanotechnology Center, Thailand, via the CARBANO project (P1752318) and the Thailand Research Fund (TRG6080004) is acknowledged. The authors are also grateful to the Collaboration Hubs for International Program (CHIRP) of Strategic International Collaborative Research Program (SICORP), Japan Science and Technology Agency (JST) and the JASTIP program–WP2 (NSTDA-Kyoto University collaboration).

Author details

Sanchai Kuboon*, Wasawat Kraithong, Jaruwan Damaurai and Kajornsak Faungnawakij

*Address all correspondence to: sanchai@nanotec.or.th

National Nanotechnology Center, National Science and Technology Development Agency, Pathum Thani, Thailand

References

[1] Chen H et al. A review on the pretreatment of lignocellulose for high-value chemicals. Fuel Processing Technology. 2017;**160**:196-206. DOI: 10.1016/j.fuproc.2016.12.007

[2] Ingram LO, Doran JB. Conversion of cellulosic materials to ethanol. FEMS Microbiology Reviews. 1995;**16**:235-241. DOI: 10.1016/0168-6445(94)00083-B

[3] Saini JK, Saini R, Tewari L. Lignocellulosic agriculture wastes as biomass feedstocks for second-generation bioethanol production: Concepts and recent developments. Biotech. 2015;**15**(3):337-353. DOI: 10.1007/s13205-014-0246-5

[4] Hendriks ATWM, Zeeman G. Pretreatments to enhance the digestibility of lignocellulosic biomass. Bioresource Technology. 2009;**100**:10-18. DOI: 10.1016/j.biortech.2008.05.027

[5] Axelsson L, Franzén M, Ostwald M, Berndes G, Lakshmi G, Ravindranath NH. Perspective: Jatropha cultivation in southern India: Assessing farmers' experiences. Biofuels Bioproducts and Biorefining. 2012;**6**:246-256. DOI: 10.1002/bbb.1324

[6] Ohtaki H. Effects of temperature and pressure on hydrogen bonds in water and in formamide. Journal of Molecular Liquids. 2003;**103-104**:3-13. DOI: 10.1016/S0167-7322(02)00124-1

[7] Petrenko VE, Gurina DL, Antipova ML. Structure of supercritical water: The concept of critical isotherm as a percolation threshold. Russian Journal of Physical Chemistry B. 2012;**6**(8):899-906. DOI: 10.1134/s1990793112080155

[8] Jimenez-Carmona M et al. Sub- and supercritical fluid extraction of trichloropyridinol from soil prior to immunoassay. Journal of Chromatography A. 1997;**785**(1-2):329-336

[9] Rodríguez-Meizoso I et al. Subcritical water extraction of nutraceuticals with antioxidant activity from oregano. Chemical and functional characterization. Journal of Pharmaceutical and Biomedical Analysis. 2006;**41**(5):1560-1565. DOI: 10.1016/j.jpba.2006.01.018

[10] Holliday RL, King JW, List GR. Hydrolysis of vegetable oils in sub-and supercritical water. Industrial & Engineering Chemistry Research. 1997;**36**(3):932-935. DOI: 10.1021/ie960668f

[11] Hodes M et al. Salt precipitation and scale control in supercritical water oxidation—Part A: Fundamentals and research. The Journal of Supercritical Fluids. 2004;**29**(3):265-288. DOI: 10.1016/S0896-8446(03)00093-7

[12] Marrone PA et al. Salt precipitation and scale control in supercritical water oxidation—part B: Commercial/full-scale applications. The Journal of Supercritical Fluids. 2004; **29**(3):289-312. DOI: 10.1016/S0896-8446(03)00092-5

[13] Bermejo MD, Cocero MJ. Destruction of an industrial wastewater by supercritical water oxidation in a transpiring wall reactor. Journal of Hazardous Materials. 2006;**137**(2): 965-971. DOI: 10.1016/j.jhazmat.2006.03.033

[14] Uematsu M, Frank E. Static dielectric constant of water and steam. Journal of Physical and Chemical Reference Data. 1980;**9**(4):1291-1306. DOI: 10.1063/1.555632

[15] Kruse A, Dinjus E. Hot compressed water as reaction medium and reactant: Properties and synthesis reactions. The Journal of Supercritical Fluids. 2007;**39**(3):362-380. DOI: 10.1016/j.supflu.2006.03.016

[16] Hunter SE, Savage PE. Recent advances in acid-and base-catalyzed organic synthesis in high-temperature liquid water. Chemical Engineering Science. 2004;**59**(22-23):4903-4909. DOI: 10.1016/j.ces.2004.09.009

[17] Akiya N, Savage PE. Roles of water for chemical reactions in high-temperature water. Chemical Reviews. 2002;**102**(8):2725-2750. DOI: 10.1021/cr000668w

[18] Marshall WL, Franck E. Ion product of water substance, 0-1000 C, 1-10,000 bars new international formulation and its background. Journal of Physical and Chemical Reference Data. 1981;**10**(2):295-304. DOI: 10.1063/1.555643

[19] Bandura AV, Lvov SN. The ionization constant of water over wide ranges of temperature and density. Journal of Physical and Chemical Reference Data. 2006;**35**(1):15-30. DOI: 10.1063/1.1928231

[20] Sasaki M et al. Cellulose hydrolysis in subcritical and supercritical water. The Journal of Supercritical Fluids. 1998;**13**(1-3):261-268. DOI: 10.1016/S0896-8446(98)00060-6

[21] Thulukkanam K. Heat Exchanger Design Handbook. 2nd ed. Boca Raton: CRC Press; 2013. p. 1260. ISBN: 9781439842133

[22] Singh J, Suhag M, Dhaka A. Augmented digestion of lignocellulose by steam explosion, acid and alkaline pretreatment methods: A review. Carbohydrate Polymers. 2015;**117**:624-631. DOI: 10.1016/j.carbpol.2014.10.012

[23] Alvira P, Tomás-Pejó E, Ballesteros M, Negro MJ. Pretreatment technologies for an efficient bioethanol production process based on enzymatic hydrolysis: A review. Bioresource Technology. 2010;**101**:4851-4861. DOI: 10.1016/j.biortech.2009.11.093

[24] Avellar BK, Glasser WG. Steam-assisted biomass fractionation. I. Process considerations and economic evaluation. Biomass and Bioenergy. 1998;**14**:205-218. DOI: 10.1016/S0961-9534(97)10043-5

[25] Adschiri T, Yoko A. Supercritical fluids for nanotechnology. The Journal of Supercritical Fluids. 2018;**134**:167-175. DOI: 10.1016/j.supflu.2017.12.033

[26] Gao P et al. Preparation of lactic acid, formic acid and acetic acid from cotton cellulose by the alkaline pre-treatment and hydrothermal degradation. Industrial Crops and Products. 2013;**48**:61-67. DOI: 10.1016/j.indcrop.2013.04.002

[27] Sakimoto K et al. Kinetic model of cellulose degradation using simultaneous saccharification and fermentation. Biomass and Bioenergy. 2017;**99**:116-121. DOI: 10.1016/j.biombioe.2017.02.016

[28] Vaquerizo L et al. Redefining conventional biomass hydrolysis models by including mass transfer effects. Kinetic model of cellulose hydrolysis in supercritical water. Chemical Engineering Journal. 2018;**350**:463-473. DOI: 10.1016/j.cej.2018.05.077

[29] Cantero DA et al. Kinetic analysis of cellulose depolymerization reactions in near critical water. The Journal of Supercritical Fluids. 2013;**75**:48-57. DOI: 10.1016/j.supflu.2012.12.013

[30] Cocero MJ et al. Understanding biomass fractionation in subcritical & supercritical water. The Journal of Supercritical Fluids. 2018;**133**:550-565. DOI: 10.1016/j.supflu.2017.08.012

[31] Suhas VK et al. Cellulose: A review as natural, modified and activated carbon adsorbent: Biomass, bioenergy, biowastes, conversion technologies, biotransformations, production technologies. Bioresource Technology. 2016;**216**:1066-1076. DOI: 10.1016/j.biortech.2016.05.106

[32] Garrote G et al. Interpretation of deacetylation and hemicellulose hydrolysis during hydrothermal treatments on the basis of the severity factor. Process Biochemistry. 2002;**37**(10):1067-1073. DOI: 10.1016/S0032-9592(01)00315-6

[33] Ruiz HA et al. Hydrothermal processing, as an alternative for upgrading agriculture residues and marine biomass according to the biorefinery concept: A review. Renewable and Sustainable Energy Reviews. 2013;**21**:35-51. DOI: 10.1016/j.rser.2012.11.069

[34] Yu Y, Wu H. Understanding the primary liquid products of cellulose hydrolysis in hot-compressed water at various reaction temperatures. Energy & Fuels. 2010;**24**(3):1963-1971. DOI: 10.1021/ef9013746

[35] Antal MJ Jr, Mok SLW, Richards GN. Mechanism of formation of 5-(hydroxymethyl)-2-furaldehyde from D-fructose and sucrose. Carbohydrate Research. 1990;**199**(1):91-109. DOI: 10.1016/0008-6215(90)84096-D

[36] Asghari FS, Yoshida H. Kinetics of the decomposition of fructose catalyzed by hydrochloric acid in subcritical water: Formation of 5-hydroxymethylfurfural, levulinic, and formic acids. Industrial & Engineering Chemistry Research. 2007;**46**(23):7703-7710. DOI: 10.1021/ie061673e

[37] Wahyudiono KT, Sasaki M, Goto M. Decomposition of a lignin model compound under hydrothermal conditions. Chemical Engineering & Technology. 2007;**30**(8):1113-1122. DOI: 10.1002/ceat.200700066

[38] Fang Z et al. Reaction chemistry and phase behavior of lignin in high-temperature and supercritical water. Bioresource Technology. 2008;**99**(9):3424-3430. DOI: 10.1016/j.biortech.2007.08.008

[39] Iroba KL, Tabil LG, Sokhansanj S, Dumonceaux T. Pretreatment and fractionation of barley straw using steam explosion at low severity factor. Biomass and Bioenergy. 2014;**66**:286-300. DOI: 10.1016/j.biombioe.2014.02.002

[40] Diop CIK, Lavoie JM, Huneault MA. Structural changes of Salix miyabeana cellulose fibres during dilute-acid steam explosion: Impact of reaction temperature and retention time. Carbohydrate Polymers. 2015;**119**:8-17. DOI: 10.1016/j.carbpol.2014.11.031

[41] Wang L, Xu H, Yuan F, Fan R, Gao Y. Preparation and physicochemical properties of soluble dietary fiber from orange peel assisted by steam explosion and dilute acid soaking. Food Chemistry. 2015;**185**:90-98. DOI: 10.1016/j.foodchem.2015.03.112

[42] Zhang LH et al. Effect of steam explosion on biodegradation of lignin in wheat straw. Bioresource Technology. 2008;**99**:8512-8515. DOI: doi.org/10.1016/j.biortech.2008.03.028

[43] Boluda-Aguilar M, Lopez-Gomez A. Production of bioethanol by fermentation of lemon (*Citrus limon* L.) peel wastes pretreated with steam explosion. Industrial Crops and Products. 2013;**41**:188-197. DOI: 10.1016/j.indcrop.2012.04.031

[44] Singh R, Varma AJ, Seeta LR, Rao M. Hydrolysis of cellulose derived from steam exploded bagasse by Penicillium cellulases: Comparison with commercial cellulase. Bioresource Technology. 2009;**100**:6679-6681. DOI: 10.1016/j.biortech.2009.07.060

[45] Champreda V et al. Development of tailor-made synergistic cellulolytic enzyme system for saccharification of stem exploded sugarcane bagasse. Journal of Bioscience and Bioengineering. 2018;**125**:390-396. DOI: 10.1016/j.jbiosc.2017.11.001

[46] Thiropoulos I et al. Life cycle impact assessment of bio-based plastics from sugarcane ethanol. Journal of Cleaner Proudction. 2015;**90**:114-127. DOI: 10.1016/j.jclepro.2014.11.071

[47] Prasad A, Sotenko M, Blenkinsopp T, Coles SR. Life cycle assessment of lignocellulosic biomass pretreatment methods in biofuel production. The International Journal of Life Cycle Assessment. 2016;**21**(1):44-50. DOI: 10.1007/s11367-015-0985-5